3-11-2011

Small Internal Combustion Engine Testing for a Hybrid-Electric Remotely-Piloted Aircraft

Isseyas H. Mengistu

SMALL INTERNAL COMBUSTION ENGINE TESTING FOR A HYBRID-ELECTRIC REMOTELY-PILOTED AIRCRAFT

THESIS

Isseyas H. Mengistu, BSE
Captain, USAF

AFIT/GAE/ENY/11-M20

DEPARTMENT OF THE AIR FORCE
AIR UNIVERSITY

AIR FORCE INSTITUTE OF TECHNOLOGY

Wright-Patterson Air Force Base, Ohio

AFIT/GAE/ENY/11-M20

SMALL INTERNAL COMBUSTION ENGINE TESTING FOR A HYBRID-ELECTRIC REMOTELY-PILOTED AIRCRAFT

THESIS

Presented to the Faculty

Department of Aeronautics and Astronautics

Graduate School of Engineering and Management

Air Force Institute of Technology

Air University

Air Education and Training Command

In Partial Fulfillment of the Requirements for the

Degree of Master of Science in Aeronautical Engineering

Isseyas H. Mengistu, BSE

Captain, USAF

March 2011

AFIT/GAE/ENY/11-M20

SMALL INTERNAL COMBUSTION ENGINE TESTING FOR A HYBRID-ELECTRIC REMOTELY-PILOTED AIRCRAFT

Isseyas H. Mengistu, BSE

Captain, USAF

Approved:

Frederick G. Harmon, Lt Col, USAF (Chairman)	14 Mar 11 Date
Christopher M. Shearer, Lt Col, USAF (Member)	17 Mar 2011 Date
Dr. Marc D. Polanka (Member)	14 MAR 11 Date

Abstract

Efficient operation of a hybrid-electric propulsion system (HEPS) powering a small remotely-piloted aircraft (RPA) requires that a controller have accurate and detailed engine and electric motor performance data. Many small internal combustion engines (ICEs) currently used on various small RPA were designed for use by the recreational hobbyist radio-control (R/C) aircraft market. Often, the manufacturers of these engines do not make accurate and reliable detailed engine performance data available for their engines. A dynamometer testing stand was assembled to test various small ICEs. These engines were tested with automotive unleaded gasoline (the manufacturer's recommended fuel) using the dynamometer setup. Torque, engine speed and fuel flow measurements were taken at varying load and throttle settings. Power and specific fuel consumption (SFC) data were calculated from these measurements. Engine performance maps were generated in which contours of SFC were mapped on a mean effective pressure (MEP) versus engine speed plot. These performance maps are to be utilized for performance testing of the controller and integrated HEPS in further research. Further follow-on research and development will be done to complete the goal of building a prototype hybrid-electric remotely piloted aircraft (HE-RPA) for flight testing. Minimum BSFC for the Honda GX35 engine was found to be 383.6 g/kW·hr (0.6307 lbm/hp·hr) at 4500 RPM and 60% throttle. The Honda GX35 was overall the better fit for incorporation into the HE-RPA.

Acknowledgments

I would like to thank my advisor Lt Col Fred Harmon for the guidance and instruction he has provided concerning my course and thesis work. Also, I thank my professors for the instruction they have provided me and my fellow classmates that have helped me here at AFIT with my graduate studies. Specifically, I am very appreciative of 2d Lt Collin Greiser, Mr. Matthew Rippl, Capt Todd Rotramel, Capt Ryan Hiserote and Capt Cary Wilson (Small Engine Research Laboratory - AFRL/RZTC) who I have worked with in a team effort to further develop the hybrid-electric remotely-piloted aircraft design envisioned by Lt Col Harmon. Also, I'd like to thank Mr. Brian Crabtree, Mr. Daniel Ryan and Mr. Christopher Harkless of the AFIT Model Fabrication Shop along with their supervisor Mr. Jan LeValley for their excellent work fabricating dozens of critical parts and their advice on various mechanical issues. Finally, I thank my family, my partner and my friends for all the continued support, love and guidance they provide. Life is truly a joy because of them. Their patience and understanding have allowed me to focus as much time as necessary to successfully complete my work.

-Isseyas Mengistu

Table of Contents

Page

Page

List of Figures Page

Page

Page

List of Tables

Page

List of Abbreviations

AFIT	Air Force Institute of Technology
AFRL	Air Force Research Laboratory
BDC	Bottom-Dead-Center
BMEP	Brake Mean Effective Pressure
BSFC	Brake Specific Fuel Consumption
CEA	Chemical Equilibrium with Applications
CI	Compression Ignition
COTS	Commercial Off-the-Shelf
DoD	Department of Defense
EM	Electric Motor
HEPS	Hybrid-Electric Propulsion System
HE-RPA	Hybrid-Electric Remotely Piloted Aircraft
ICE	Internal Combustion Engine
ISR	Intelligence, Surveillance, and Reconnaissance
IOL	Ideal Operating Line
LPG	Liquefied Petroleum Gas
MEP	Mean Effective Pressure
MON	Motor Octane Number
ON	Octane Number
OSD	Office of the Secretary of Defense
PC	Personal Computer
R/C	Radio Control
RON	Research Octane Number
RPA	Remotely Piloted Aircraft
RPM	Rotations/Revolutions per Minute
SAE	Society of Automotive Engineers
SFC	Specific Fuel Consumption
SI	Spark Ignition
SOP	Standard Operating Procedure

TDC	Top-Dead-Center
TPS	Throttle Position Sensor
USAF	United States Air Force

Nomenclature

Symbol	Description (Units)
A	Area (m^2)
F	Force (N) [lbf]
F/A	Fuel-to-air ratio
h	Specific Enthalpy (kJ/kg)
H	Enthalpy (kJ)
m	Mass (kg, g) [lbm]
$\dot{m}$	Mass flow rate (g/min) [lbm/hr]
$BMEP$	Brake mean effective pressure (kPa)
n_R	Number of crank revolutions per power stroke
N	Crankshaft rotational speed (rad/s)
P	Power (W) [hp]
Q_{HV}	Heating value (J/kg)
Q_{LHV}	Lower heating value (J/kg)
$\bar{S}$	Piston speed (m/s)
$BSFC$	Brake specific fuel consumption (g/kW·hr)
t	Time (s) [min, hr]
T	Temperature (K)
T	Torque (N·m) [lbf·ft]
W	Weight (N) [lbm]
W	Work (J)
V	Volume (cm^3) [gal]
$\dot{V}$	Volumetric flow rate [gal/hr]
η_f	Fuel conversion efficiency
η_{mech}	Mechanical efficiency
η_v	Volumetric efficiency
ρ	Density (g/cm^3)
θ	Angle (rad) [degrees]

Subscript	Description
a	Air, Ambient
c	Compression, Clearance, Combustion
d	Displacement
EM	Electric motor
f	Fuel
HV	Heating value
i	Initial, Inlet
p	Piston
prod	Products
reac	Reactants
R	Required, Reaction, Rotation
v	Volume
x	Unknown Variable
y	Unknown Variable

SMALL INTERNAL COMBUSTION ENGINE TESTING FOR A HYBRID-ELECTRIC REMOTELY-PILOTED AIRCRAFT

I. Introduction

1. Background

Today's battlefield has found a tremendous amount of use for small remotely-piloted aircraft (RPA). Small RPA are specified as those having maximum gross takeoff weight of less than 55 pounds [1]. The size and portability of these assets have allowed individual service members to conduct numerous types of missions. These missions typically include intelligence, surveillance and reconnaissance (ISR) and target acquisition. Non-military uses for small RPAs include border monitoring, chemical, biological and radiological detection, weather data collection, and scientific research [2]. The application of persistence is critical to the effectiveness of these missions. Persistence is the principal attribute of RPA over manned aircraft [3], and a RPA's range and endurance capabilities are analogous to persistence. These capabilities are directly linked to the performance of the RPA's propulsion system.

Currently, small RPA utilize numerous types of propulsion systems. Rechargeable lithium-ion batteries and an electric motor (EM) power the less than five pound United States Air Force (USAF) RQ-11B Raven RPA to achieve an endurance of 1-1.5 hours [4]. The Wasp III is a one pound RPA. It is powered by an electric motor as well, and it has an endurance of 45 minutes [5]. The Naval Research Laboratory's Ion Tiger RPA weighs 37 pounds and employs a 0.550 kW (0.75 hp) hydrogen fuel cell enabling demonstration flights of greater than twenty hours [6].

The internal combustion engine (ICE) has been a prolific source of power for hobby radio-controlled (R/C) model aircraft. Along with many other R/C model aircraft components, small ICEs have found a home in RPA. The Scan Eagle RPA has a maximum takeoff weight of 44 pounds and uses a single cylinder two-stroke ICE producing 1.5-1.9 peak horsepower [7]. The Scan Eagle has endurance capabilities of greater than 20 hours [8] but payload is sacrificed for additional fuel storage. Propulsion via an ICE still provides an excellent platform for achieving great endurance for small RPA, when cost is considered. Using an ICE avoids the challenges of storing and transporting hydrogen used in some fuel cells.

Most small RPA using the aforementioned non-ICE propulsion sources, currently provide less endurance but are superior to ICEs in the aspect of acoustic signature. A key component to ISR and target acquisition is executing the mission while remaining undetected and unbeknownst by the objective. Minimizing the acoustic signature of an operating RPA is crucial to achieving this aspect of stealth. In recent years, it has been suggested and shown by Harmon [9] and Hiserote [10] that a parallel hybrid-electric propulsion system (HEPS) composed of an ICE, EM and batteries is a viable propulsion system for small RPA. The use of a HEPS on a small RPA can improve fuel consumption and increase range while reducing acoustic and thermal signatures. The central focus, of the overall work that this effort falls under, is taking Harmon and Hiserote's conceptual design of a hybrid-electric RPA (HE-RPA) and developing a prototype.

2. Motivation and Problem Statement

Developing a propulsion system that maximizes endurance and range capability is a challenge facing small RPA design because of the desire for persistent ISR. Accurate and reliable performance maps for an engine and EM are required (along with a controller), to optimize the performance of a HEPS on a small RPA. The engine performance parameters most critical to a propulsion controller are specific fuel consumption (SFC), torque, power, and engine speed. The controller references the engine performance data to decide how the propulsion system as a whole operates. The controller determines whether to propel the RPA using the EM, ICE, or both in combination, after referencing the map and utilizing real-time engine speed and possibly cylinder pressure information. The design of a controller for this project's hybrid-electric propulsion is the focus of research done by Greiser [11]. Optimizing the RPA's entire propulsion system by properly matching a propeller to the HEPS is another key to maximizing range and endurance. This propeller matching optimization is the motivation of Rotramel's [12] work.

Accurate and reliable performance data from manufacturers and researchers has been found to be sparse for ICEs producing the required power levels common to small RPA (one-half to several horsepower). Also, it is not uncommon for small ICE manufacturers to inflate advertised peak power ratings for their engines. These small ICEs have been traditionally used by the R/C hobby aircraft community which usually has little need for detailed and accurate performance data. Also, due to considerations of the existing logistical supply chain for supplying fuel to military aircraft, having RPA propulsion systems capable of running on JP-8 or Diesel fuel is desired by the Department of

Defense (DoD) [13]. Many small RPA currently have engines that run on gasoline or hobbyist glow fuel (the latter being a mixture of methanol, nitro-methane and oil). For these reasons, testing a number of small ICEs to establish accurate and reliable performance parameter measurements for use as a essential part of a HEPS is seen as a worthy research effort. Also, exploring the capability of running small ICEs on Diesel or JP-8 fuel is an important part of trying to ease logistical supply chain difficulties for DoD RPA operation.

3. Objectives

This research effort's goal is to test and compare the engine performance of two ICEs. The aim of the comparison is to select the better performing engine and determine the feasibility of the choice for incorporation into the HEPS. Engine performance maps in which contours of brake specific fuel consumption (BSFC) are mapped on a break mean effective pressure (BMEP) versus engine speed plot are to be generated. This effort will compare the BSFC of both engines and provide the data necessary to establish the ideal operating line (IOL) where the engine will be operated as part of the HEPS. The engines will be tested with the manufacturer's recommended fuel (gasoline in both cases) as well as diesel fuel. Also, to further determine the better performing engine, a qualitative analysis will be done in which the operating characteristics of the engines are compared.

4. Methodology

The research objectives will be achieved through engine testing via an engine test stand. An engine test stand will be developed using a dynamometer. Initially, the

dynamometer itself will be tested and calibrated. Engine mounts, an engine to dynamometer coupling, a fuel flow system, and a throttle control system must be designed and built, or purchased. These parts will be installed and integrated together into a functioning test stand. Software tools necessary for testing and data analysis must be developed (or otherwise procured) as well.

5. Scope

This effort is limited to testing two possible ICE choices for incorporation into the HEPS. The entire HEPS will not be tested in this effort; however, building it will be a side effort of this research. Greiser's [11] work seeks to test the possible operating modes of the HEPS to verify controller effectiveness. Time permitting, the engines will be run and tested on diesel fuel. No development of models to generate performance maps and engine performance data will be done, although it was initially considered.

6. Thesis Overview

Chapter I introduced the reader to background information concerning the subject areas this effort is involved with. It discussed the objectives of this effort and the motivation behind achieving these goals. In this thesis, Chapter II serves as a review of applicable research gained from literature. The author sought to first learn about the fundamentals of hybrid-electric propulsion, ICEs, fuel, and combustion. Current research and knowledge gains in small RPA design, HEPS design, ICE testing, and engine performance modeling was then tackled by the author. Chapter III lays out the method in which the experimental research was conducted. Detailed analysis of research results are

explored in Chapter IV. Lastly, chapter V summarizes results, offers conclusions and proposes areas for further related research.

II. Literature Review

1. Chapter Overview

There has been considerable research and development in the areas of HEPS and ICE technology for automotive applications. This research has focused on various aspects of design, manufacture, testing, operation and performance. As ICE testing is the main thrust of this effort, this chapter summarizes ICE essentials and discusses research areas relevant to aforementioned objectives. Information concerning hybrid-electric propulsion is first explored, since the overall goal of this project is developing, designing and building a HEPS that is incorporated into a small RPA prototype. Also, fundamentals of combustion fuels are investigated and discussed to better understand how to effectively operate ICEs on various fuels. One of the initial objectives was to test the ICEs on heavy fuels, but this was not accomplished due to time constraints.

2. Hybrid-Electric Propulsion

Hybrid-electric propulsion technology is one example of the more general interest area of hybrid power technology. A hybrid system combines two or more sources capable of generating power into a single power system. One widespread application of hybrid technology is in vehicle propulsion. The commonly used term, hybrid-electric, describes a system that utilizes one or more heat engines together with one or more EMs in a certain configuration. In propulsive vehicles, hybrid-electric technology is primarily implemented in one of three principal configurations [14]. The three configurations are a series configuration, a parallel configuration and a power-split or series-parallel configuration. The series and parallel configurations are further discussed in the

following sections. The power-split configuration is a combination of the other two configurations and is not expanded on.

2.1. Series Configuration

A heat engine (ICE, gas-turbine, etc.) is used to run a generator in a hybrid-electric power-train with a series configuration. The generator supplies power to an EM that propels the vehicles. The generator also provides power (unused by the EM) to an energy storage system (batteries, capacitors, flywheels, etc.) for future use. A simple diagram of a hybrid-electric series configuration is shown in Figure 1. A main benefit of a series configuration is that the engine running the generator can be designed to operate at a consistent and optimum engine speed. This is because the engine is not directly mechanically linked to the driving of the vehicle. A drawback to a series configuration is that the EM must be sized based on the capability to provide the maximum power output the vehicle requires. This leads to a more massive EM and overall system. Due to the weight downside associated with series configurations, they find most use in high-torque, low-speed, large vehicles like buses, commercial trucks and locomotives [14].

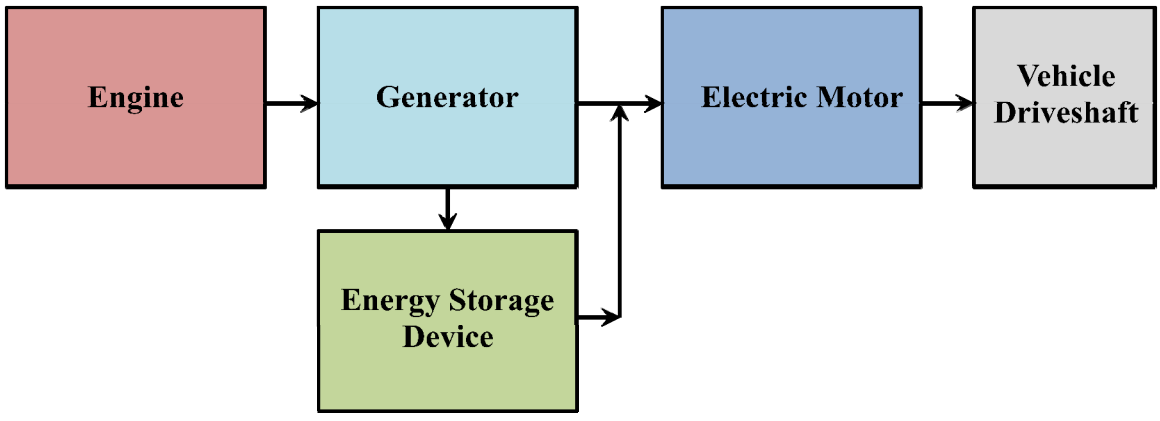

Figure 1: Hybrid-electric series configuration diagram

2.2. Parallel Configuration

In a parallel hybrid-electric system, a heat engine and an EM are used in combination to turn a single driveshaft through individual mechanical linkages. This hybrid architecture allows for the engine to power the vehicle alone, the EM to power the vehicle alone or for the engine and the EM to both power the vehicle jointly. A simple diagram of a hybrid-electric parallel configuration is shown in Figure 2. The three major types of parallel hybrid-electric systems are called mild, power-assist and dual-mode [14]. The types are nominally classified based on the sizing and intended function of the EM. The EM is relatively small in a mild system. It is used to aid in acceleration and utilizes regenerative braking to recharge batteries during decelerations. The power-assist parallel system uses a larger EM and larger energy storage system to aid in vehicle acceleration and propulsion and can warrant a modest downsizing of the engine [14]. Mild hybrids are often only capable of propelling the vehicle in electric-only mode (in which the EM singly powers the vehicle) for short distances, if at all. Finally, the dual-mode parallel hybrid-electric system utilizes a yet even larger EM and larger energy storage bank to aid further in vehicle acceleration and propulsion as well as being capable of extended-range sustained electric-only mode. Also, dual-mode parallel systems allow for further downsizing of the engine.

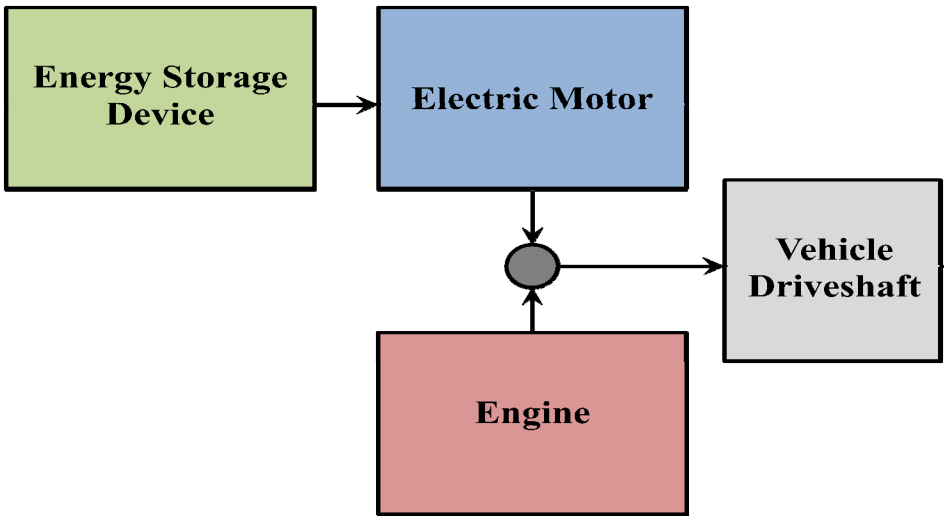

Figure 2: Hybrid-electric parallel configuration diagram

Over the last decade, the major thrust behind hybrid-electric technology research and application has been the automotive industry. Accordingly, the ICE (common to most automobiles) has been the heat engine of choice for most HEPS designs. Selecting the appropriate size and type of ICE is critically important for an HEPS and its performance in vehicle propulsion. Therefore, ICE fundamentals are extensively investigated in the next section.

3. Internal Combustion Engines

At the dawn of powered flight, the ICE was the sole propulsion source for aircraft. The ICE was used as the power source to rotate propellers which generated the thrust necessary for an aircraft to achieve flight. In the original era of powered flight, various ICE configurations were developed to produce sufficient and efficient thrust for aircraft of the period. In the quest for aircraft capable of higher speeds, it was found that propeller driven aircraft were speed limited. Higher propeller rotational speeds were

required to create the thrust needed for increased aircraft speed. The result of these increased speeds, were that the tips of the propeller began to approach the speed of sound producing shockwaves at the tips and dramatically increasing drag. The ICE powered propeller aircraft had a speed limit. The invention of the turbojet engine in the 1930s provided a method of propulsion for aircraft to break the propeller speed limit. The turbo-jet engine had superior thrust-to-weight properties than the ICE which allowed for larger aircraft to be built [15]. Advanced turbo-machinery, like the turbo-fan engine and turbo-prop engine, power a wide range of flight regimes. They have relegated the ICE to power mostly smaller and slower aircraft, where it is still the most effective propulsive platform (though fuel-cells and EMs are more efficient). Thus, the ICE is an excellent source of propulsion for propeller driven small RPA. The growth of small RPA has increased research in small ICE design and performance.

The ICE is a type of heat engine that develops mechanical power by means of converting the energy stored in the chemical bonds of fuel [16]. This chemical energy is converted to kinetic energy by means of a rapid oxidation process [17]. This rapid oxidation is commonly referred to as burning or combustion. The mixture of fuel and oxidizer (most often air) acts as a working fluid against specific mechanical components in the engine both before and after combustion. Two major types of ICEs are the spark-ignition (SI) engine (also called the Otto or gasoline/petrol engine) and the compression-ignition (CI) engine (also called the Diesel engine). The two engine cycles that either SI or CI engines usually operate with are the two-stroke cycle and the four-stroke cycle. These two engines and two cycles will be the focus of the next few sections.

3.1. Engine Components and Cycles

The reciprocating ICE's main features are shown for one cylinder in Figure 3. The piston travels back and forth through a cylinder, and the piston is attached to a crankshaft by means of a connecting rod. The linear motion of the piston is translated into rotational motion through the connection between crankshaft and connecting rod.

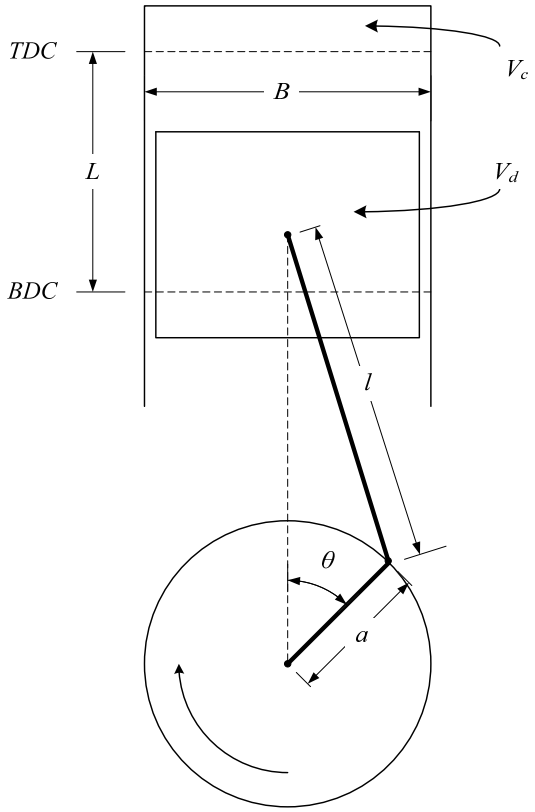

Figure 3: Cylinder geometry

The piston travels to and from positions of top-dead-center (TDC) and bottom-dead-center (BDC). The stroke (L) is the distance between TDC and BDC while the bore (B) represents the diameter of the cylinder. With knowledge of the crank radius (a) and connecting rod length (l), the position of the piston can be determined at any crank angle (θ). The crank angle is measured as the change in angle of the crankshaft from the

position of the crankshaft when the piston is at TDC where the crank angle is 0°. The compression ratio (r_c) is another important feature of cylinder geometry. Compression ratio represents the ratio of maximum cylinder volume to minimum cylinder volume [16]. The maximum cylinder volume is the sum of displaced cylinder volume (V_d) and cylinder clearance volume (V_c), whereas the minimum cylinder volume is the clearance volume.

In 1876, the first SI reciprocating engine was successfully operated. It was developed by Nicolaus A. Otto with his proposed engine cycle comprised of four piston strokes. This cycle came to be known as the Otto cycle. The intake stroke starts with the piston at TDC and finishes with the piston located at BDC. A fresh fuel-air mixture is ingested into the cylinder during the piston travel of the intake stroke. The compression stroke happens prior to ignition. As the piston moves from the BDC to TDC position, the fuel-air mixture is compressed, increasing pressure in the process. An expansion or power stroke, where the piston travels from TDC to BDC, follows spark-ignition (occurring at some point near TDC) and near constant-volume combustion. Finally, an exhaust stroke expels the remaining products of the fuel-air mixture combustion from the cylinder as the piston travels from BDC to TDC.

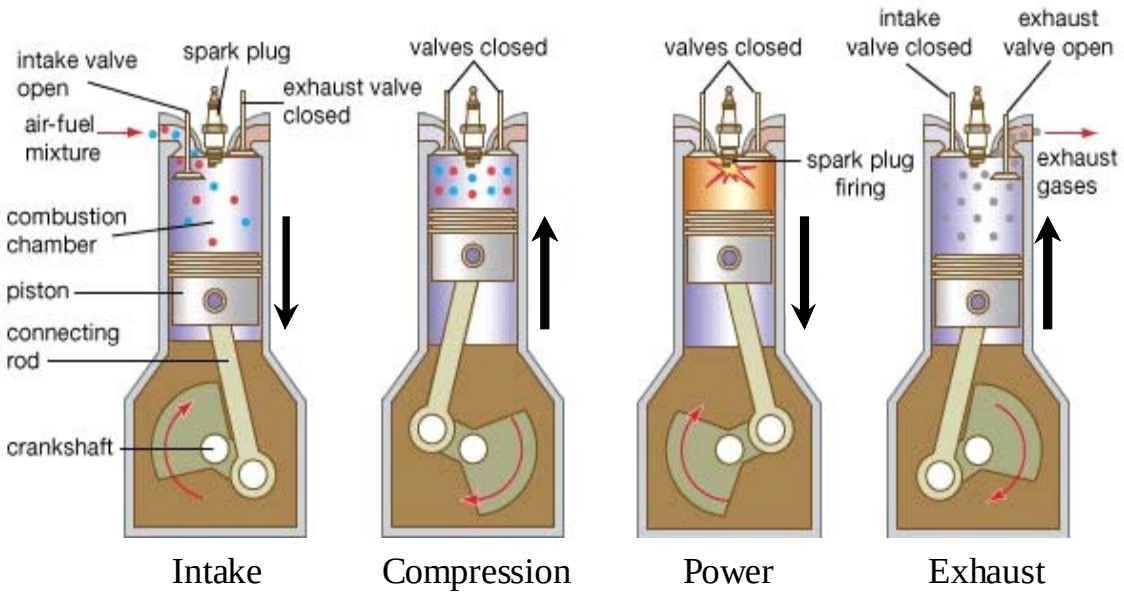

Figure 4: Four-stroke operating cycle [18]

Engines operating on the Otto cycle are said to be four-stroke engines. An illustration of the stages of the four-stroke operating cycle is shown in Figure 4.

Another dominate type of engine cycle is the two-stroke operating cycle. The primary advantage of two-stroke engines over the four-stroke variety is their higher power output per displaced volume [16]. This is due to the two-stroke variety having one power stroke per one crankshaft revolution as opposed to the four-stroke engine having one power stroke per two crankshaft revolutions. The two-stroke cycle only consists of a compression stroke and a power or expansion stroke. An illustration of the stages of the two-stroke operating cycle is shown in Figure 5. The two-stroke engine lacks individual exhaust and intake strokes so its gas exchange processes into and out of the cylinder are more complex.

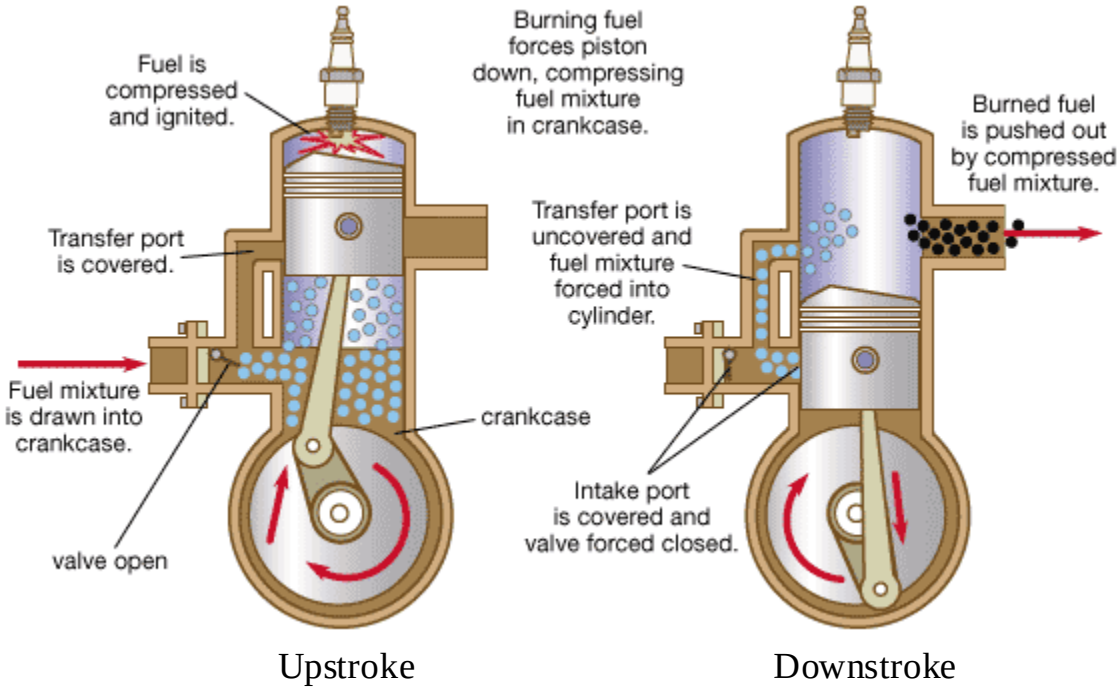

Figure 5: Two-stroke operating cycle [18]

This simplicity of design generally leads to two-stroke engines being less massive compared to four-stroke engines with similar displacement. Lacking the intake and exhaust stokes, most two-stroke engines don't have intake and exhaust valves but rather intake and exhaust ports. To achieve the required gas exchange processes a process called scavenging is used. In scavenging, a fresh fuel-air mixture is taken into the cylinder through a port in the cylinder wall and exhausts the remaining combustion products out of the cylinder through another port. By specific positioning of the ports on the cylinder wall, the traveling piston reveals and covers the intake and exhaust ports at the most appropriate time. In a crankcase scavenged SI two-stroke engine, the compression stroke closes both ports as the piston travels from BDC to TDC compressing the cylinder fuel and air content. Fresh fuel and air enters the crankcase and is pressured

there first during upward piston travel. Pressurization of the fresh charge is required so that it will have a higher pressure than that of the burnt gases from the previous cycle. This allows for effective displacement of the burnt gases. In the power stroke, the piston approaches BDC from TDC (as in the four-stroke cycle). The exhaust port is first uncovered and then the intake port is revealed during piston travel. When the intake port is uncovered, the pressurized fresh charge enters the cylinder from the crankcase and most of the burnt gas from the previous cycle is expunged through the exhaust port. Scavenging results in some of the fresh charge being directly exhausted before it is combusted, as well as leaving some of the burnt gases from the previous cycle in the cylinder. These losses are much greater in two-stroke engines compared to four-stroke engines. This results in two-stroke engines generally being less efficient than four-stroke engines.

Engines based on both two-stroke and four-stroke cycles find considerable and wide-ranging use in a variety of applications. Four-stroke engines dominate the passenger automotive vehicle landscape while, two-stroke engines have been used extensively in small portable devices such as chainsaws and lawnmowers, smaller vehicles like snowmobiles and motorcycles, and light aircraft like small RPA. The increased importance of efficiency, fuel consumption and growing interest in minimizing environmental impact by reducing engine exhaust emissions have lead to four-stroke engines becoming more common place in areas that are traditional two-stroke engine strongholds. The additional cost associated with four-stroke engine manufacture and power reduction has before limited their introduction into such areas, but the benefits now sometimes outweigh the negatives. Both engines tested for this research operate

using the four-stroke cycle. The other large classification of engines is whether the engine requires SI or CI.

3.2. Engine Gas Cycles

The SI engine's defining characteristic is the spark plug. It supplies an electrical discharge that ignites some of the fuel-air mixture. The ignition gives birth to a turbulent flame that propagates throughout the cylinder. The fundamental assumption (though not always valid) of the ideal SI engine cycle is that combustion occurs rapidly enough to effectively occur at constant volume. In addition to the gas cycle having constant volume heat addition; it is assumed heat is rejected from the system at constant volume as well. A pressure versus volume plot for the gases in an ideal SI Otto cycle is shown in Figure 6, whereas Table 1 summarizes the processes taken place over the cycle in Figure 6.

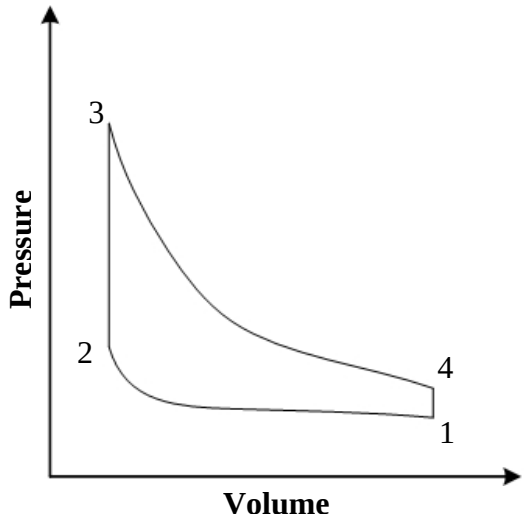

Figure 6: SI engine cycle pressure versus volume

Table 1: SI engine cycle processes [19]

Cycle Stage	Process Description
1 to 2	isentropic compression
2 to 3	constant-volume heat addition
3 to 4	isentropic expansion
4 to 1	constant-volume heat rejection

The CI engine and cycle has commonly been referred to as the Diesel engine and cycle. The ideal Diesel cycle operates with the fundamental assumption (though not always valid) that heat is added to the system (through combustion) at approximately constant pressure. This is illustrated in Figure 7. The CI engine is most distinguished from SI engines by its lack of a spark plug for ignition. It relies on spontaneous ignition of the cylinder fuel-air mixture content. This process is called auto-ignition. Diesel engines typically have higher compression ratios than that of SI engines. These higher ratios are needed to compress air in the cylinder to high enough pressures and temperatures to facilitate auto-ignition. Before the piston reaches TDC, fuel is injected into the cylinder and mixes with the compressed air. The fuel-air mixture now has a temperature and pressure above the fuel's ignition point and it auto-ignites. Auto-ignition can also occur in SI engines, but it is undesirable because the engine is not designed to handle the higher pressures and temperatures. These unfavorable detonations are commonly called knock, because of the distinctive pinging sound they generate that is audible to the human ear.

Table 2: CI engine cycle processes [19]

Cycle Stage	Process Description
1 to 2	isentropic compression
2 to 3	constant-pressure heat addition
3 to 4	isentropic expansion
4 to 1	constant-volume heat rejection

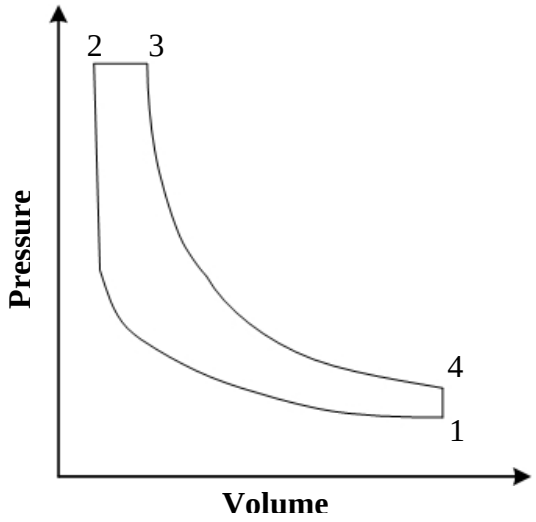

Figure 7: CI engine cycle pressure versus volume

3.3. Cylinder Configuration

SI and CI ICEs come in various cylinder configurations. Most (non-radial) engine configurations utilize one, two, three, four, five, six, eight, ten and twelve cylinders. Engine cylinder configuration impacts engine vibration and smoothness because of the consequences the configuration has on engine balance. Six and eight cylinders are often aligned in a V-shape which is well balanced and linearly compact. Six and eight cylinder engines are also commonly arranged in a linear or straight configuration. The straight cylinder arrangement provides superior balance for six cylinders but is relatively long in comparison to the V-shape configuration. Two cylinder designs are most often arranged

in a V-shape design or horizontally opposed (boxer) design while four cylinder engines are commonly in an in-line configuration. Due to the nature of the two-stroke and four-stroke work cycles, torque spikes are experienced, especially in single cylinder engines. The ICEs in consideration for use for this thesis are both single cylinder designs. The implication of single cylinder engine torque spikes on operation and testing were found to be significant. The torque spikes can damage the engine-dynamometer coupling or the dynamometer itself. In study of a small single cylinder four-stroke ICE, Wilson [20] found that vibrations from the torque spikes caused numerous couples to fail. This limited testing to engine speeds under 6000 Revolutions Per Minute (RPM). This effort will seek to find or develop a dynamometer engine couple sufficient for testing at higher engine speeds. Wilson suggested developing a method for dampening out engine test stand vibrations and using a larger coupling. The couple used by Wilson that limited testing to 6000 RPM was rated for torque 37 times that of what the test engine averaged.

3.4. Performance

Engine performance is central to this research. The two most common figures of merit are torque (T) and power (P). However, the engine performance parameters that allow for equivalent comparison between engines of varying size are *MEP* and *SFC* [16]. Mean effective pressure (MEP) is the amount of work per cycle (W_c) divided by the cylinder volume (V_d) displaced per cycle [16]. Equation 1 shows the *MEP* relation. Equation 2 shows that W_c is found by multiplying power times the number of crank revolutions for each power stroke (n_R) and then dividing by the crankshaft rotational speed (N). The crankshaft rotational speed is commonly referred to as engine speed.

$$MEP = \frac{W_c}{V_d} \quad (1)$$

$$W_c = \frac{Pn_R}{N} = T \cdot n_R 2\pi \quad (2)$$

MEP is often expressed in units of kPa or lb/in^2. *MEP* is directly related to torque. This relation is shown by substituting the expression for W_c in Equation 2 into Equation 1. Torque is the engine parameter most readily measured via a dynamometer. Engine speed is also measured in a dynamometer apparatus. Power is calculated from torque and angular speed measurements by means of Equation 3.

$$P = 2\pi NT \quad (3)$$

Power is most often expressed in units of kW and hp while torque is given in N·m and lbf·ft. An engine's output power and torque values are crucial to ensuring the engine can sufficiently supply the work demand of the desired function it is supporting. For most engine applications, how effectively the engine can deliver work is also very important.

This effectiveness in converting the chemical energy stored in fuel to useful work is described by relating fuel consumption to power output. *SFC* is the fuel mass flow ($\dot{m}_f$) rate divided by power output.

$$SFC = \frac{\dot{m}_f}{P} \quad (4)$$

SFC is given in units of g/kW·h and lbm/hp·h. To supplement *SFC*, a dimensionless parameter that links engine output to required fuel energy input was developed as a

means to better compare engines. Fuel energy refers to the energy possibly available by combustion of the supplied fuel. It is equivalent to the mass of fuel supplied to the engine per cycle (m_f) multiplied by the chemical heating value intrinsic to the fuel (Q_{HV}). The parameter is an empirical engine efficiency called fuel conversion efficiency (η_f) or thermal efficiency. The efficiency is shown in its different forms in Equation 5.

$$\eta_f = \frac{W_c}{m_f Q_{\mathrm{HV}}} = \frac{P}{\dot{m}_f Q_{\mathrm{HV}}} = \frac{1}{\mathrm{SFC}\ Q_{\mathrm{HV}}} \qquad 5$$

This efficiency parameter assumes that the fuel energy supplied to the engine is entirely converted to thermal energy. This however, is not the usual case because the assumption requires complete combustion of the fuel with air. Of vital importance to the combustion process is the ratio of air-to-fuel (*A/F*) or fuel-to-air (*F/A*) shown in Equations 6 and 7.

$$(A/F) = \frac{\dot{m}_a}{\dot{m}_f} \qquad 6$$

$$(F/A) = \frac{\dot{m}_f}{\dot{m}_a} \qquad 7$$

Even with a stoichiometric (chemically balanced) *A/F* mixture or an oxygen rich mixture 100% complete oxidation of the fuel is not achieved. This is due to the complex mechanisms involved with the hundreds of elementary reactions that occur with hydro-carbon fuel combustion [21]. Volumetric efficiency (η_v) is a parameter developed to measure and engine's ability to induct air into the cylinder. It is not used with two-stroke engines because of the cycle's lack of a discrete process for air intake. It is described by the ratio of air's volumetric flow rate into the engine ($\dot{m}_{a,i}$) by the rate of volume

displaced by the piston. Volumetric efficiency $\rho_{a,i}$ represents the ambient inlet air density and is shown in Equation 8.

$$\eta_v = \frac{2\dot{m}_{a,i}}{\rho_{a,i} V_d N} \quad (8)$$

Engine power, torque and *MEP* can be expressed in terms of the earlier introduced parameters. These relations (Equations 9 to 12) better show how and what power and torque correlate to.

$$P = \frac{MEP\ A_p \bar{S}_p}{4} \quad (\text{four} - \text{stroke cycle}) \quad (9)$$

$$P = \frac{MEP\ A_p \bar{S}_p}{2} \quad (\text{two} - \text{stroke cycle}) \quad (10)$$

$$T = \frac{MEP\ V_d}{4\pi} \quad (\text{four} - \text{stroke cycle}) \quad (11)$$

$$T = \frac{MEP\ V_d}{2\pi} \quad (\text{two} - \text{stroke cycle}) \quad (12)$$

Power is directly proportional to piston area (A_p) and mean piston speed ($\bar{S}_p$) while torque is proportional to displaced volume. Lastly, *MEP*'s relationship to these parameters is shown in Equation 13.

$$MEP = \eta_f \eta_v Q_{HV} \rho_{a,i}\ (F/A) \quad (13)$$

Performance maps that show contours of constant *SFC* are plotted on a chart of *MEP* versus engine speed, are essential for comparing engines of differing size, type and configuration. SI and CI engines operating two-stroke and four-stroke cycles often have minimal fuel consumption at roughly 60% of the maximum engine speed and 60% of maximum *MEP* [19]. Performance maps enable viewing an engine's performance characteristics throughout its entire loading and speed range possible. Examples of performance maps are shown in Figure 8.

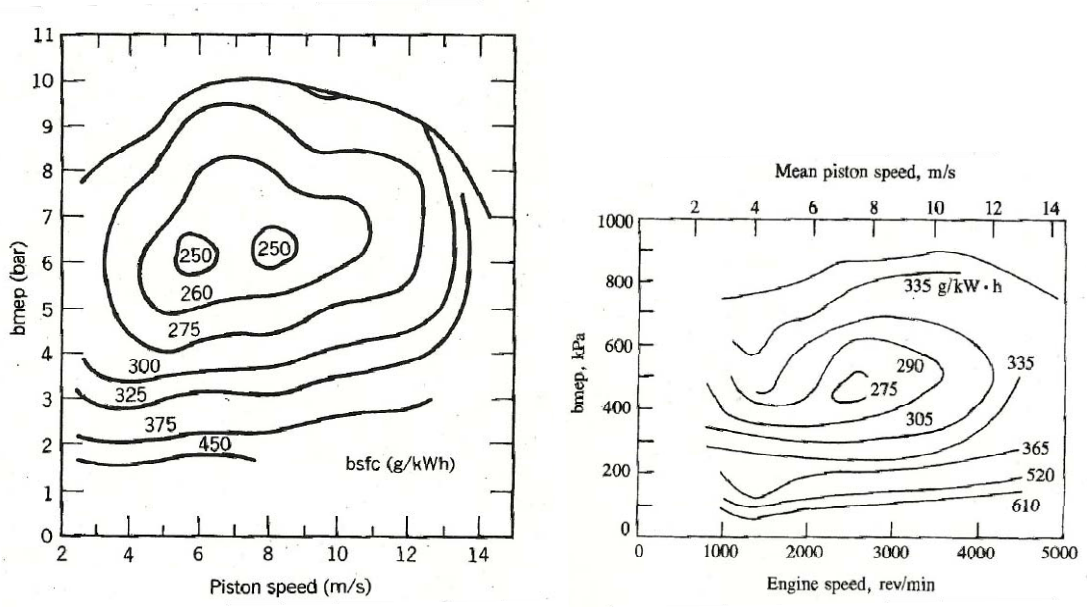

a.) b.)

Figure 8: Engine performance map examples (a.) [19] (b.) [16]

The contours of constant *SFC* create islands of efficiency on the map that clearly show at what speed and load the engine should be operated at to minimize *SFC* and maximize efficiency. Two secondary but important parameters for engine comparison are engine specific power and engine specific volume shown in Equations 14 and 15 respectively.

$$\text{specific power} = \frac{\text{engine weight}}{\text{rated power}} \quad (14)$$

$$\text{specific volume} = \frac{\text{engine volume}}{\text{rated power}} \quad (15)$$

Proper comparison requires consistency in the development of engine weight and volume. What components and secondary items are considered as the engine must be unvarying. One of the two-stroke engine's qualities is its superior specific weight to that of the four-stroke engine. Two-stroke engines generally weigh less because they are less complex than four-stroke engines.

3.5. Predictive Modeling

The testing of engines to determine performance parameters is time consuming. Considerable effort by researchers and industry has been put forth into modeling real engine operation. Developing accurate models is quite involved and challenging because of the complex and numerous processes involved in an ICE. Models hope to predict engine behavior over a wide range of operating conditions and variables. This allows for evaluating engine concepts and designs without the effort and cost associated with actually building and testing a design. Predicting engine performance from fundamental governing equations alone is quite daunting and most models developed have more limited objectives [16]. More commonly, models have been developed to predict the separate processes in ICES relating to friction, heat transfer, fluid flow, chemical kinetics, combustion and turbulence. For example the computer software programs CHEMKIN and Cantera have been developed to model chemical kinetics and related combustion

processes in reacting flows. Increased computing power has allowed for advances in modeling techniques and approaches.

Artificial neural-network models are being used to predict engine performance parameters and to also model individual engine processes. The networks develop a mathematical function that is composed from different input functions. For input, the neural-network approach requires a number of experimentally found data points of the parameters of interest. In one study [22], a neural-network model was developed to predict the output power of a two-stroke SI engine. A conventional simulation model to predict power was developed using simplified ideal relations with many assumptions. This power was used as one input into the neural network model. The model also used experimentally found data points of power and SFC as functions of measured *A/F* ratio, engine speed and throttle position. *A/F* ratio, engine speed and throttle position were thus used as input neurons. Using machine training and learning rules, the neural-network model sought to minimize the error between the model's power prediction and the experimental values of power. This hybrid model approach produces predictions with decent accuracy and the study suggests the model could be used to predict power for different engines of similar displacement. The model's reliance on experimental data and the variance in engine design, materials and quality could inject significant error however.

Recently, Menon et al. [23] have looked at the performance of small ICEs due in large part to their increased use and value in small RPA. The study sought to generate a numerical model of a small ICE to examine the factors limiting small engine performance. The model was generated by solving a set of governing equations

(conservation of energy, mass and species) for the non-combustion portions of the engine cycle. For this two-stroke engine model, a complete mixing scavenging model was assumed in which fresh charge instantly mixes with the remaining charge (burned gas products) in the cylinder to form a uniform mixture. Models for heat loss and friction loss were also incorporated. Combustion and gas mixture composition was modeled using the computer software tool CANTERA. Two sets of ordinary differential equations (ODEs) were formed and solved for numerically using various solvers in MATLAB. From these solutions, engine performance parameters were solved for by first calculating work using the 1st Law of Thermodynamics. Experimentally, engine performance data was measured using an in-house developed dynamometer. The two-stroke engine specifically looked at was a AP Engines manufactured Yellowjacket glow-plug two-stroke engine with 2.83 cm^3 of displacement. Simulation results were then compared to performance data calculated from experimental measurements. Plots of efficiency and power versus engine speed showed the results did not compare well. A suggested reason for error is the scalability of the heat and friction loss models to engines with very small displacements.

Presently, models that can accurately predict performance parameters of small displacement ICEs are immature. The complex nature of the processes involved in ICE operation make creating an all-inclusive model to predict engine MEP and SFC quite challenging. Though modeling provides significant advantages to propulsion system designers and developers, full scale engine testing remains the best approach for creating engine performance maps.

4. Fuels

Both SI and CI engines require fuels to feed the combustion processes that ultimately lead to the generation of useful work. Commonly SI engines use gasoline and CI engines use Diesel fuel. Kerosene fuel is the main ingredient of jet fuels primarily used in jet turbine engines that power many large aircraft. The fundamental characteristics of these fuels, their origin and composition and their use in combustion engines are presented here.

4.1. Crude Oil

Petroleum (or crude oil) is the general term for the naturally occurring hydro-carbon mixtures found on earth [24]. The elemental composition of petroleum is mainly carbon, hydrogen, nitrogen, oxygen and sulfur. The ranges of the proportions of the elements comprising petroleum are summarized in Table 3.

Table 3: Elements in petroleum

Element	% Mass Present
Carbon	83.0-87.0
Hydrogen	10.0-14.0
Nitrogen	0.1-2.0
Oxygen	0.05-1.58
Sulfur	0.05-6.0

Other elements and minerals present in crude oil are nickel, vanadium and iron. These metals exist in very small quantities in petroleum, mostly measured in tens to hundreds of parts per million. Though these metallic elements are only present in small concentrations, they can have significant negative effects on refinery and distillation operations and equipment.

The exact composition of crude oils from different sources varies. The components of a particular crude oil mixture and its properties depend on many factors including location, age and type of organic source material. Carbon and hydrogen are the bulk of the material in crude oil. These two elements bond together and form molecules commonly referred to as hydro-carbons. The basic formula for a hydro-carbon follows the form of Equation 16.

$$C_x H_y \qquad 16$$

Carbon number refers to the number of carbon atoms present in the hydro-carbon molecule [25]. In Equation 16, the carbon number value is represented by *x*. The simple formula in Equation 16 may dangerously mislead one to assume hydro-carbon structure is simple, while usually the contrary is more accurate. Hydro-carbons are structured in various chains and rings of different ratios, design and chemical bonds.

There are thousands of different ways hydrogen atoms and carbon atoms can combine to form hydro-carbons. When a hydro-carbon molecule has all carbon-carbon single bonds it is referred to as saturated because it contains the maximum possible number of hydrogen atoms [26]. An unsaturated hydro-carbon has at least one double or triple carbon-carbon bond present. The single carbon-carbon bonds in saturated hydro-carbons generally tend toward exhibiting molecular stability; whereas the double and triple carbon-carbon bonds in unsaturated hydro-carbons tend to exhibit molecular instability. Stability is important because the more molecularly stable the hydro-carbon, the more difficult it usually is to refine. Another important characteristic of hydro-carbon structure is whether carbon atoms form chain or ring-shaped molecules. Similar types of hydro-carbons are grouped together in main categories. The similarities include

hydrogen to carbon atomic ratio and bonding structure. The major classes include paraffins (alkanes), naphthenes (cyclanes) and aromatics. Olefins (alkenes) and acetylenes (alkynes) are sometimes present in crude oil but are usually rare. In general, paraffins are saturated hydro-carbons with no ring structure (only having straight or branched chains). Naphthene hydro-carbons are saturated as well but contain at least one ring structure. Hydro-carbons classified as aromatics are unsaturated and contain ring structures [24]. The classic example of an aromatic hydro-carbon is C_6H_6 (Benzene). Concerning a naming custom, saturated hydro-carbons (paraffins and naphthenes) have names ending with *ane* while unsaturated hydro-carbons (aromatics and olefins) have names ending with *ene*.

Crude oils are often qualitatively classified by the amount of paraffins, naphthenes and aromatics it contains. This led to a naming convention of describing a particular crude oil as naphthenic or paraffinic crude oil [26]. The concentration of these different groups of hydro-carbons in a crude oil is central to how processing and refining is conducted and dictates the amount and type of petroleum products that can be produced.

4.2. Petroleum Products as Fuels for Combustion

Through different processes (mainly distillation), petroleum feedstock is refined to create a wide range of useful products. Thermal separation physically divides crude oil into different groups of hydro-carbons from which products including lubricants, waxes, asphalt, solvents, and fuels are obtained. The separated groups of hydro-carbons are called straight-run distillation fractions and are stratified based on boiling temperature range. The group with the lowest boiling temperature range (-160°C to 0°C) contains gases with carbon numbers of one through four. Vapor recovery units capture the gases

which include CH_4 (methane), C_2H_6 (ethane), C_3H_8 (propane) and C_4H_{10} (*n*-butane). The light straight run gasoline distillate has the next highest boiling temperature range (25°C to 90°C) and contains hydro-carbons with five to six carbon atoms. Light straight run gasoline can often be mixed directly into the final gasoline blend [26]. Heavy straight-run naphtha is next with a boiling range of 85°C to 190°C and having carbon numbers between six and ten. The next distillate is kerosene with a boiling range of 160°C to 275°C and carbon number ranging from nine to fifteen. The remaining distillates include light and heavy atmospheric gas oils (boiling range of 250°C to 340°C and 315°C to 410°C respectively). Light and heavy vacuum gas oils have the highest boiling point range from 370°C to 575°C and high carbon numbers ranging from 22 to 45. The remaining crude oil is called residuum and can't be further distilled without causing destruction of hydro-carbons because of extreme heating. Some of the residuum material is used to form asphalt.

After distillation, further refining processes are used to extract more products from petroleum and improve quality by removing impurities. Catalytic cracking is one such process and is used to withdraw additional gasoline not originally present in crude oil. The cracking process causes heavier fractions of petroleum to degrade into smaller hydro-carbon molecules falling in the gasoline range. Also, the chemical products derived from petroleum product intermediates (commonly called petrochemicals) are extremely useful. Some examples of petrochemicals include adhesives, polymers, gels, plastics and resins.

Of concern to this effort are the products derived from petroleum that are utilized as fuel for combustion engines that power aircraft. Three major refinery products used as

popular fuels are gasoline, diesel and kerosene. Gasoline is the dominate fuel used in SI ICEs, while diesel fuel is predominately used in CI ICEs. Kerosene is the basis for jet fuels which are used in gas-turbine engines.

4.3. Gasoline

Gasoline is a mixture of hundreds of different hydro-carbon molecules. The composition of gasoline varies depending on the crude oil source and refining process. Gasoline is composed of hydro-carbons having carbon numbers between four and fourteen. The average properties of gasoline are most similar to that of C_8H_{18} (iso-octane). Hydro-carbons with carbon numbers of three or lower (CH_4, methane; C_3H_8, propane; etc.) are too volatile to be blended in as component of gasoline. Conversely, hydro-carbons with carbon numbers of fifteen and higher are too heavy and non-volatile to be used in gasoline mixtures. Gasoline is the fuel of choice for passenger automobiles using SI ICEs. Its high volatility allows for easy carburetion and good ignition properties in varying environmental conditions. Gasoline dominates the refining of crude oil. If ICE cylinder compression ratios are too high the problem of engine knock can be experienced which is described later.

4.4. Diesel

Diesel fuel is a blend of light to middle distillate fuels. A typical diesel fuel mixture has the average hydro-carbon structure of $C_{10.8}H_{18.7}$. The fraction of petroleum distillation between gasoline and kerosene is the primary component of diesel fuel and is sometimes called gas oil. Diesel fuel exhibits less volatility than gasoline, but more volatility than kerosene. Originally, diesel fuel found most use in the large, slow and heavy CI engines used in railroad, marine, industrial and heavy-construction equipment

applications. The largest barrier to diesel fuel use in smaller CI engines with greater engine rotational speeds was how to effectively deliver a combustion ready fuel charge to the engine cylinder. Carburetors were insufficient because of the low volatility of diesel fuel. The solution came in the form of fuel injection.

4.5. Kerosene

Kerosene is a fuel made up from crude oil fractions that exhibit boiling between temperatures of 150°C to 300°C. Properties of kerosene on average closely relate to that of $C_{13}H_{25.5}$. Kerosene fuel is largely consumed by gas-turbine engines used in large aircraft. Kerosene has low volatility which aids in fuel storage safety but can impede engine startup and low temperature engine operation. The wide range of operating conditions for large aircraft challenge the ability of kerosene based jet fuels to achieve proper combustion.

4.6. Octane Rating

A major property of fuels for use in combustion engines is octane number (ON). The ON of a fuel for the layman has come to be a general indicator of fuel quality but it is really a parameter used to evaluate the fuel's performance in two specific tests. Auto-ignition or knock in SI ICEs is an undesirable and abnormal combustion event that occurs within the cylinder. Engine knock happens when the fuel-air mixture detonates instead of achieving uniform combustion (deflagration) initiated by a spark. Detonation involves supersonic combustion and is characterized by a shock wave that propagates through the cylinder and causes a distinctive knocking sound. Detonation usually results in cylinder pressures higher than the engine was designed to withstand which is why knocking is often damaging to engine components. Engine knocking is also associated with losses in

efficiency. CI ICEs are designed to purposely operate with detonation in the cylinder and have cylinders devised to handle the resulting higher pressures. The causes of engine knock are related to engine design, environment and fuel characteristic. To relate the occurrence of knock to actual fuel types the ON was created. Octane number characterizes various fuels' resistance to exhibit engine knock in ICEs. The higher the ON, the less likely the fuel is to experience engine knock [27]. A fuel must be tested to establish its octane rating.

Two testing methods were developed to determine the ON of a fuel. The two methods of testing are the Research Octane Number (RON) and the Motor Octane Number (MON). Both methods test a fuel at specific operating conditions, with MON testing conditions being more severe. RON testing uses an inlet mixture temperature of 52°C and engine speed of 600 RPM. MON testing uses an inlet mixture temperature of 149°C and engine speed of 900 RPM [27].

A single cylinder SI engine designed by the Cooperative Fuel Research Committee (now Coordinating Research Council, Inc.) is used for testing. The engine has the ability to vary compression ratio from three to 30. The octane rating scale uses C_7H_{16} (*n*-heptane) and C_8H_{18} (iso-octane) as its two reference fuels. The two fuels have volatility properties that are reasonably similar, as show in Table 4.

Table 4: Reference fuels for octane rating

Fuel Name	Formula	Melting Point (°C)	Boiling Point (°C)	Density (g/mL)	Heat of Vaporization (MJ/kg)
n-heptane	C_7H_{16}	-90.70	98.4	0.6840	0.365 at 25°C
iso-octane	C_8H_{18}	-107.45	99.3	0.6919	0.308 at 25°C

The lower end of the scale is defined as the knocking characteristic exhibited by testing *n*-heptane and the ON is labeled zero. The upper end of the scale uses iso-octane and its ON is defined as 100. An electronic knock meter placed in the cylinder head is used to quantitatively measure knock. To determine ON the fuel of interest is tested using either the RON or MON methods or both. A mixture of specific amounts of the reference fuels *n*-heptane and iso-octane is formed and tested to attempt to match the knocking data recorded initially for the fuel of interest. Once the knocking data is closely matched, the amount (percentage by volume) of iso-octane in the blend is the ON assigned to the fuel of interest. Thus, if the matching blend is 90% iso-octane by volume, the octane number is 90. In the United States of America, the mean of the *RON* and *MON* values is used to describe fuel resistance to engine knock and is called the antiknock index. The relationship is shown in Equation 17.

$$antiknock\ index = \frac{RON + MON}{2} \qquad 17$$

Octane number is not primarily related to the energy content of a fuel [26]. Correlations attempting to relate ON to energy content are often confusing and misleading, especially when considering both the energy density and the specific energy of fuels. Ultimately, energy content is only a function of the molecules present in the fuel mixture. However, in engines, transferring chemical energy (in chemical bonds) to heat energy and finally to mechanical energy is a matter of combustion.

4.7. Combustion and Volatility

Combustion is the rapid oxidation of a chemical resulting in the release of heat or light or both [21]. The basic reactants in combustion are a fuel and an oxidizer. A

stoichiometric combustion process involves the precisely necessary amount of oxidizer reacting with fuel resulting in complete combustion of the reactants. Complete hydro-carbon combustion has all the reactant carbon and reactant hydrogen formed into CO_2 and H_2O as products. If the amount of oxidizer present in the reaction is less than stoichiometric, the result is incomplete combustion with un-reacting excess fuel essentially becoming a product. This scenario is said to be fuel rich. In the opposite scenario, where more than the stoichiometric amount of oxidizer is present, the reaction is said to be fuel lean. The true combustion reaction of hydro-carbons with air as the oxidizer involves hundreds of intermediate reactions and many different products. Evaluating these reactions is most accurately done using a computer program to calculate chemical equilibrium reactions and analyze chemical kinetics, like the National Aeronautics and Space Administration's Chemical Equilibrium with Applications (CEA) program, CHEMKIN and Cantera. The simplified general reaction (global reaction) is a helpful illustration of the net effects of combustion. Hydro-carbon combustion with atmospheric air and only carbon dioxide, water and nitrogen as products follows the formula in Equation 18.

$$C_xH_y + a(O_2 + 3.76N_2) \rightarrow xCO_2 + (y/2)H_2O + 3.76aN_2 \quad [21]\ (2.30) \qquad 18$$

where

$$a = x + (y/4) \quad [21]\ (2.31) \qquad 19$$

Air is a composition of oxygen, nitrogen, argon, water vapor and carbon dioxide and other elements and molecules. Since oxygen and nitrogen are the dominant components of air, the composition of air is assumed to be solely oxygen and nitrogen in concentrations of 21% and 79% by volume. This equates to 3.76 moles of N_2 for every 1

mole of O_2 in air. Actual combustion is incomplete and products such as CO, NO, NO_2 and soot are also formed. For iso-octane, the balanced stoichiometric global reaction is shown by Equation 20.

$$C_8H_{18} + 12.5(O_2 + 3.76N_2) \rightarrow 8CO_2 + 9H_2O + 12.5(3.76N_2) \quad 20$$

The heat energy content released by the reaction is called the enthalpy of reaction (ΔH_R) or enthalpy of combustion. This change in specific enthalpy (Δh_R) is measured in kJ/kg_{fuel} and is found by subtracting the specific enthalpy of the reactants from that of the products and is summarized in Equation 21. The molecular weight of fuel is denoted by MW_f.

$$\frac{\Delta H_R}{MW_f} = \Delta h_R = -\Delta h_c = h_{prod} - h_{react} \quad 21$$

The heat of combustion (Δh_c) is equivalent to the enthalpy of combustion in magnitude but opposite in sign. Heat of combustion values were determined using the CEA program for C_8H_{18} (iso-octane) and Jet-A (civil equivalent of JP-8) kerosene based jet fuel. The results of these calculations are shown in Table 5. Complete calculation data can be found in Appendix A.

Table 5: Combustion equilibrium reaction calculations

Fuel Name	Heat of Formation (kJ/kmol)	Lower Heating Value (kJ/kg)	Specific Heat of Combustion, (kJ/kg_{mix})	Specific Heat of Combustion, (kJ/kg_f)
Jet-A ($C_{12}H_{23}$)	-303,403	44,316	-119.79	-35,271
iso-octane (C_8H_{18})	-259,160	44,791	-144.71	-41,151

Diesel fuel combustion calculations were not conducted because the fuel was unavailable in the CEA database of reactants. The calculation shows that for complete combustion iso-octane releases more heat per mass than Jet-A (kerosene). Fuels are not ideally combusted however. For this effort, the combustion of fuels in ICEs is of interest. Combustion in SI ICEs requires fuel be vaporized (or at least atomized) to achieve proper combustion. Volatility represents a fuel's vaporization properties.

Fuel volatility is described by a fuel's boiling temperature range and vapor pressure properties. Vapor pressure is the measure of the amount of pressure a fuel exerts at a certain temperature. Flash point temperature is a measure also used to examine fuel volatility. It defines the minimum temperature where a fuel-air mixture becomes flammable. Flammability limits are measured as the flash point on the low end (not enough fuel vapor for ignition) and a fuel rich flammability limit on the high end (not enough air or oxidizer for ignition). In ICEs high volatility is favored in fuels because it allows for easier ignition and shorter more stable flame propagation. Contrarily, higher volatility makes fuel handling more difficult. More care must be taken in properly venting fuel tanks to prevent dangerous rises in tank pressure. In general, a fuel's boiling point represents the point at which its vapor pressure achieves atmospheric pressure. This permits boiling or the vaporization of the fuel. As relative density increases in fuels, boiling point temperature increases; thus, as fuels increase in density they usually have lower volatility. Heavy fuels like diesel and kerosene are less volatile than gasoline. Kerosene, diesel and gasoline fuels have different knock, volatility and combustion properties. They are each well suited for primary use in their specific engine and combustion type. It is predicted using kerosene and diesel fuel in a SI ICE designed for

gasoline fuel will result in reduced engine performance in terms of fuel consumption, efficiency and power.

4.8. Heavy Fuels Effect on ICE Performance

Performance of an SI ICE using different fuels was examined by research done by M.S. Shehata [28]. The fuels tested were gasoline ($C_{8.26}H_{15.5}$), kerosene ($C_{12}H_{26}$) and Liquefied Petroleum Gas (LPG). LPG was 93% propane (C_3H_8) by mass and the remaining mixture was made up of ethane (C_2H_6), propene or propylene (C_3H_6) and butane (C_4H_{10}). Actual cylinder pressure was measured and compared to reconstructed cylinder pressure values using Fast Fourier Transforms. Engine performance parameters of MEP and SFC were calculated using equations from Heywood [27] and measured values of cylinder pressure. These parameters were plotted versus crank angle. Rotational engine speeds where data between the fuels was compared were 1588 RPM for gasoline, 1549 RPM for kerosene and 1535 RPM for LPG.

It was found that the net heat release of gasoline was higher than that of kerosene (which agrees with the rough CEA calculations done earlier). The peak net heat release of LPG was higher than kerosene but less than gasoline. Peak cylinder pressure was highest in kerosene, then gasoline and then LPG. Peak cylinder pressure location didn't correspond to the location of peak net heat release. Exhaust gas temperature was plotted versus crank angle and showed gasoline to have the higher values over LPG over the entire range of crank angle. Torque and exhaust gas temperature data was taken for the different fuels and wide open throttle. The highest peak torque was achieved by LPG, followed by gasoline and then kerosene. Exhaust gas temperature of kerosene was higher than gasoline and LPG at crank locations corresponding to the time before the beginning

of combustion. Table 6 summarizes how the parameters measured compare amongst the different fuels.

Table 6: Measured performance parameters of different fuels

Fuel	Peak Cylinder Pressure (kPa)	Peak Net Heat Release (J/deg)	Peak Exhaust Gas Temperature (K)	Torque (N·m)
Gasoline	4200	53	1880	800
Kerosene	4500	37	1600	560
LPG	3200	47	1820	1040

How the different parameters relate to each other is difficult to ascertain because it is not intuitive. It was believed parameters would trend in a like manner or be inversely proportional. Properties of duration of combustion and specific heat ratio variance was investigated by the researcher as well, but was not seen as applicable to the focus of this effort. Unfortunately SFC, MEP and efficiency parameters were only presented for gasoline so no comparison is drawn between the fuels concerning performance in these areas. Comparisons of these parameters may clear up the trends amongst the interrelations.

Based on the research, developing a model to accurately predict small ICE performance was seen as out of reach, especially in the available time for this effort. The research also showed that running SI ICEs on Diesel and JP-8 fuel would be difficult and create a number of hurdles. Testing the ICEs on heavy-fuels remained a secondary objective of this effort. The research gained from literature reinforced the necessity of engine testing to produce engine performance maps. Next, the main objectives of this effort were attacked by establishing a methodology.

III. Methodology

1. Chapter Overview

This chapter discusses the design and development of the various components of the dynamometer test stand utilized to test the engines for this effort. The dynamometer test stand parts include the test stand, mounting hardware, dynamometer, data acquisition computer, data harness, instruments and sensors, fuel delivery hardware, ventilation system, safety shield, throttle control and engine starting equipment. Also, this chapter details the experimental methods used for the engine testing conducted.

2. Dynamometer Test Stand

For this effort and future small engine testing a commercial off-the-shelf (COTS) dynamometer was purchased. The dynamometer purchased was a DYNOmite™ dynamometer system from Land and Sea, Inc. who manufacture customized engine or chassis dynamometer systems for car, truck, motorcycle, snowmobile and watercraft dynamometer testing. The dynamometer purchased (Figure 9) was a DYNOmite™ Mini Eddy Dyno 96v. This dynamometer was capable of testing small ICEs and EMs that produce up to three horsepower. A 96 V direct current eddy-current absorber was used by the dynamometer as a brake to load the engine. A reaction cradle was incorporated into the dynamometer and a linkage attached the cradle to a 25 pound load cell. Engines were mounted to the cradle and their engine shafts coupled to the absorber via a belt pulley and gears for testing purposes in this effort.

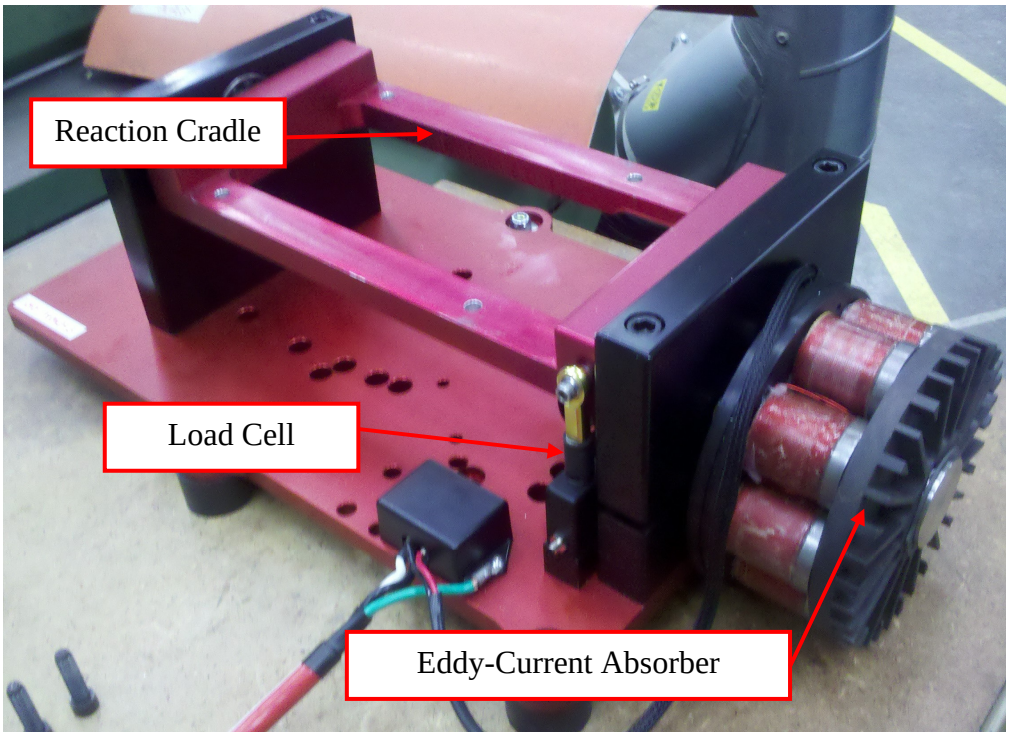

Figure 9: DYNOmite™ Mini Eddy Dyno 96 V dynamometer

Data were transmitted from the dynamometer to the DYNOmite™-Pro Data Computer and Controller (Figure 10) via a 28 channel harness. The harness was capable of passing engine RPM, absorber RPM, torque, exhaust gas temperature, fuel flow, air flow and other data from the dynamometer system. Also, DYNO-MAX 2010 Pro Software (Version 10.10) was supplied with the dynamometer for data recording and analysis of data fed from the data computer and controller via a universal serial bus cable. The software was installed on a desktop personal computer (PC) running the Microsoft Windows XP® operating system. Software features are discussed in a subsequent section.

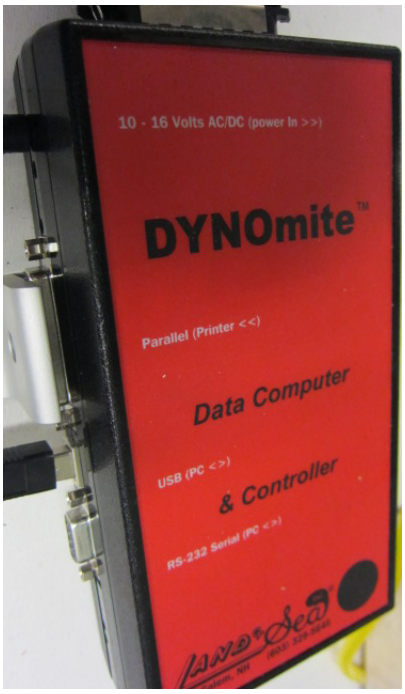

Figure 10: DYNOmite™ data computer and controller

With the dynamometer procured, a testing stand was required to house the dynamometer system. No suitable test stand was available so a test stand was designed and built. The basic design called for a table like structure with an open frame for mounting the dynamometer as well as a solid table surface for mounting sensors and control equipment. The test stand was assembled from T-slotted aluminum framing from 80/20 Inc. Polycarbonate panels were used to form an enclosure surrounding the dynamometer on four sides for safety during operation as well as help contain exhaust. Engine exhaust was directed outside the laboratory via a fan and ducting implanted through the polycarbonate rear panel. No panel was placed beneath the dynamometer. One side was left open to give control and fuel lines access to the dynamometer. The dynamometer test stand is shown in Figure 11.

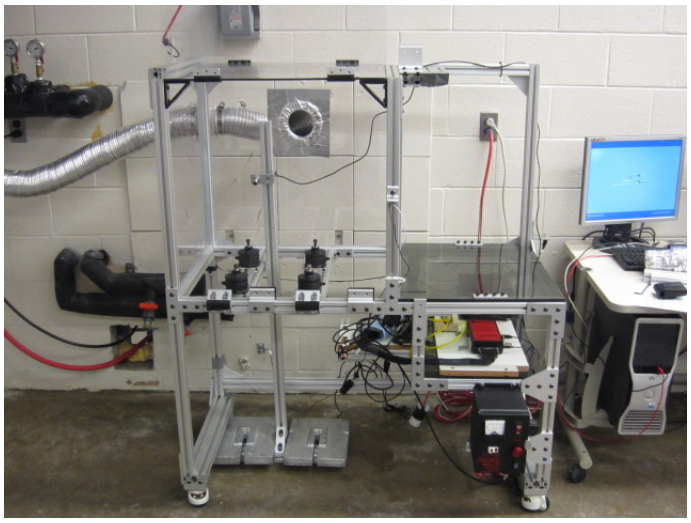

Figure 11: HE-RPA dynamometer test stand

The dynamometer itself was bolt mounted to four air filled shock-absorber (Figure 12). The shock-absorbers allowed for leveling the dynamometer and more importantly, helped limit the transfer of vibration to the rest of the test stand.

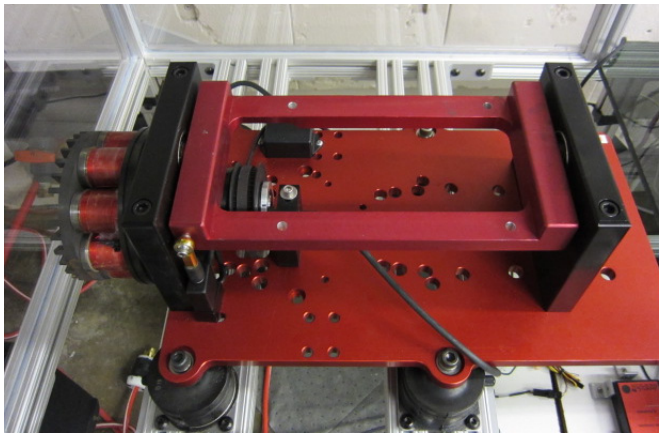

Figure 12: Dynamometer mounted to the test stand

3. Engines

The work of Hiserote [10] showed that for the HE-RPA design it was best to size the ICE for the cruise segment of a nominal ISR mission and the EM for the endurance segment of the same mission. The cruise segment required that the ICE generate roughly 265.7 W (0.356 hp) of power [10]. With this information, two COTS engines providing power in the required range were selected for testing. The engines were the Honda GX35 (Honda) four-stroke spark ignition (SI) engine [29] with a displacement of 35.8 cm^3 and the Fuji-IMVAC BF-25EI (Fuji) four-stroke SI engine [30] [31] with a displacement of 24.5 cm^3. Peak power of the Honda engine was manufacturer rated for 1.3 hp @ 7000 RPM and peak power of the Fuji was manufacturer rated for 1.6 hp @ 7500 RPM. Both engines are small single cylinder designs using a carburetor to meter fuel and are intended for use with gasoline only. Also, more manufacturer engine specifications are listed in Table 7 for easy comparison.

Table 7: ICE manufacturer's specifications

	Honda GX35	Fuji-IMVAC BF-25EI
Displacement (cm^3)	35.8	24.5
Mass* (kg)	2.700	1.770
Height x Width (mm)	230 x 204	190.5 x 165
Bore x Stroke (mm)	39 x 30	24 x 24
Peak Power (kW)	0.97 @ 7000 RPM	1.19 @ 7500 RPM
Peak Power (hp)	1.3 @ 7000 RPM	1.6 @ 7500 RPM
Peak Torque (N·m)	1.6 @ 5500 RPM	1.37 @ 5000 RPM
Peak Torque (lbf·ft)	1.18 @ 5500 RPM	1.01 @ 5000 RPM

* measured dry mass (i.e. no oil in engine)

Images of both engines are shown in Figure 13 and Figure 14.

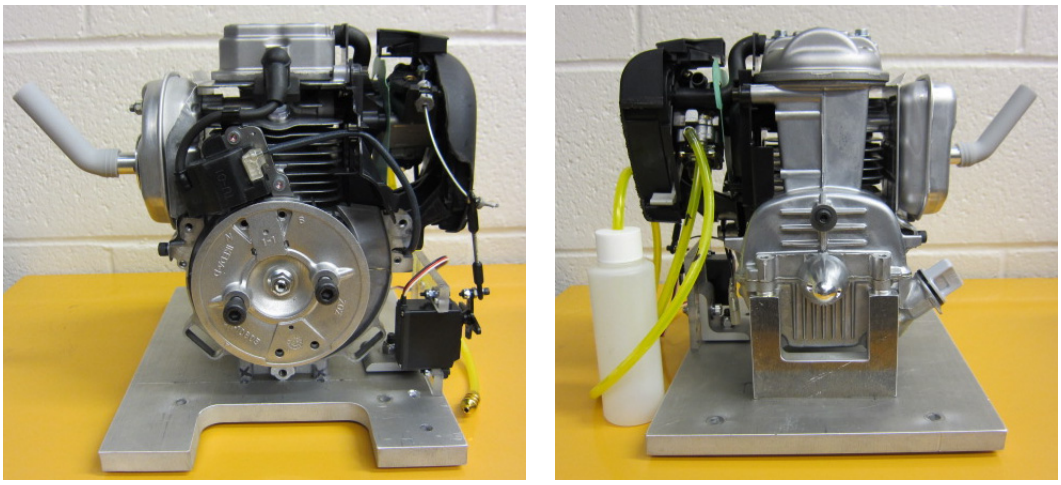

(a.) (b.)

Figure 13: Honda GX35 (a.) front view (b.) rear view

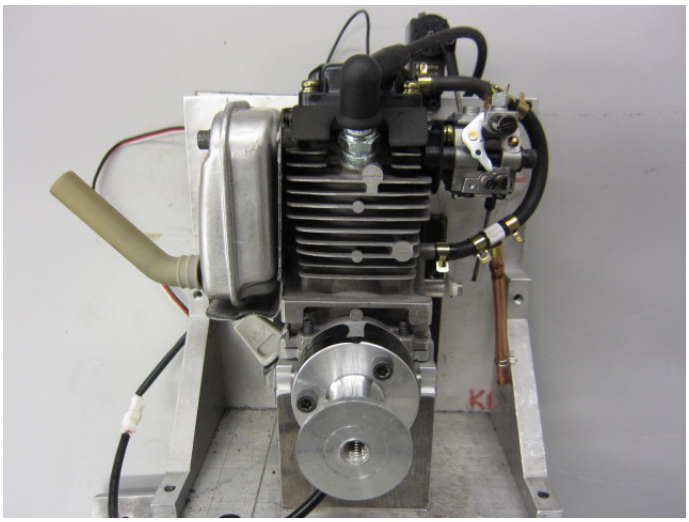

Figure 14: Fuji-IMVAC BF-25EI

One of the motivations for this research was that, currently, many of the manufacturers of small ICEs in use in hobbyist R/C controlled model aircraft have

inaccurate and at times, inflated figures for claimed power and torque. Also, the author was unable to find any manufacturer supplied data concerning SFC. This was not found to be unusual, since SFC is not usually important to hobbyists or users of lawn mowers, weed-whackers and other small gas powered machinery in which these engines are predominately used. The author expected the power and torque claims for the Honda to correspond well with the power and torque results from dynamometer testing. This expectation was founded, for the Honda, by the statement that the manufacturer tested the model in accordance with the Society of Automotive Engineers (SAE) J1349 Standard. This standard titled *Engine Power Test Code - Spark Ignition and Compression Ignition – Net Power Rating* establishes a method for dynamometer testing to resolve loaded engine power [32]. Engine manufacturers use this standard so that level comparisons of engine power rating can be made across different engine designs, sizes, models and manufacturers. The net torque and net power versus engine speed plots shown in Figure 15 were supplied by Honda and were presumably from engine testing following the SAE J1349 Standard.

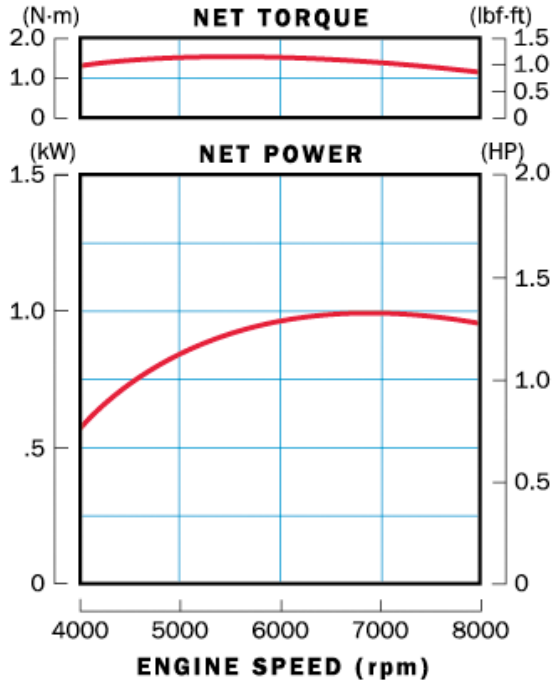

Figure 15: Honda GX35 manufacturer's supplied torque and power chart [29]

Fuji-IMVAC made no mention of the testing method conducted to produce net power output numbers. For this reason and the test results of Wilson's work testing the larger Fuji-IMVAC BF-34EI [20], it was suspected that the smaller Fuji (tested in this effort) would have tested power output figures less than the manufacturer's claims. As can be seen in Table 7, Fuji-IMVAC claims a higher power output for its 25 cm^3 engine over the larger Honda 35 cm^3 engine.

For incorporation into the small RPA, a critical parameter of engine performance is the engine specific power which is more commonly called power to weight ratio. The formula for specific power was shown earlier in Chapter II.3.4 and the inverse relation is shown here as Equation 22.

$$\text{power to weight ratio} = \frac{\text{rated power}}{\text{engine weight/mass}} \qquad 22$$

A comparison of the power-to-weight ratios of the two engines using their claimed peak power ratings was done. The results are shown in Table 8.

Table 8: Claimed ICE specific power

	Honda GX35	Fuji-IMVAC BF-25EI
Peak Power (kW)	0.97 @ 7000 RPM	1.19 @ 7500 RPM
Mass (kg)	2.700	1.965*
Specific Power (kW/kg)	0.36	0.61

*This mass of the Fuji engine includes the electronic ignition module mass

A power to weight ratio of 1.23 kW/kg (0.75 hp/lbm) was used by Hiserote for sizing of the ICE during the conceptual design of a small RPA with a HEPS [10]. This power to weight ratio more closely mimics the average value a 2-stroke engine would exhibit. The claimed specific power of both these 4-stroke engines is less than half of the proposed design power-to-weight ratio. Also, the Fuji has a claimed specific power rating nearly double that of the Honda engine. If the specific power measurements were validated through testing and thereby remained consistent with manufacturer's claims, the Fuji would clearly have a weight benefit over the Honda for use in the HEPS of the small RPA prototype.

4. Fuel Delivery System, Hardware and Sensors

A 1480 cm^3 gasoline fuel tank was mounted to a platform above the dynamometer test stand. Two brass tubes were mounted through a stop in the fuel tank. One tube was used as a vent, while the other fed fuel to the engine. Fuel was first drawn through a fuel filter pick-up placed in the fuel tank and then a second hobbyist in-line fuel filter. Fuel passed through a fuel flow sensor next that measured fuel flow. The fuel flow sensor was

provided by Land and Sea, Inc., and it accompanied the dynamometer package. The fuel flow sensor was an Omniflo® Turbine Flow-meter made by Flow Technology™. The flow-meter was a tangential flow transducer capable of accurately measuring low fluid flows by using a tangential rotor design coupled with a precision pivot sapphire bearing. The flow-meter is shown in Figure 16.

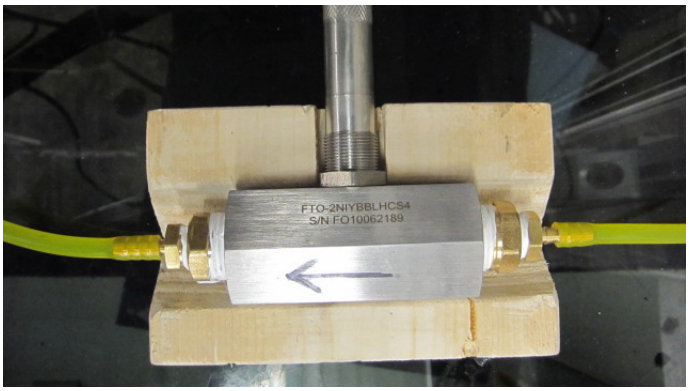

Figure 16: Flow Technology™ fuel flow-meter

The turbine's rotor rotation (caused by passage of a flow) was sensed by a modulated carrier pickoff that then relayed a proportional electrical frequency output to the dynamometer. The unit used in this research was factory calibrated to measure flows in a range of 0.18 gal/hr to12 gal/hr. This range approximately corresponded to a capability of measuring gasoline fuel mass flow in the range of 1.09 lbm/hr to 57.6 lbm/hr. Lastly the fuel exited the fuel flow-meter and went through a final hobbyist fuel filter before entering the engine carburetor.

Designs for various flanges and engine mounts were drawn and then submitted to the Air Force Institute of Technology's (AFIT) Fabrication and Model Shop where they were fashioned. These parts were used to mount sprockets to the engine shaft as well as mount

the engine to the reaction cradle. Drawings of the various plates and mounts are included in Appendix B.

All ICEs were tested using factory spark timing. Sparking was initiated by a magneto on the Honda engine and by a battery powered electronic spark ignition module on the Fuji. Precise and remote throttle operation was desirable for increased flexibility concerning engine testing. To operate the throttle and choke valves of the engines, electronic servomechanisms (servos) were used. These servos used had components that included a body and a rotating wheel. One end of a cable or threaded metal shaft was physically attached to a specific location on the servo wheel and the other end attached to the throttle or choke lever on the engine. A battery-powered controller was used to dictate the servo's motion. The unit used for control was a MT-1 R/C Multiple Tester made by Grand Wing System U.S.A. Inc [33]. The controller is shown in Figure 17.

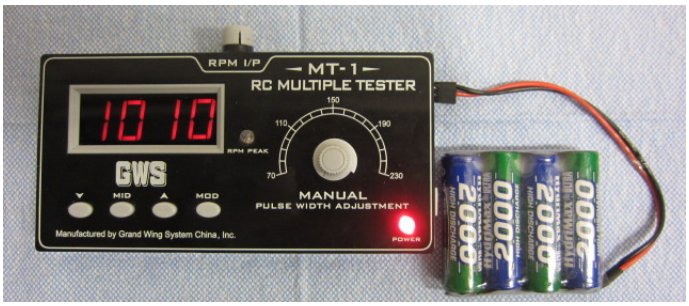

Figure 17: Servomechanism controller

The servo wheel rotated a particular amount depending on the pulse sent from the tester. This servo rotation was used to actuate the throttle or choke causing it to open or close. The tester allowed specific pulse-width-modulation to be established. The minimum pulse-width step possible to be sent to the servo from the tester was 1μs. Manipulating the pulse-width step allowed for dividing the range of throttle from idle to wide open into

definite segments. The established segments are explored later. Though the servo was actuated using a defined pulse-width this did not correspond to an exactly precise throttle position because of hysteresis. A throttle position sensor (TPS) was procured but was unable to be incorporated into this research effort. With a TPS, the actual throttle position would be known and when used in concert with the servo (in a closed or open loop) would direct the servo to actuate to open or close the throttle to any position.

Starting the engines was achieved using a high torque EM used to start engines in R/C aircraft via their propellers. The engines tested in this effort had a through engine shaft design resulting in a protruding threaded bolt on the backside of the engines. Propeller nuts were attached to the threaded bolts, and the cup attachment on the high torque EM fit over and tightly gripped the cone of the prop nut. The engines were started by this method using the starter EM and 12 V battery shown in Figure 18.

Figure 18: Prop starter EM and battery

5. Data Acquisition Software

The supplied DYNO-MAX software was used to operate the dynamometer, record data and do some data analysis. A screen shot of the main data acquisition console of the

DYNO-MAX software is shown in Figure 19. The software allowed for adjusting console setup to meet specific testing needs. Gauges and ranges had the ability to be altered and moved to customize the console setup. The information received by the software program from the data computer and controller was limited to absorber RPM, measured torque, engine temperature and fuel flow. Hundreds of built in formulas were available from the software to calculate other parameters including engine power, BSFC, and BMEP. These formulas also used information about the engine's specifications that was input into the *Active Run Information* window [34]. The information included local weather data (ambient temperature, relative humidity, altitude and relative pressure), engine dimensions (bore, stroke, and displacement) and fuel density. The active run information was also used to correct data to SAE standards and standard-day conditions.

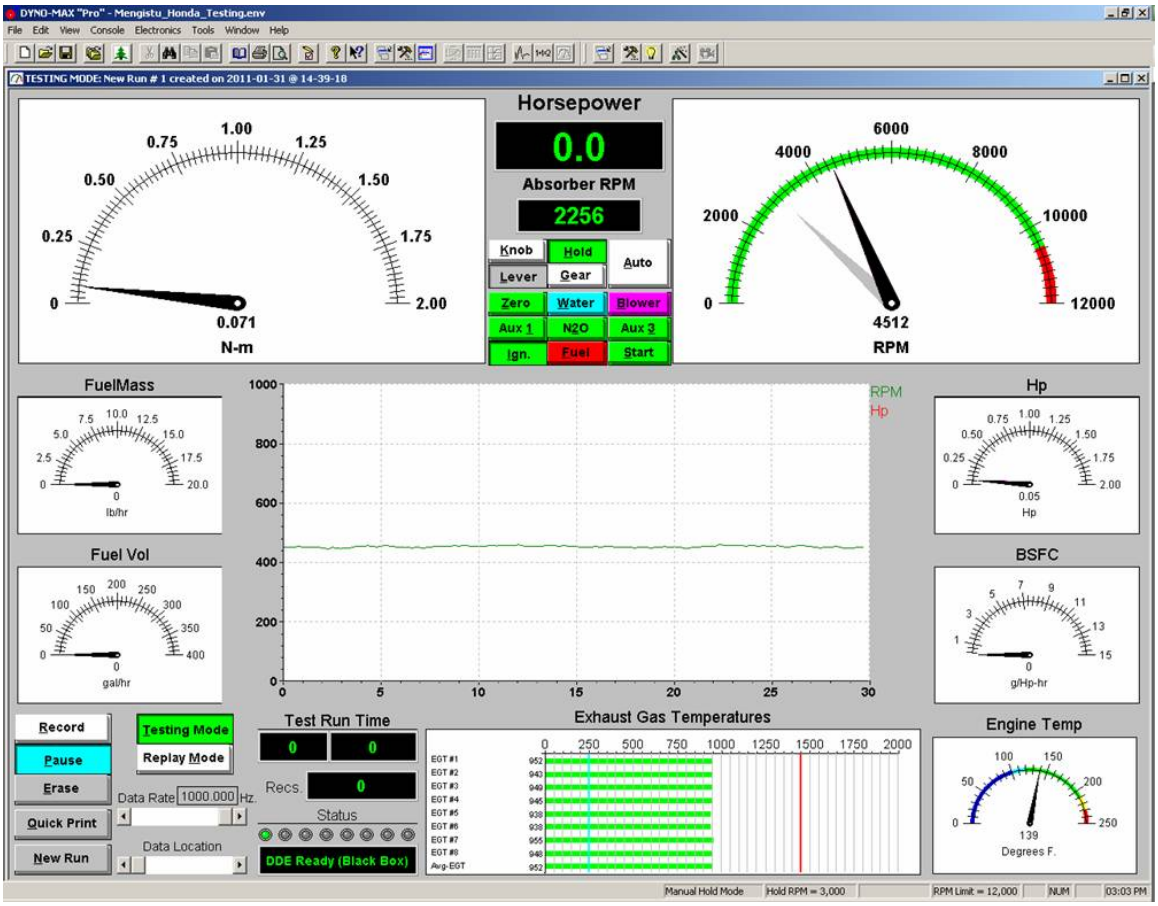

Figure 19: DYNO-MAX data acquisition software screenshot

6. Testing Procedure

The essential data sought by this investigation was torque, engine speed and fuel flow. First, a dynamometer torque measurement calibration was conducted. Next, initial engine testing was done to check the operation of all mechanical and electrical parts. Also, the engines were broken in through initial testing. This initial testing also provided an opportunity to familiarize with the dynamometer setup and data acquisition software. The familiarization with the dynamometer (as well as the need to meet safety requirements) led to the establishment of standard operating procedures (SOPs) for

engine and EM testing using the dynamometer. A checklist document (included in Appendix C) was created that included step by step instructions such as:

- Ensure sprocket-engine flange is securely fastened to engine shaft
- Examine oil pan dip stick to ensure sufficient oil is present in crankcase

After initial testing and finalization of SOPs, baseline tests were done to establish how varying the throttle position (dictated by the servo) corresponded to engine RPM, torque, power and fuel flow measurements with no additional loading provided by the dynamometer absorber. Lastly, engine testing was done to establish a matrix of data points to generate engine performance maps. Engine throttle was adjusted and RPM, torque and fuel flow measurements were taken at a series of varying engine loads. Each test was run for two minutes and the data points were the mean values of the measurements. The process was repeated and at all possible throttle positions. After data collection, the data was analyzed and the results were presented.

IV. Analysis and Results

This chapter details the outcomes of the testing done in this effort. The data collected during testing is also examined to draw conclusions and verify or disprove hypotheses made.

1. Dynamometer Calibration

Before testing was conducted and measurements taken, the dynamometer was calibrated. Initial torque-arm calibration was done by the factory, so a re-calibration test was done to ensure initial calibration accuracy. A dead-weight style test was used for the torque-arm calibration. A calibration bar with bolts that mount directly to the dynamometer's reaction cradle was supplied with the dynamometer. With the dynamometer system turned on, the calibration bar was affixed to the reaction cradle. The calibration bar had screw eye hooks at both its ends. The distance from the eye hook to the center of the reaction cradle was designed and measured to be 1.0 ft. With no mass attached to the calibration bar, the dynamometer was zeroed using the DYNO-MAX software. A known torque was generated by hanging a weight of known mass from the eye hook and was calculated using Equation 23.

$$T = F \cdot d \qquad 23$$

The calibration setup is illustrated in Figure 20.

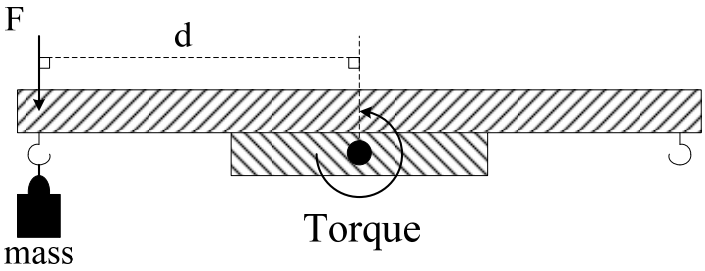

Figure 20: Torque arm calibration setup illustration

Two separate masses were used utilizing laboratory hardware items. One mass was a sprocket with a mass of 0.1644952 kg. The other mass was a C-clamp with a mass of 0.1641053 kg. The calibration bar is shown alone in Figure 21 and attached to the dynamometer in Figure 22.

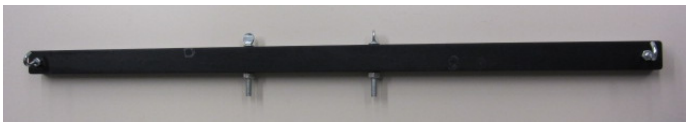

Figure 21: Calibration bar alone

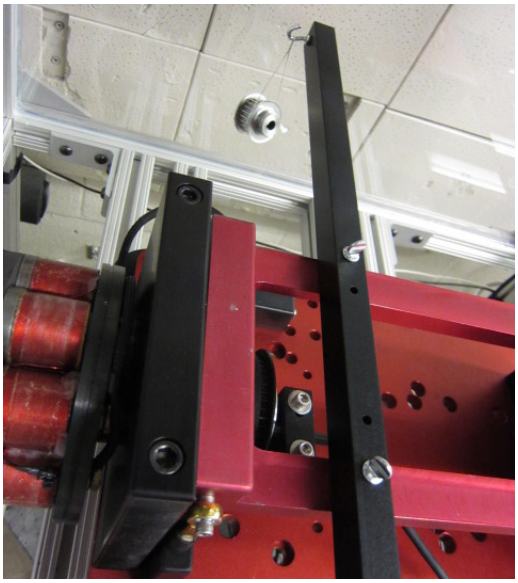

Figure 22: Calibration bar attached to dynamometer

The moment arm length (center of the calibration bar to the screw eye hook) was measured to be 1 ft or 0.3048 m. The results of the calibration are shown in Table 9.

Table 9: Torque arm calibration results

Dead-weight	Mass (kg)	Arm Length (m)	Calculated Torque (N·m)	Measured Torque (N·m)	Torque Differential (N·m)
Sprocket	0.1644952	0.3048	0.4919	0.501	0.0091
C-clamp	0.1641053	0.3048	0.4907	0.503	0.0123

The results showed that the initial calibration would provide sufficient accuracy. The measured and calculated torques differed by less than ± 0.02 N·m. For this research effort, torque measurements within ± 0.05 N·m was seen as adequate for developing engine performance maps. Significant torque ripples and spikes due to the single cylinder piston engines being tested were expected. It was believed the torque spikes would lead to fluctuating torque measurements impairing the ability to attain torque measurements with higher accuracy than ± 0.02 N·m.

Another calibration was done in regard to dynamometer operation. Greiser [11] and Harmon [9] calculated the gear-ratio between the dynamometer sprocket and the sprocket mounted to the engine shafts. A magnetic pick-up mounted to the dynamometer was used to measure absorber RPM. The pickup face was the absorber sprocket shown in Figure 23 . This calibration would ensure the proper engine RPM was calculated by the DYNO-MAX software based on measured absorber RPM. The number of grooves or gear teeth were counted on the sprockets and compared. The gear-ratio was calculated to be 2 to 1 and this data was entered into the software. Greiser also compared the RPM measurement via the optical RPM sensors used by his C-based controller and LabView

GUI for data collection. Using an EM operating at very low RPM, the number of pulses (generated by the optical sensor) was recorded for a minute. The rotations of the dynamometer absorber sprocket were physically counted by eyesight and compared to that of the optical sensor measurements and the magnetic pick-up inherent in the dynamometer system. The rotations were found to be effectively equivalent across all three measuring techniques and the calculated 2 to 1 gear-ratio was determined to be valid.

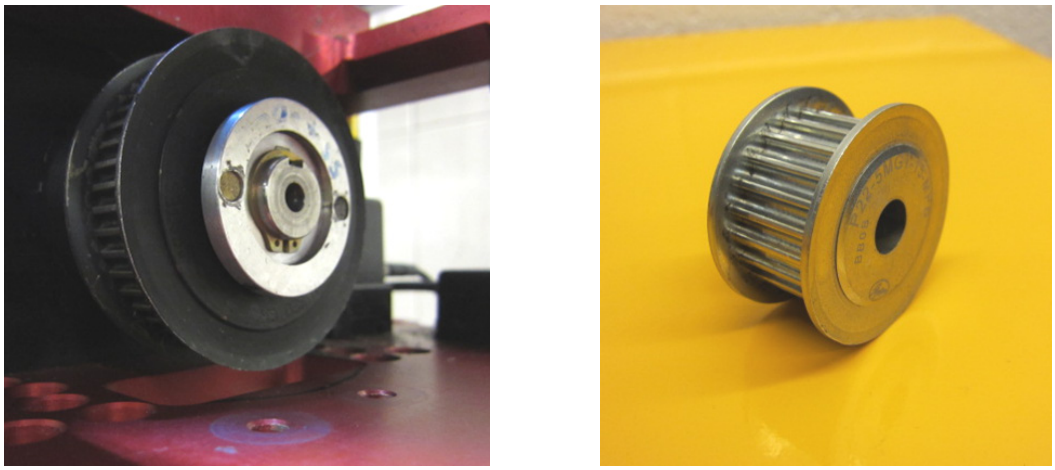

(a.) (b.)

Figure 23: Sprockets used in testing (a.) absorber sprocket (b.) engine shaft sprocket

2. Fuel Flow-meter Calibration

A series of simple calibration tests were performed to ensure the factory calibrated fuel flow-meter was accurately and precisely measuring fuel flow. The calibration was performed using the Honda GX35 engine. The engine was run at a series of specific throttle settings and operated for a specific period of time. Using a scale, the mass of the fuel tank was measured at 30 s intervals. The fuel mass measurements over time were

plotted and fitted with an ordinary least squares line. The time rate of change was equivalent to the fuel mass flow rate during the test. This method of fuel mass flow rate measurement was used by Menon in similar research focused on small ICE testing [35]. The calibration test setup is shown in Figure 24.

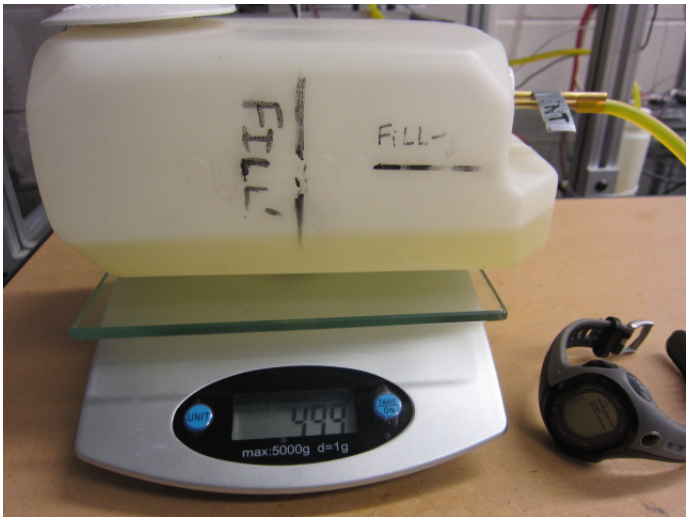

Figure 24: Fuel mass flow rate calibration test setup

Table 10: Fuel tank mass measurements (1st series of tests)

Time (s)	Fuel Tank Mass (g) 7100 RPM Average	Fuel Tank Mass (g) 8300 RPM Average	Fuel Tank Mass (g) 8900 RPM Average
0.0	~	528	~
0.5	592	525	565
1.0	591	522	561
1.5	589	519	558
2.0	587	517	554
2.5	585	514	551
3.0	583	511	548
3.5	581	508	544
4.0	579	506	541
4.5	577	503	~
5.0	575	500	~

The Honda was run unloaded (not mechanically connected to dynamometer load) at three throttle settings corresponding to average engine speeds of 7000 RPM, 8300 RPM and 8900 RPM respectively. The results of the tests' fuel tank mass measurements using the scale are summarized in Table 10 and plotted in Figure 25.

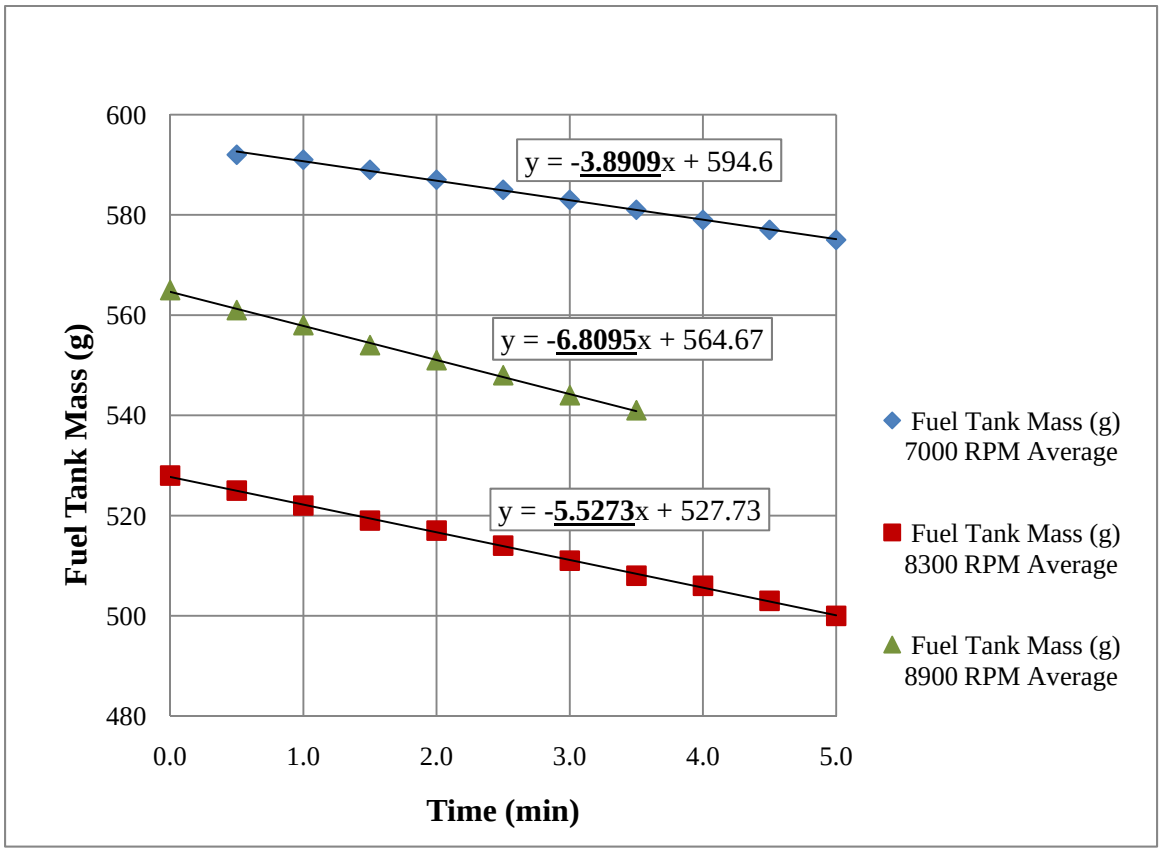

Figure 25: Fuel tank mass measurements over time using scale (1st series of tests)

Table 11: Comparison of mean fuel mass flow rates (1st series of tests)

Ave. Engine Speed	Ave. Fuel Mass Flow Rate (g/min) from Scale	Ave. Fuel Mass Flow Rate (g/min) from Flow-meter
7000	3.891	11.711
8300	5.527	31.125
8900	6.810	44.423

The comparison of the mass flow rates calculated from fuel tank mass measurements with those calculated from flow-meter data and DYNO-MAX software is shown in Table 11. The calibration test showed that the fuel mass flow rate measurements from the flow-meter and scale measurements differed by greater than a factor of three. This very large discrepancy between the values first led the author to search for something amiss with parameters in the data acquisition software.

The flow-meter used in the dynamometer test stand calculated volumetric flow rate and then the DYNO-MAX software converted this data to a fuel mass flow rate using user input information about the fuel's relative density and local weather data. The DYNO-MAX data acquisition console (Figure 19) is programmed to show and record measured and calculated dynamometer data. Calculated dynamometer data was found by use of default formulas stored in the DYNO-MAX software. The formula used for fuel mass flow rate calculation was examined to ensure correctness. The formula displayed in the *Formula List* window of DYNO-MAX is shown in Figure 26.

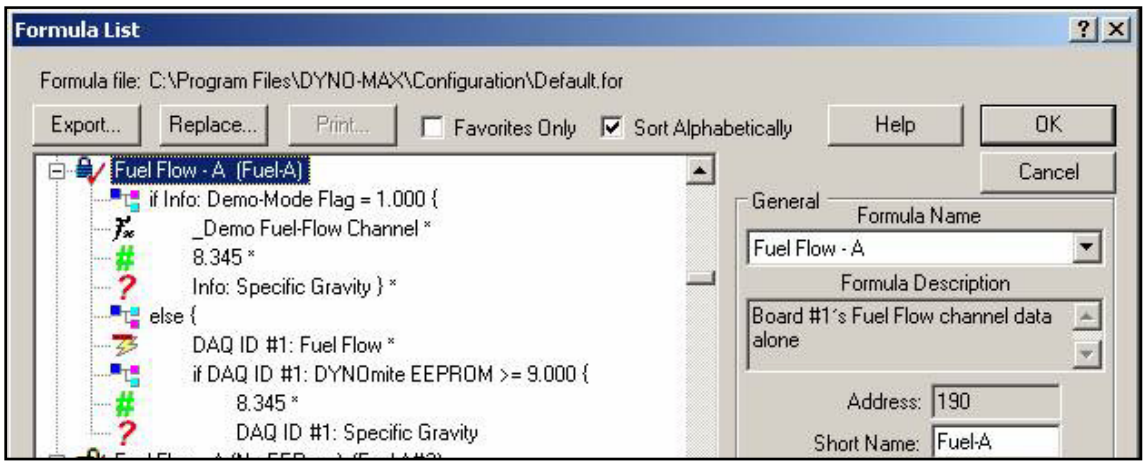

Figure 26: DYNO-MAX software formula list for fuel mass flow rate calculation

The formula in mathematical form is shown in Equation 24.

$$\dot{V} \cdot 8.345(\text{lbm/gal}) \cdot \text{fuel relative density} = \dot{m} \qquad 24$$

where 8.345 lbm/gal is the density of water at 4°C, and $\dot{V}$ is volumetric flow rate The formula was evaluated for known volumetric and mass fuel rates and was determined to be correct so the author moved on to examining the fuel flow channel settings.

The factory set calibration values were checked for accuracy by comparing values present in the *Calibrate DYNOmite™ Channels* window (Figure 27) to the values listed in the DYNOmite™ manual [34] and software *Help* index.

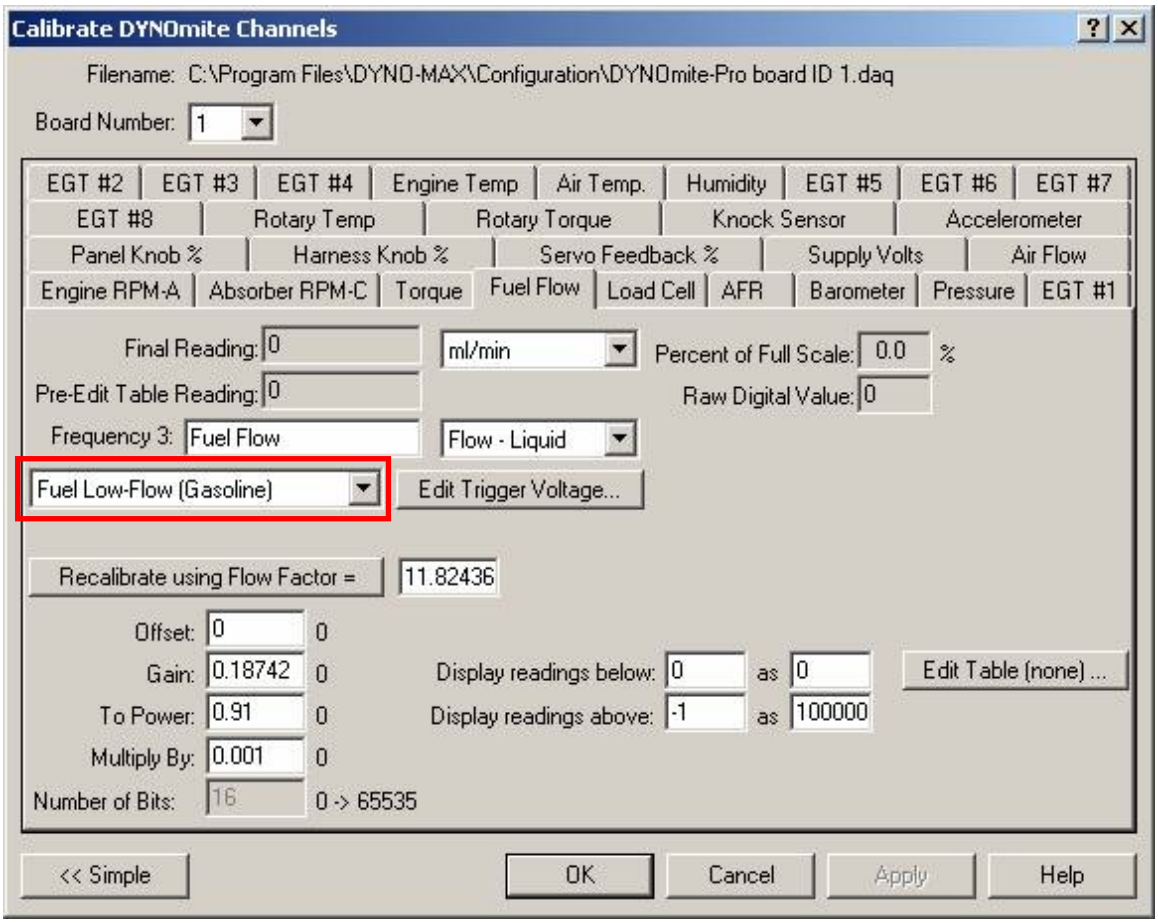

Figure 27: DYNO-MAX software fuel flow calibration window

The gain, power and multiplier values did not correspond. Immediately, it was found that the fuel flow channel was initialized with settings for a *Standard Flow Transducer* and not the *Low Flow Transducer* used in this dynamometer setup. The channel gain, power, multiplier and flow factor values were changed by selecting *Fuel Low-Flow (Gasoline)* from the drop down menu highlighted by the red box in Figure 27. Following these changes, a second series of calibration tests were conducted to determine if flow-meter measurements were improved.

Table 12: Fuel tank mass measurements (2nd series of tests)

Time (min)	Test 1 Fuel Tank Mass (g) 8000 RPM Average	Test 2 Fuel Tank Mass (g) 8000 RPM Average
0.5	740	600
1.0	738	598
1.5	735	~
2.0	732	~
2.5	730	591
3.0	727	588
3.5	725	585
4.0	723	582
4.5	720	580
5.0	717	577
5.5	715	~
6.0	712	~
6.5	709	~

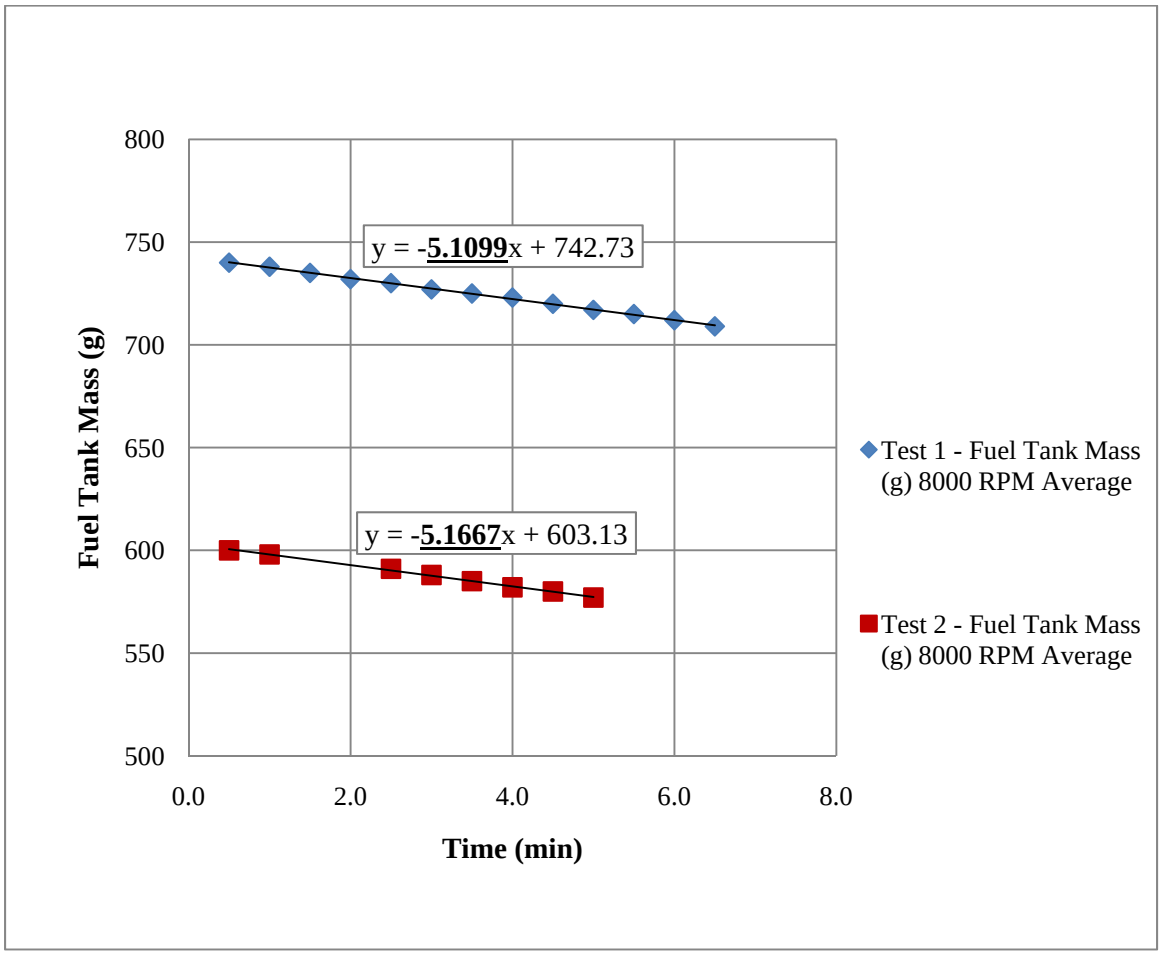

Figure 28: Fuel tank mass measurements over time using scale (2nd series of tests)

Table 13: Comparison of mean fuel mass flow rates (2nd series of tests)

Test	Ave. Engine Speed	Ave. Fuel Mass Flow Rate (g/min) from Scale	Ave. Fuel Mass Flow Rate (g/min) from Flow-meter
1	8000	5.110	4.108
2	8000	5.167	4.044

The results of the second series of calibration tests brought the flow-meter measurements closer to the fuel mass flow rate calculated from the fuel tank mass measurements, but the error was still significant. After consultation with technicians from Land and Sea, Inc.

(the manufacturer of DYNOmite™ dynamometers) and Flow Technology™ (makers of the fuel flow sensor) it was determined volumetric and mass flow rates below the minimum of the calibrated range for this fuel flow sensor (11.35 cm^3/min or 0.18 gal/hr and 8.3 g/min respectively) would be measured inaccurately and imprecisely by the fuel flow sensor and DYNO-MAX software. It was decided this fuel flow sensor could not be used to reliably measure fuel flow and calculate fuel consumption. Unfortunately, a fuel flow sensor that could accurately measure these lower flows could not be obtained in time for this effort. The method of calculating fuel mass flow rate from fuel tank mass measurements (like that used by Menon [23] [35]) was used for all testing where fuel consumption was required.

3. Initial Testing

After calibration tests, initial engine testing was done to gain operational experience with the dynamometer test setup and data acquisition process using the DYNO-MAX software. At the outset, the Honda GX35 engine was setup for testing. The Honda GX35 is shown in Figure 29 as it was mounted to the dynamometer test setup for initial testing. All aspects of the engine testing system were inspected for proper function using the establish SOPs. Testing of the servo operating the throttle showed it worked properly. Fuel flowed from the fuel tank through the fuel flow-meter and into the carburetor appropriately. The exhaust fan properly ventilated the dynamometer engine enclosure. The engine cut off switch properly stopped the engine.

Using the original configuration shown in Figure 29, the Honda engine was tested for approximately ten minutes. Engine throttle was opened and closed and dynamometer

loading was varied over the testing period. The data acquisition computer logged data to the PC and was recorded via DYNO-MAX software. The DYNO-MAX software dampened and collated recorded data over the entire test run for plotting purposes. Surprisingly, torque and power measurements from this initial test run had decent agreement with the manufacturer's ratings. A comparison of the data from the initial test run and the manufacturer's claimed performance data is shown in Table 14. Initial test power and torque measurements are plotted in Figure 30.

Table 14: Comparison of initial data and manufacturer claims for the Honda engine

Measurement	Initial Test Data	Manufacturer Claim
Peak Torque (N·m)	1.383 @ 5800 RPM	1.60 @ 5500 RPM
Peak Torque (lbf·ft)	1.020 @ 5800 RPM	1.18 @ 5500 RPM
Peak Power (kW)	0.910 @ 7000 RPM	0.97 @ 7000 RPM
Peak Power (hp)	1.221 @ 7000 RPM	1.30 @ 7000 RPM

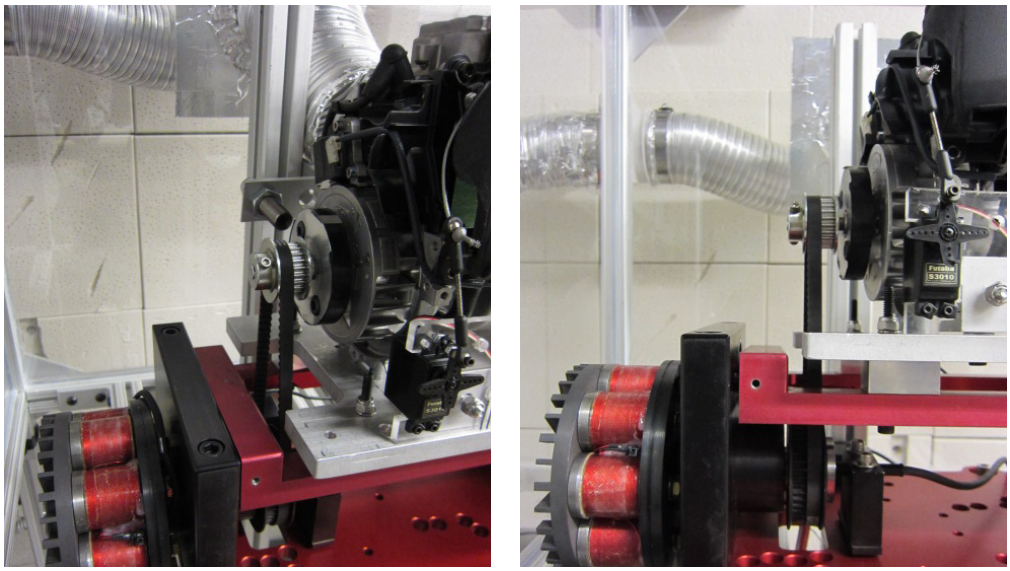

(a.) (b.)

Figure 29: Honda GX35 mounted to dynamometer (a.) angled view (b.) side view

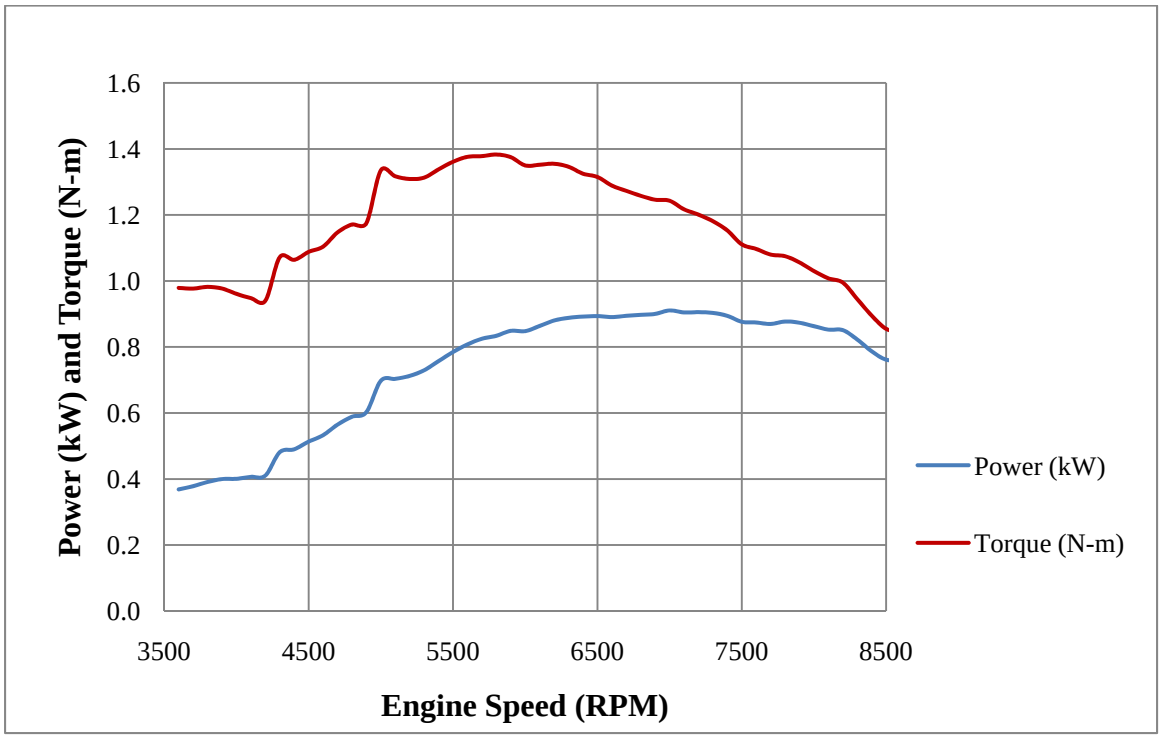

Figure 30: Initial torque and power versus engine speed plot for Honda

This initial mounting configuration caused excessive wear of the belts leading to premature belt failure. The tension in the belt applied a force on the sprocket mounted on the engine shaft causing misalignment due to lack of support on the free end of the sprocket. A new testing configuration was devised and implemented to support the engine shaft on both sides of the sprocket on which the belt was seated. A mounted support bearing was fitted to a block on the free end of the sprocket and a longer engine shaft extension was fit through the sprocket and into the bearing. The ball bearing was rated for speeds up to 32000 RPM, which well exceeded the 11000 RPM maximum the Honda engine was capable of achieving. The bearing's load capacity was 450 lbf. The bearing is shown in Figure 31 and a diagram of the belt-sprocket-bearing configuration is shown in Figure 32.

Figure 31: Mounted bearing for engine shaft support [36]

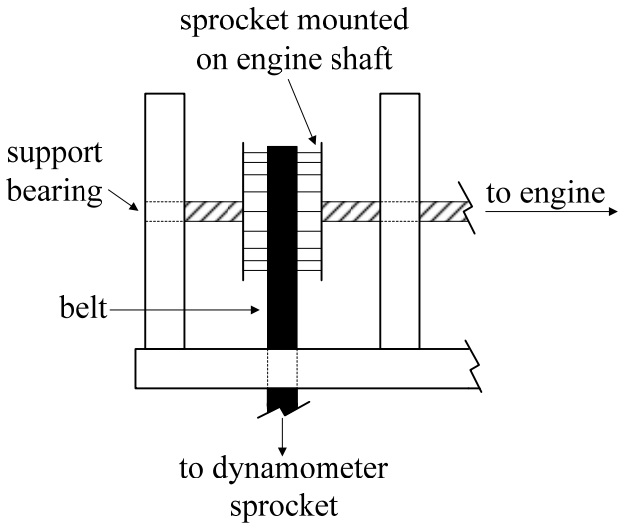

Figure 32: Engine testing hardware configuration diagram

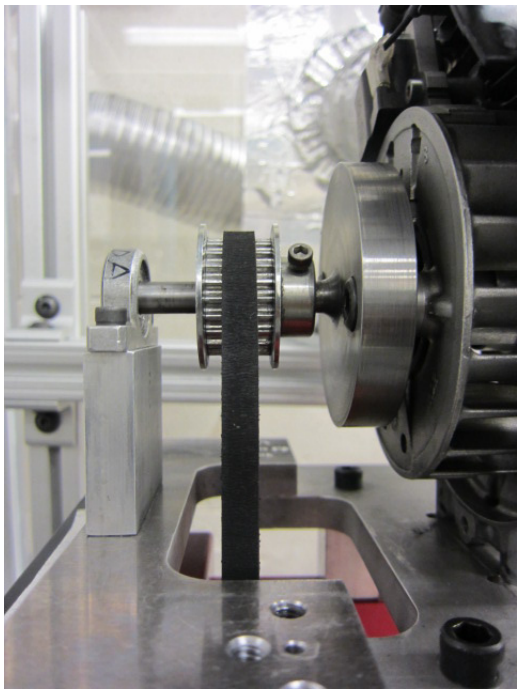

Figure 33: Engine testing hardware configuration photograph

The addition of the bearing did not entirely solve the problem of excessive belt ware and premature belt failure. The bearing only mitigated the problem and allowed for more tests to be conducted between belt failures. The synchronous timing belts used in testing were manufactured by Gates Corporation. Initially, belt alignment was blamed for the failures. Belt technology and alignment literature was investigated to better understand belt maintenance and failure [37] [38]. A diagram of belt misalignment concern areas is shown in Figure 34.

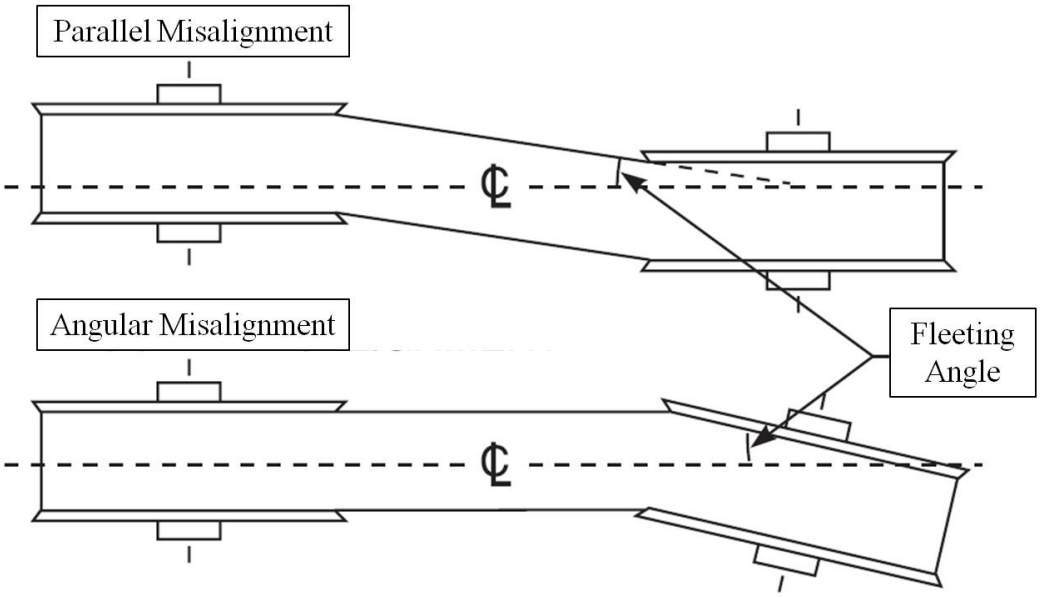

Figure 34: Diagram of common belt misalignment areas [38]

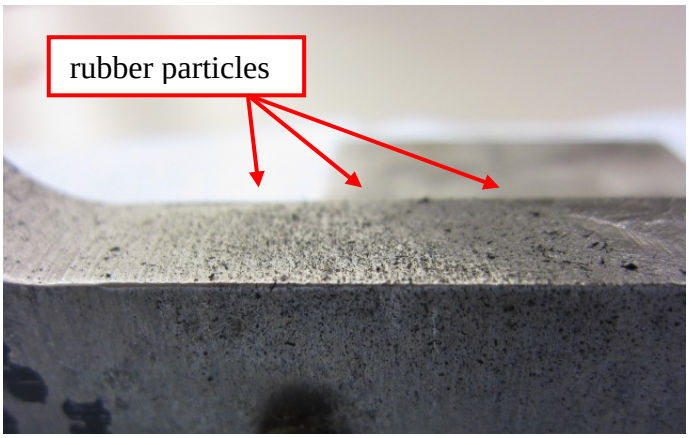

Figure 35: Rubber particles thrown from belt and collected on mounting plate

(a.) (b.)

Figure 36: Belts suffering complete failure (a.) (b.)

The belt alignment for original testing was done by naked-eye physical inspection by the author. It was assumed the flexibility in the belt would absorb additional stresses imposed on the belt because of slight misalignment. During engine testing, minute rubber particles were found clinging and collecting to dynamometer and engine mounting hardware after being thrown from the belt (Figure 35). Belt width was less than the width of the sprockets. The belts were not remaining centered in the sprocket (believed to be due to misalignment) and drifted to either wall of the sprocket. It was thought the sprocket walls were causing belt side-wall damage eventually wearing away belt material causing failure. To combat the failures, misalignment was tackled by the technicians of the AFIT Model and Fabrication Shop.

The dynamometer setup was brought to the technicians and the various bearings and spacers were leveled and aligned as best as possible. A tensioner device was fabricated by the technicians to guide the belt in a groove preventing side-wall damage as well as

applying variable tension to absorb torque fluctuations and vibration associated with the single cylinder ICEs being tested. The tensioner devices are shown in Figure 37.

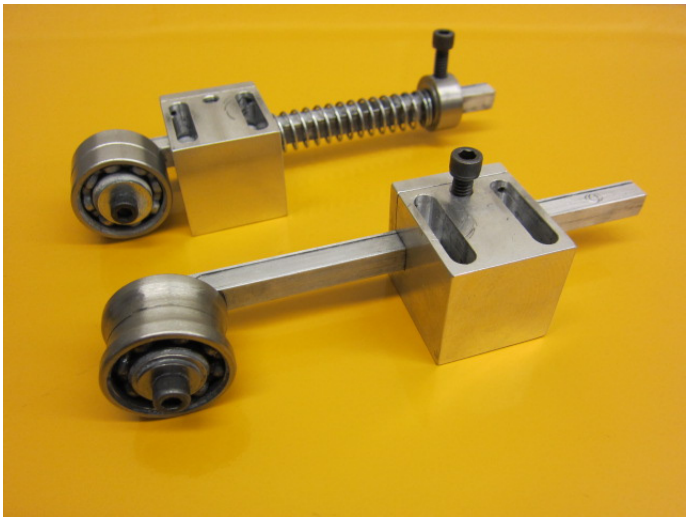

Figure 37: Tensioner devices for engine to dynamometer belts

The test setup alignment and incorporation of the tensioner resulted in the belt remaining centered on the sprocket and not rubbing the side-wall. The overall ability to conduct engine testing was improved, however belt failure still occurred frequently after a few hours of engine testing total. A second type of belt was recommended by the dynamometer manufacturer. The Poly Chain GT Carbon belts (also made by Gates Corporation) were described as having higher power rating than the Power Grip belts but failure still occurred. The synchronous belts used were found to have much less flexibility than was expected. Flexibility of the belt was hoped would absorb vibration and torque fluctuations from the single cylinder engines being tested in this effort. The short-term solution was to have enough spare belts on hand to allow for continued testing.

4. Throttle Position Establishment

The ability to adjust throttle position in increments was necessary to generate data points over the entire engine operating range. The goal was to open and close the throttle in roughly 10% increments between idle and wide-open throttle (WOT) (100% throttle). Specific pulse-widths were established using the MT-1 R/C Multiple Tester. These pulse-widths resulted in specific actuation of the Honda and Fuji-IMVAC servomechanisms. The author used physical naked-eye inspection to judge how open the throttle valve was compared to the value of the pulse-width sent from the controller. The throttle position and pulse-width increments were established through numerous iterations via a guess, check and revise process. The pulse-width to throttle setting correspondence is shown in Table 15.

Table 15: Controller pulse-width to throttle position correlation

Pulse-width (μs)	Honda Throttle Position (% of WOT)	Pulse-width (μs)	Fuji-IMVAC Throttle Position (% of WOT)
1415	idle	1055	idle
1460	10	1145	10
1505	20	1235	20
1550	30	1325	30
1595	40	1415	40
1640	50	1505	50
1685	60	1595	60
1730	70	1685	70
1775	80	1775	80
1820	90	1865	90
1865	100	1910	100

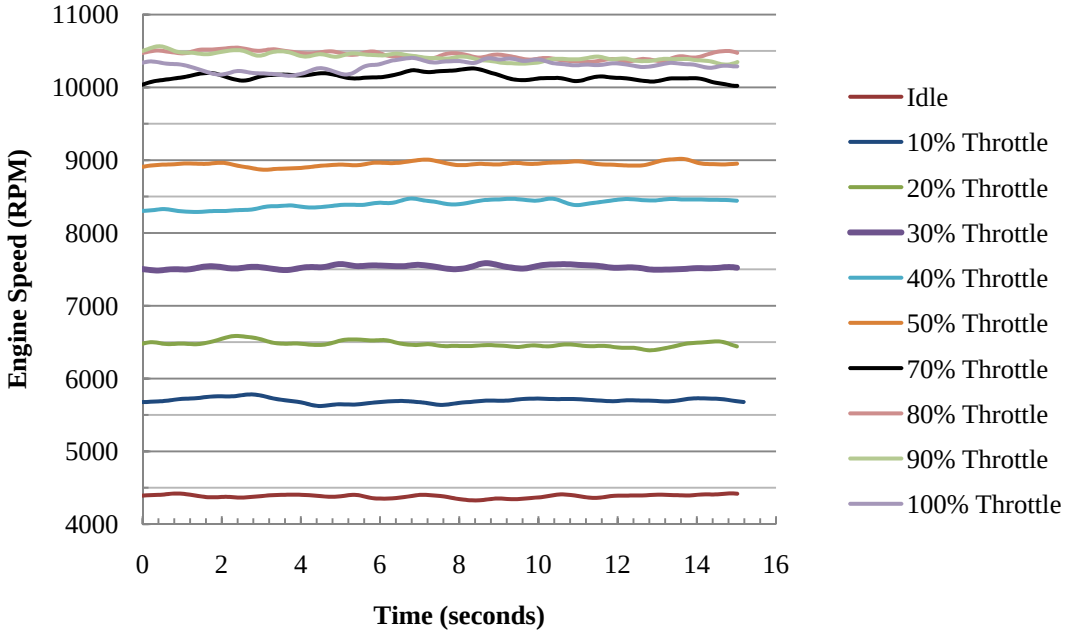

Figure 38: Honda no-load RPM over time plot for various throttle position settings

Examining the plot in Figure 38, showed that the RPM corresponding to 70%, 80%, 90% and 100% (or WOT) were crowded and overlapping in the region between 10000 and 10500 RPM. The established pulse-widths approximately dividing throttle position into 10% increments (in the physical degree of throttle valve openness) did not correlate well into even 10% increments of engine speed between idle and WOT.

5. Honda GX35 Engine Test Results

Testing of the Honda was done before any initial testing of the Fuji engine. First, an automated dynamometer test using the dynamometer to sweep through engine speed was initially setup to ensure repeatability of experiment. Essentially, the automated test consists of the DYNO-MAX software adjusting the load on the engine to vary RPM. This test required running the engine at more open throttle settings to achieve RPM close

to maximum of the allowable engine speed range. Starting at high RPM, the software would increase the load to the engine resulting in a reduction in engine speed. However, proper matching of RPM when switching from manual load control to automated load control was required to not stall the engine and was very difficult and inconsistent to achieve. The author was unable to alter the default automated load control settings so the automated test was somewhat of a black-box.

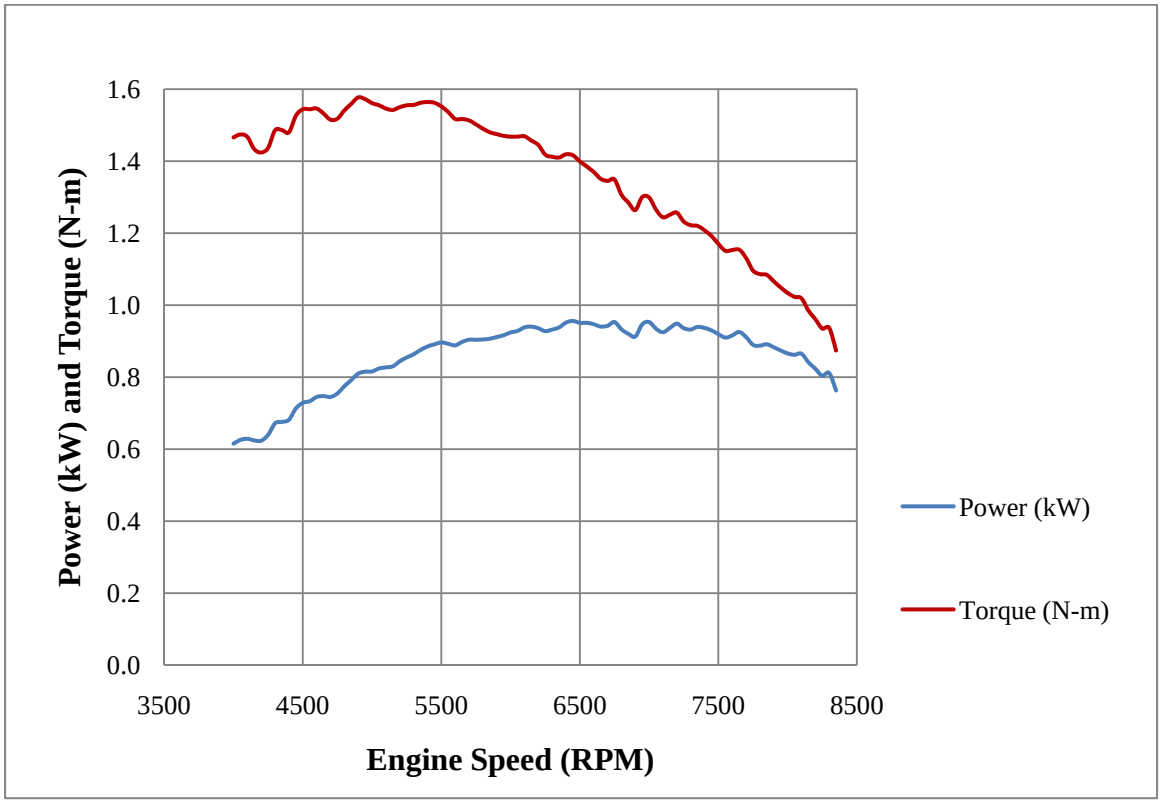

Figure 39: Honda power and torque versus engine speed (SI units)

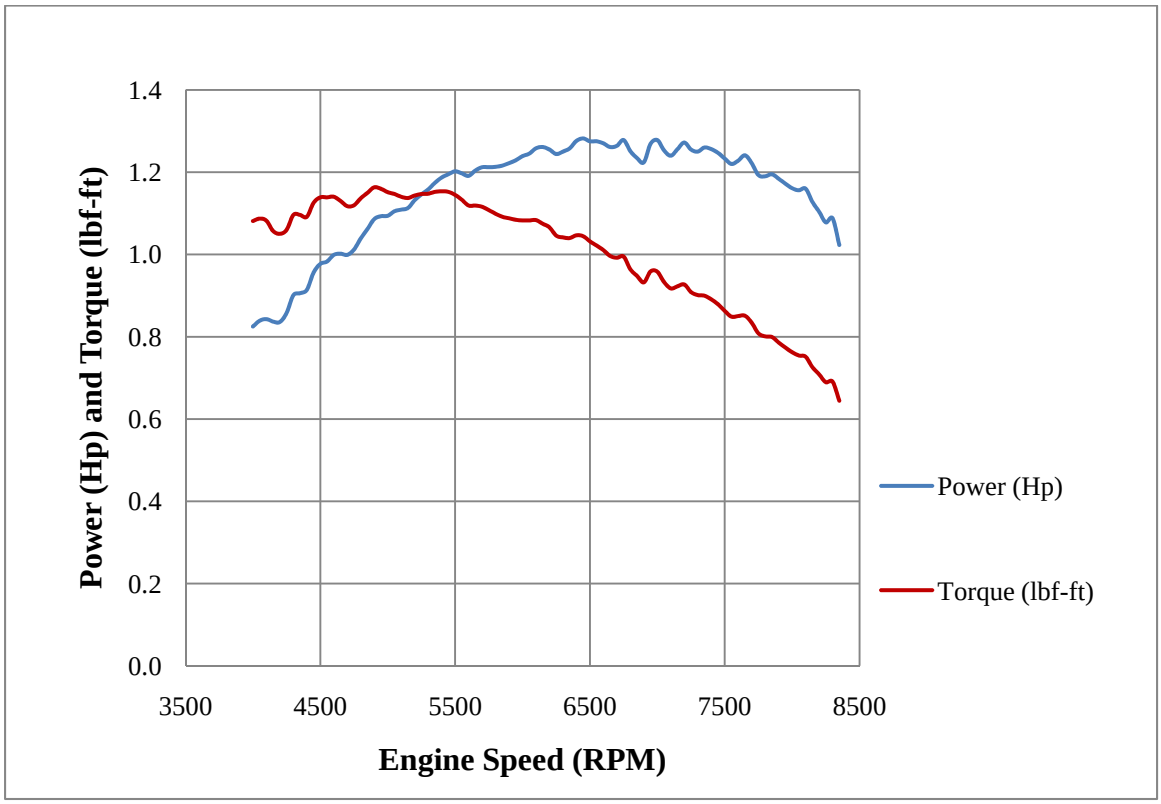

Figure 40: Honda power and torque versus engine speed (English units)

It was decided that the automated test would not be used due to difficulties with the automated test stalling the engine. Power, torque and BSFC measurements needed to populate the desired performance maps would need to be made by a different method.

Measurements of power, torque and BSFC for use in producing performance maps were made by selecting a throttle setting, manually applying a set load and running the engine under those steady conditions for a specific duration of time. Each throttle setting had eight loadings applied to it and the duration of each test was 2 min. The throttle settings to be tested would be 30%, 40%, 50%, 60%, 70%, 80%, 90%, and 100%. Fuel tank measurements were taken at 30 s intervals and fuel flow rate was determined using the same method as in the calibration tests. The process was repeated over all throttle

settings. The mean value of the power, torque and BSFC measurements and calculations were used to establish single values representing a single point on the performance map. The performance map was to contain 64 points in total. An example of the data for the performance map points for a single throttle setting is shown in Table 16.

Table 16: Honda power, torque and BSFC values at 50% throttle

RPM Average	Torque (N·m)	BMEP (kPa)	Power (kW)	BSFC (g/kW·hr)
4500	1.5373	539	0.7216	394.1
5000	1.3720	481	0.7156	436.0
5500	1.2470	437	0.7184	456.0
6000	1.1611	407	0.7336	461.3
6500	1.0049	352	0.6841	526.2
7000	0.9198	323	0.6724	574.7
7500	0.7307	256	0.5775	694.0
8000	0.5858	205	0.4935	863.2

Engine testing was only able to produce reliable data for 30%, 40%, 50%, 60%, and 100% throttle. Thus, only a partial performance map was able to be generated. At 70%, 80% and 90% throttle, a consistent engine speed was not able to be maintained when a consistent load was applied. Why this was happening could not be solved during within time for this effort. The data for 100% throttle were not included in the performance map because of the discontinuity caused by the missing data for 70%, 80%, and 90% throttle. Also, the engine test at 30% throttle could not produce engine speed of 8000 RPM or greater so data at 8000 RPM for engine tests at all throttle's were left out at well. The performance map contained 28 points total instead of the originally expected 64 points in total. The performance map of BMEP versus engine speed with plotted contours of BSFC is shown in Figure 41. The plot shows that the lowest fuel consumption occurred

near an engine speed of 4500 RPM and a BMEP of around 450 kPa. From the data points used, actual minimum BSFC for the Honda was found at 60% throttle to be 383.6 g/kW·hr (0.6307 lbm/hp·hr) at 4500 RPM.

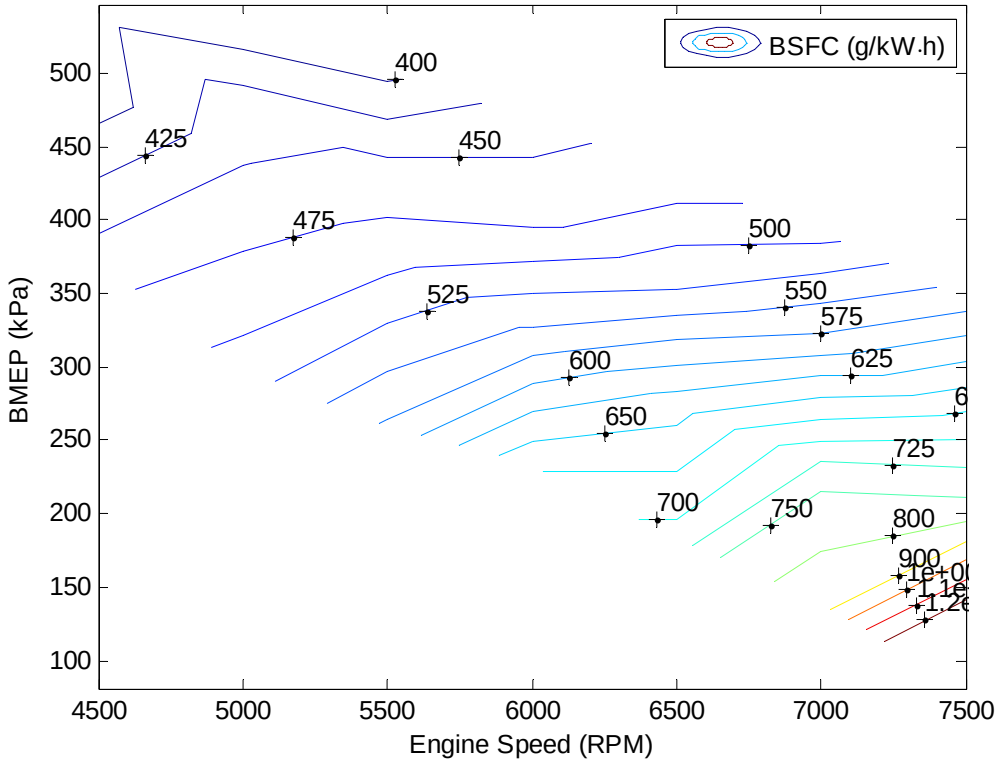

Figure 41: Honda performance map of BMEP versus engine speed with BSFC contours

The Honda performance map using engine torque instead of BMEP is shown in Figure 42. This performance map shows that to operate the engine at lower BSFC at a given engine speed, the engine should tend (for the most part) to have the highest possible torque demand requested of it. To lower BSFC during engine operation at a given torque, engine speed should generally be minimized. This trend does not hold true at numerous locations between engines speeds of 5000 and 6000 RPM at torque above

1.00 N·m. Peak torque for the Honda was found at 60% throttle to be 1.5601 N·m at 4500 RPM.

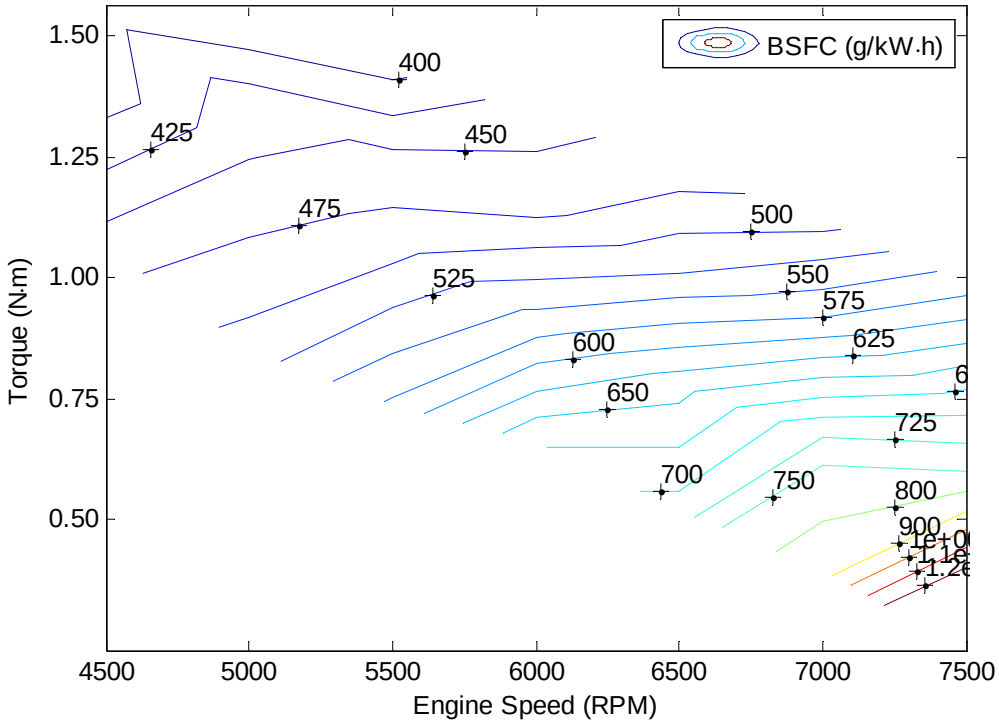

Figure 42: Honda performance map of torque versus engine speed with BSFC contours

For the Honda, peak power was found at WOT to be 1.0808 kW at 7700 RPM. Figure 43 shows contours of constant power mapped over values of torque and speed. At a given engine speed, power increases as torque increases. At a given torque, power increases as engine speed increases. This type of map is useful as a decision add when trying to operate at minimum power required or used. Figure 44 shows the maximum torque and maximum power developed by the Honda utilizing information from the performance map data points. This graph is effectively the plot of the torque and power measured at 60% throttle.

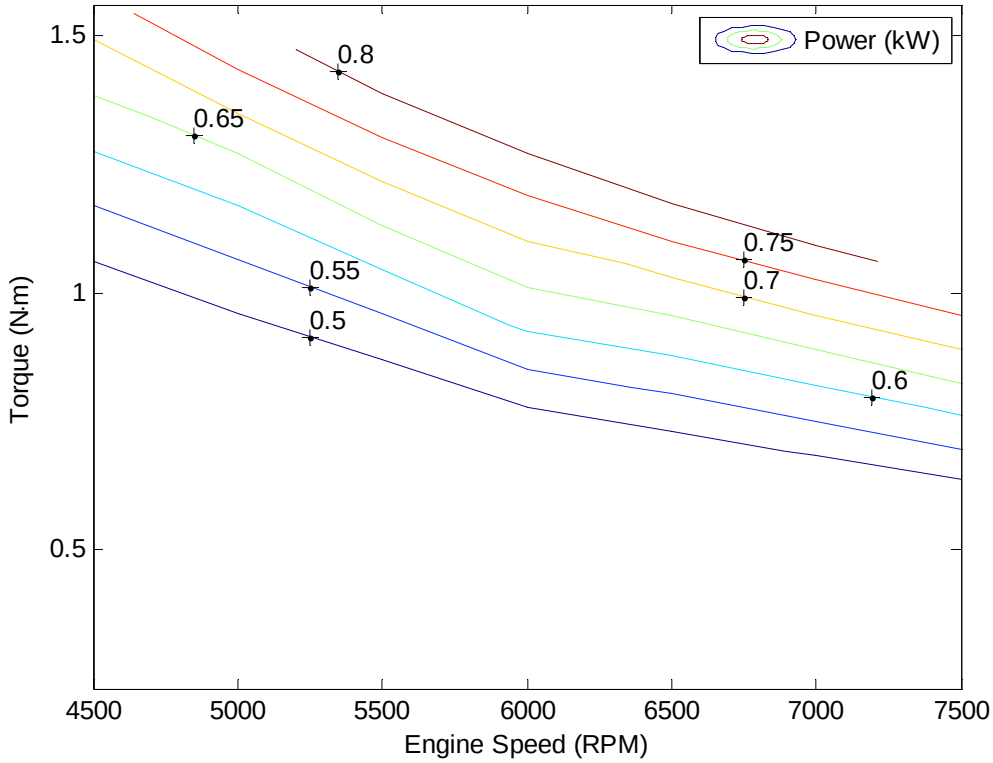

Figure 43: Honda map of power versus torque and engine speed

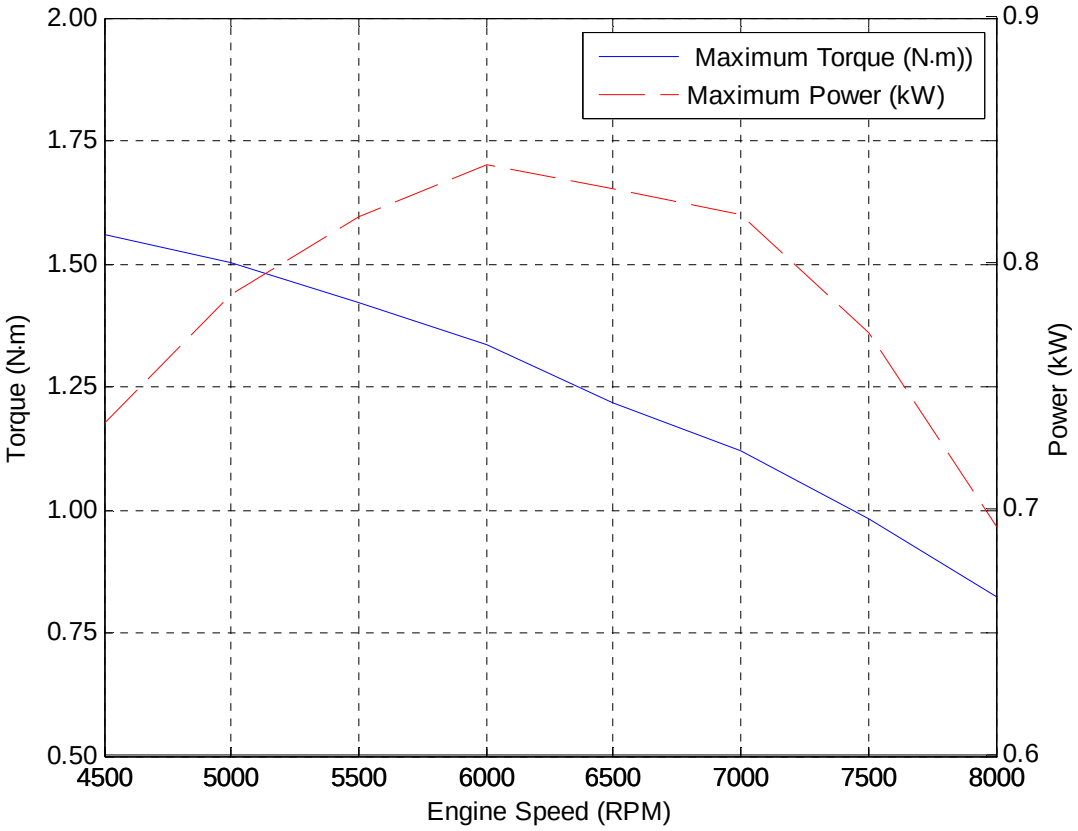

Figure 44: Honda maximum torque and power versus engine speed

The performance map created from engine testing the Honda was provided to Greiser [11] for incorporation as a reference for his HEPS controller. Engine testing of the Fuji was next.

6. Fuji-IMVAC BF-25EI Engine Test Results

Testing of the Fuji-IMVAC BF-25EI was found to be more difficult than the testing of the Honda GX35. Unlike the Honda, the Fuji engine was specifically designed to power small R/C aircraft. A flange, used to attach propellers to the engine shaft, was included with the purchase of the Fuji engine. This eliminated the need to design an

engine flange from scratch like was needed for the Honda. Initially the idle engine speed of the Fuji was running high. The engine was idling around 6000 RPM. After consulting with technicians at Fuji-IMVAC and fine adjustment of the low-speed carburetor adjustment needle the engine idle speed was reduced to 4500 RPM. This 4500 RPM idle speed was within the 1400 to 9000 RPM range claimed by the engine manufacturer, but much higher than the 1400 RPM minimum engine speed. The carburetor was examined for blockages and none were found. Fuel and air lines were examined for leaks and none were found. The spark-plug was cleaned and plug gap checked to be set at the recommended distance of 0.6 mm. In addition to the high idle speed, the Fuji was difficult to start and rough running. The most critical setback to testing the Fuji was the engine shaft to dynamometer coupling. Testing the Fuji resulted in belt failure within minutes. Prior to belt failure, at a set throttle setting, the torque measured by the dynamometer varied wildly. A consistent torque measurement was unable to be obtained. The difficulties with the Fuji engine were not resolved in time to produce test results for this effort. Although engine performance data was not produced from testing the Fuji, much was learned about its operating characteristics. These lessons learned were used in the feasibility comparison between the Fuji and the Honda.

7. Comparison of Engine Design and Operating Characteristics

The overarching rationale of all the objectives of this effort was to determine which engine would be the most efficient and feasible choice for incorporation into the HEPS used to power the HE-RPA. Criteria were developed to compare overall operating and design characteristics of the Honda and Fuji engines. These characteristics included cost,

mass, size, engine starting ease, engine noise at idle, ignition system reliability. Each characteristic had five points available in total to award to either engine. More points correlated to exhibiting the characteristic in a positive way. For characteristics were quantitative values could be compared (e.g. cost) points were awarded based on the multiplicative factor separating the values. For example, if the Honda engine cost $300 and the Fuji engine cost $200, the Honda engine would receive 2 points and the Fuji engine 3 points. Qualitative characteristics (e.g. engine starting ease) were based on the opinion of the author and two other colleagues working on engine testing. The results of the study are shown in Figure 45.

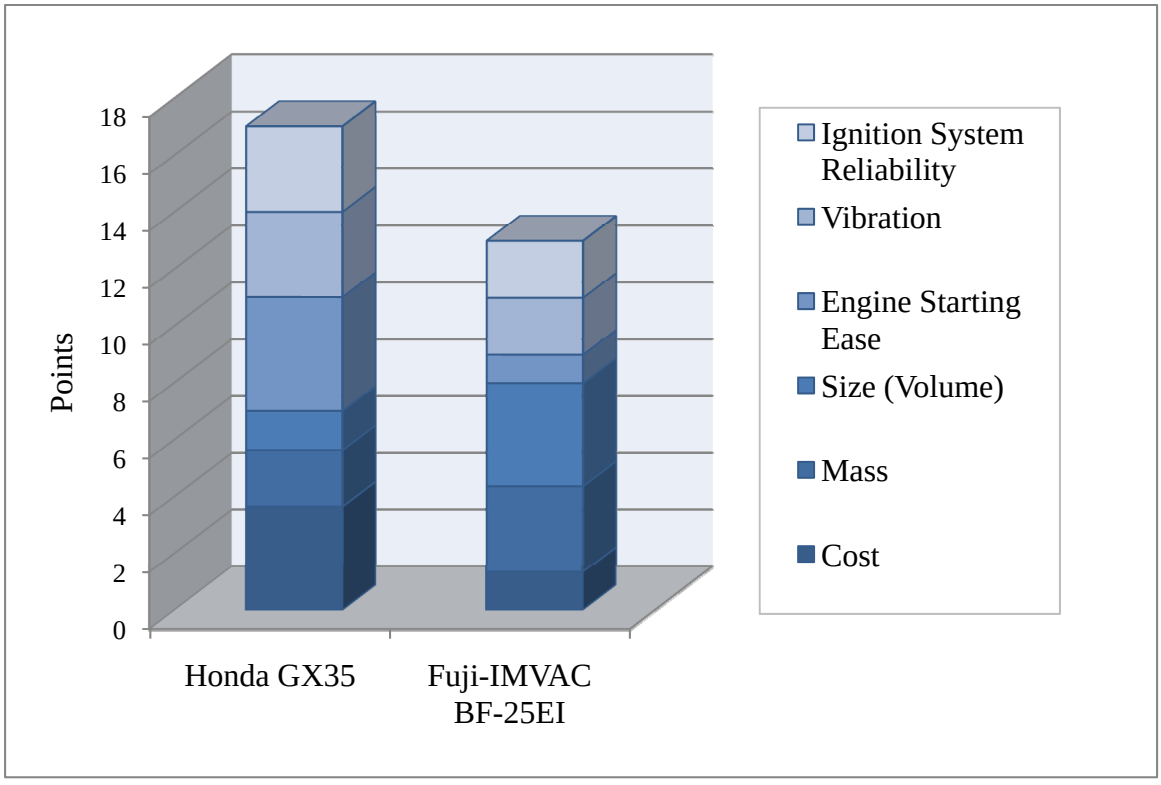

Figure 45: Engine characteristic comparison bar graph with category contribution

The Honda engine received 17 points and the Fuji 13 points. With no regard to torque, power and BSFC considerations the Honda engine exhibits better characteristics.

Although torque, power and BSFC data are very important, how these other engine characteristics impact the entire RPA and its other systems is also very important. The Honda did better in the comparison mostly due to the Honda being 2.7 times cheaper than the Fuji, displaying less vibration and being easier to start. Achieving a benefit from cost savings assumes equivalent durability and maintenance schedule between the engines. Though durability tests were not conducted, the reduced vibration apparent with the Honda leads one to believe the durability of the Honda would be on par with the Fuji (if not better). One of the ideas for operation of the HE-RPA is to shut off the ICE, while the EM is powering the aircraft alone. The ability to restart the engine easily and reliably is critical to success in this scenario. The magneto on the Honda acts as flywheel. The inertia of the flywheel resists change which steadies the rotation of the engine shaft. The lack of a flywheel on the Fuji makes it more susceptible to excessive vibration due to fluctuating torque. The Fuji's strongest characteristics in this study were its lesser volume and mass. The Fuji is 1.5 times less massive and 2.6 times smaller than the Honda. These characteristics are critically important when considering the main point of this effort is to determine the engine most fit to be used in a small HE-RPA.

V. Conclusions and Recommendations

1. Conclusions of Research

This research effort successfully tested one ICE to accurately measure engine performance data. A partial engine performance map was generated for the Honda engine showing contours of BSFC mapped on BMEP versus engine speed plots. Only performance parameters found at 30%, 40%, 50%, 60% and 100% throttle were able to be accurately measured. Only the data found at 30%, 40%, 50% and 60% throttle were incorporated into the engine performance map. Measured performance data for the Honda GX35 corresponded well with the performance data claimed by the manufacturer. For the Honda, peak power was found at WOT to be 1.0808 kW at 7700 RPM whereas manufacturer specification was for peak power to be 0.97 kW at 7000 RPM. Concerning data actually used in the formation of the Honda performance maps, values at 60% throttle produced peak torque and minimum BSFC. At 60% throttle, peak torque for the Honda was found to be 1.5601 N·m at 4500 RPM and minimum BSFC for the Honda was 383.6 g/kW·hr (0.6307 lbm/hp·hr) at 4500 RPM. Even at 60% throttle, peak torque nearly matches the manufacturer peak torque claim of 1.6 N·m at 5000 RPM. It is most likely the manufacturer obtained peak torque and power measurements at WOT.

The Fuji-IMVAC BF-25EI was not successfully tested using the dynamometer test setup due to repeated belt failure and large fluctuations in torque measurements. No solution was found in the time available to produce suitable engine test results. However, lessons learned from the operating characteristics of the Fuji showed it is not the better fit for incorporation into the HE-RPA and that the Honda GX35 is the better fit.

2. Recommendations for Future Research

The effort provided a good foundation for continued small ICE testing. Also, this effort, in part, resulted in the construction of a dynamometer test setup that is ideal suited for further EM and HEPS testing. There are a multitude of avenues to take to further small ICE testing and related research. Suggested ideas for future research are explored in this section.

- **Finish initially intended tests**

First and foremost, the objectives originally presented in this effort should be revisited. An attempt should be made to resolve the problems that arose in testing of the Fuji-IMVAC BF-25EI engine. If the operating characteristics of the Fuji cannot be improved it should not be further considered for use in the HE-RPA. The Honda engine should be retested to ensure repeatability of the experimental results first found and to complete the engine performance map. Engine testing on Diesel fuel was also not achieved on either engine. This should be done because of the DoD motivation to simplify fuel logistics, reduce cost and possibly improve performance.

- **Different engines**

The overall assessment of rated engine power was that Honda GX35 exceeded the theorized power required for climb, 0.3679 kW (0.4934 hp), and cruise, 0.2657 kW (0.356 hp), of the HE-RPA calculated by Hiserote [10]. One of the proposed advantages of the HEPS is the overall RPA weight reduction from downsizing of the ICE. There is another COTS Honda engine that would provide sufficient power as the ICE component of the HEPS if manufacturer peak torque and power claims hold true. The Honda GX25 is a smaller version of the Honda GX35 engine tested in this effort. The Honda GX25

engine has a displacement of 25 cm^3 and claims peak power to be 0.72 kW (1.0 hp) at 7000 RPM and peak torque of 1.0 N·m (0.74 lbf·ft) at 5000 RPM [39]. The Honda GX25 mass is estimated to be 0.45 kg (1.0 lbm) less than the GX35. It is believed the GX25 will have similar operating characteristics to the GX35, which is why it is recommended that the Honda GX25 be procured and tested for possible incorporation into the HEPS.

Through collaboration with CLMax Engineering LLC, the author learned of another small COTS ICE for possible use in the HE-RPA. The Subaru Robin EH025 [40] is a single cylinder four-stroke spark ignition (SI) engine with a displacement of 24.5 cm^3, which is the same displacement as the Fuji-IMVAC BF-25EI engine. The Subaru engine is manufacturer rated peak power output of 0.81 kW (1.1 hp) at 7000 RPM and rated peak torque of 1.18 N·m (0.87 lbf·ft) at 5000 RPM. Upon physical inspection of a loaner Subaru Robin EH025, the author found the Subaru engine's exterior to appear to be identical to its Fuji-IMVAC BF-25EI counterpart. It has be suggested by some in the hobbyist R/C community, that the Fuji and Subaru share the exact same design but have internal components of differing quality. The only physically apparent difference between the Subaru and the Fuji is that the Subaru uses a magneto to power for creating a spark while the Fuji uses an electronic spark ignition system. Also, the Subaru recommendation for lubrication is to use SAE 10W-30 engine oil, while the Fuji recommends SAE 5W-20 engine oil. Examining and comparing manufacturer specifications revealed performance differences between the Fuji and Subaru engines. The Fuji has claims of higher peak power and peak torque ratings higher than the equivalently sized Subaru.

The parent company of Subaru Robin Industrial Engines (the distributer of the Subaru Robin EH025) and actual manufacturer of Subaru Robin Power Products is Fuji Heavy Industries Ltd. of Japan. The author contacted the North American distributor of Fuji-IMVAC engines and Subaru Robin Industrial Engines to determine if the companies equivalently sized engines shared more than just physical similarity. Officials from both companies responded that they knew of no share of design or parts between the engines. It is recommended that the Subaru Robin EH025 be procured and tested for possible incorporation into the HEPS also. However, it is important that first the mechanical system of coupling engine to dynamometer be improved, before different engines are tested.

- **Dynamometer testing repeatability**

A series of tests under identical settings could not be precisely conducted when collecting data measurements used to produce engine performance maps. The inability to properly use the automated loading function of the dynamometer was the primary reason behind failing to repeat identical tests. Fixing the problems with automated testing should be done. The two main benefits from this would be validation of engine test results and reducing the time required to conduct engine testing.

- **Engine to dynamometer coupling**

For dynamometer testing of the engines, the engine shafts were coupled to the dynamometer using toothed belts made of fiberglass, neoprene, nylon and carbon-fiber fitted on sprockets. These belts were primarily used because they were recommended and initially supplied by the dynamometer manufacturer. Unfortunately, engine testing was significantly impeded by the premature failure of these types of belts. Developing a

coupling system that avoids frequent belt failure would greatly improve engine testing capability.

Due to the dynamometer's reaction cradle location and setup, a belt system still remains the best option for engine to dynamometer coupling. A number of belt changes could be attempted. The increased surface area of a wider belt may better absorb the vibrations. Also, a v-belt should be considered for use as they tend to be much more flexible than synchronous belts. Though a v-belt is more susceptible to slippage, it is less prone to failure from overload, vibration and torque fluctuations. Ultimately, in the future, further consultation with a belt manufacturer should be attempted, and a belt design manual [41] should be used to develop a permanent solution to belt failure.

- **Fuel flow measurement**

Fuel flow measurement was an essential source of data for calculating and recording fuel consumption. The supplied fuel flow-meter's range of measurement was found to be insufficient. The flow-meter was unable to accurately measure flows below 1.0 lbm/hr. The fuel flow-meter was abandoned for use in this effort's engine testing. Instead, fuel mass flow was directly found using a scale to measure the fuel mass consumed during testing. This method was found to be sufficient, but in no way ideal. Using the scale was cumbersome. Also, taking scale measurements required increasing the duration of individual engine tests to allow for more fuel mass measurements to better define the fuel mass flow. Engine testing would be more automated and flexible if an accurate and precise fuel flow-meter was found and incorporated into the dynamometer test setup. Similar small ICE testing was done by Wilson [20] and the fuel flow-meter used in that research produced good results. The fuel flow-meter used by Wilson was a Model 213

Piston Flow-meter manufactured by Max Machinery, Inc [42]. It is suggested that this flow-meter be acquired.

- **Engine performance**

Engine performance was analyzed for the ICEs tested in this effort using factory recommended settings. Fuel-air ratios could be adjusted to run the engine leaner or richer and analyze the engine performance gains or losses. An air mass flow-meter manufactured by TSI, Inc. [43] was purchased to be used by the dynamometer test setup, but was unable to be incorporated. Installation of the flow-meter would allow calculation of actual fuel-air ratio. Also, use of the air mass flow-meter would allow for volumetric efficiency calculation.

Future research could look into improving performance with after-market components (carburetor, spark plug, etc.). Also, changes to engine spark-timing similar to work done by Wilson [20] could be attempted. Developing or incorporating an electronic ignition system to replace the Honda GX35's magneto is another possible area for future research. Eliminating the large magneto on the Honda GX35 would most likely increase the engine's power-to-weight ratio and lead to significant overall RPA weight reduction when incorporated into an aircraft.

- **Engine modeling**

At the onset of this effort, the author considered developing or implementing models to represent small ICE operation and predict engine performance (torque, power, BSFC, etc.). Developing an engine performance model that would utilize ideal models of individual engine cycle processes or one that would use more realistic models of fluid-transfer, combustion, heat-transfer and kinetics was seen as not fitting into the time

constraint of this research effort. Thus, the modeling subject was not taken-on, but is seen as a good area to consider for future research. This engine performance model could be developed or procured to compare actual test results to predictions. An accurate small ICE performance model would aid in the engine selection portion of the design process for a HE-RPA. This would reduce the need to test similar ICEs of larger and smaller displacement and give insight on to the performance effects of design and operating variable changes.

- **Throttle position**

Throttle position establishment using the servo controller was adequate for the testing involved in this effort but increased throttle position accuracy and precision is desirable. Attaining the ability to open and close throttle position in finer increments is also desirable. These improvements would lead to greater flexibility in testing engines over their entire operating range, but more importantly improve the capability of the HEPS controller. The open-loop controller developed by Greiser [11] must have confidence in the accuracy of servo actuation's correspondence to throttle position as well as fine control as possible. For example, to optimize HEPS performance for a HE-RPA during a mission segment, the controller should not be limited to selecting 10% or 20% throttle when the optimal engine performance would be attained from 15% throttle. The use of a throttle position sensor (TPS) would also enhance throttle position accuracy and precision.

A TPS was ordered to accurately measure throttle valve position regardless of servo actuation but was not incorporated into engine testing in this effort because of time constraints. The TPS is a 500 Series single ear rotary position sensor manufactured by

CTS Corporation [44]and is intended for use on small engines. When opening or closing the throttle valve the TPS data could be used to more accurately establish a throttle position map to be used by the current open-loop controller design. In the future, the TPS could be used more effectively by incorporating real-time throttle position data from the sensor as feedback into a closed-loop controller design.

These recommendations for future research offer a wide range of directions for efforts to go in. Exploring these avenues will lead to improvements in the ability to test small ICEs and EMs intended for use in a HEPS for a HE-RPA. Improved testing, will hopefully lead to lessons learned and data analysis that shed light on how to improve HEPS performance. All this effort in-turn, would be for achieving the ultimate goal of building a HEPS for a HE-RPA that is designed for minimum fuel and energy consumption and maximum efficiency.

VI. Appendices

1. Appendix A: CEA Output for Fuel Combustion Equilibrium Reactions

```
******************************************************************************
         NASA-GLENN CHEMICAL EQUILIBRIUM PROGRAM CEA2, MAY 21, 2004
                  BY  BONNIE MCBRIDE AND SANFORD GORDON
      REFS: NASA RP-1311, PART I, 1994 AND NASA RP-1311, PART II, 1996

******************************************************************************
 problem    phi,eq.ratio=1,
       hp   p,atm=1,  t,k=2400
 react
   fuel=C8H18(L),isooct moles=1  t,c=25
   oxid=Air moles=12.5  t,c=25
 output  short
 end
         THERMODYNAMIC EQUILIBRIUM COMBUSTION PROPERTIES AT ASSIGNED PRESSURES
 CASE =
             REACTANT                          MOLES         ENERGY      TEMP
                                                           KJ/KG-MOL       K
 FUEL        C8H18(L),isooct                1.0000000    -259160.000    298.150
 OXIDANT     Air                           12.5000000       -125.530    298.150

 O/F=   15.13131  %FUEL=  6.199125  R,EQ.RATIO= 1.000000  PHI,EQ.RATIO=
1.000000

 THERMODYNAMIC PROPERTIES

 P, BAR             1.0132
 T, K             2261.88
 RHO, KG/CU M    1.5327-1
 H, KG/KG         -144.71
 U, KG/KG         -805.79
 G, KG/KG        -21795.0
 S, KJ/(KG)(K)     9.5718

 M, (1/n)          28.448
 (dLV/dLP)t      -1.00302
 (dLV/dLT)p        1.0895
 Cp, KJ/(KG)(K)    2.2440
 GAMMAs            1.1787
 SON VEL,M/SEC      882.7

 MOLE FRACTIONS
 *Ar              0.00863
 *CO              0.01302
 *CO2             0.11078
 *H               0.00042
 *H2              0.00288
 H2O              0.13418
 *NO              0.00232
 *N2              0.71820
 *O               0.00030
 *OH              0.00335
 *O2              0.00591

 * THERMODYNAMIC PROPERTIES FITTED TO 20000.K
```

```
*******************************************************************************
         NASA-GLENN CHEMICAL EQUILIBRIUM PROGRAM CEA2, MAY 21, 2004
                  BY  BONNIE MCBRIDE AND SANFORD GORDON
      REFS: NASA RP-1311, PART I, 1994 AND NASA RP-1311, PART II, 1996

*******************************************************************************

 problem    phi,eq.ratio=1,
     hp   p,atm=1,  t,k=2400
 react
   fuel=Jet-A(L) moles=1  t,c=25
   oxid=Air moles=9  t,c=25
 output  short
 end
         THERMODYNAMIC EQUILIBRIUM COMBUSTION PROPERTIES AT ASSIGNED PRESSURES
 CASE =
             REACTANT                          MOLES         ENERGY      TEMP
                                                           KJ/KG-MOL       K
 FUEL        Jet-A(L)                       1.0000000    -303403.000    298.150
 OXIDANT     Air                            9.0000000       -125.530    298.150

 O/F=   14.66948  %FUEL=  6.381831  R,EQ.RATIO= 1.000000  PHI,EQ.RATIO=
1.000000

 THERMODYNAMIC PROPERTIES

 P, BAR            1.0132
 T, K             2269.67
 RHO, KG/CU M    1.5406-1
 H, KJ/KG         -119.79
 U, KJ/KG         -777.48
 G, KJ/KG        -21687.0
 S, KJ/(KG)(K)     9.5024

 M, (1/n)          28.693
 (dLV/dLP)t      -1.00315
 (dLV/dLT)p        1.0932
 Cp, KJ/(KG)(K)    2.2540
 GAMMAs            1.1772
 SON VEL,M/SEC      879.9

 MOLE FRACTIONS
 *Ar              0.00868
 *CO              0.01411
 *CO2             0.11752
 *H               0.00042
 *H2              0.00265
 H2O              0.12134
 *NO              0.00244
 *N2              0.72292
 *O               0.00033
 *OH              0.00333
 *O2              0.00627

 * THERMODYNAMIC PROPERTIES FITTED TO 20000.K
```

2. Appendix B: Drawings for Engine Brackets, Flanges & Mounts

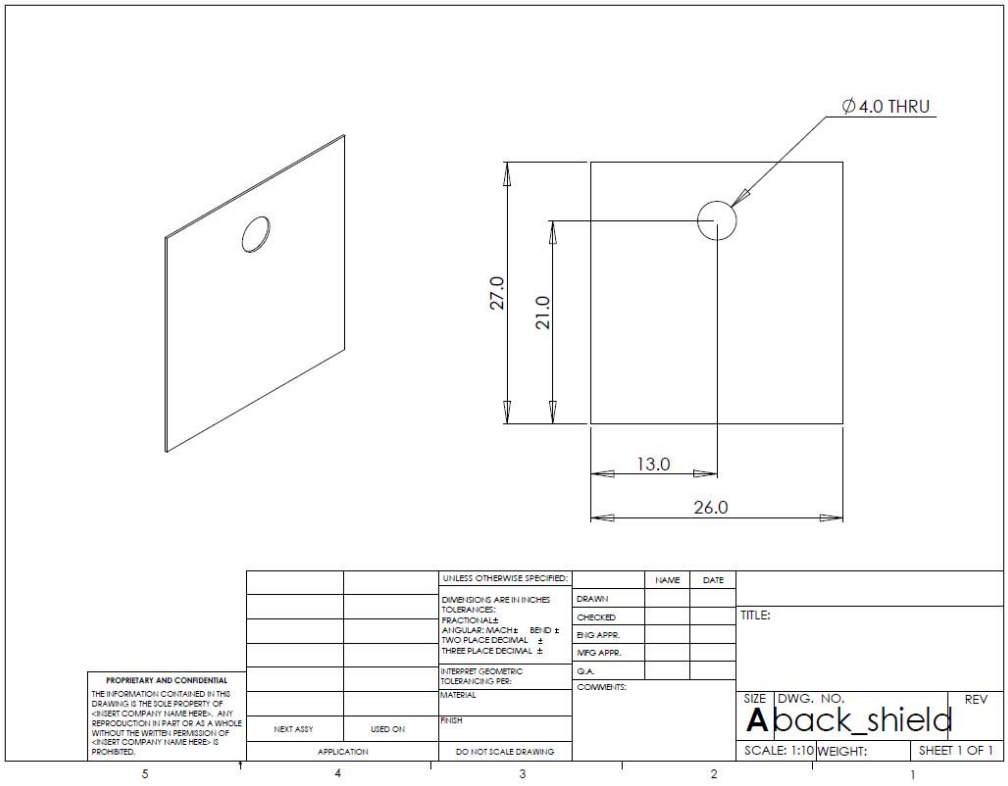

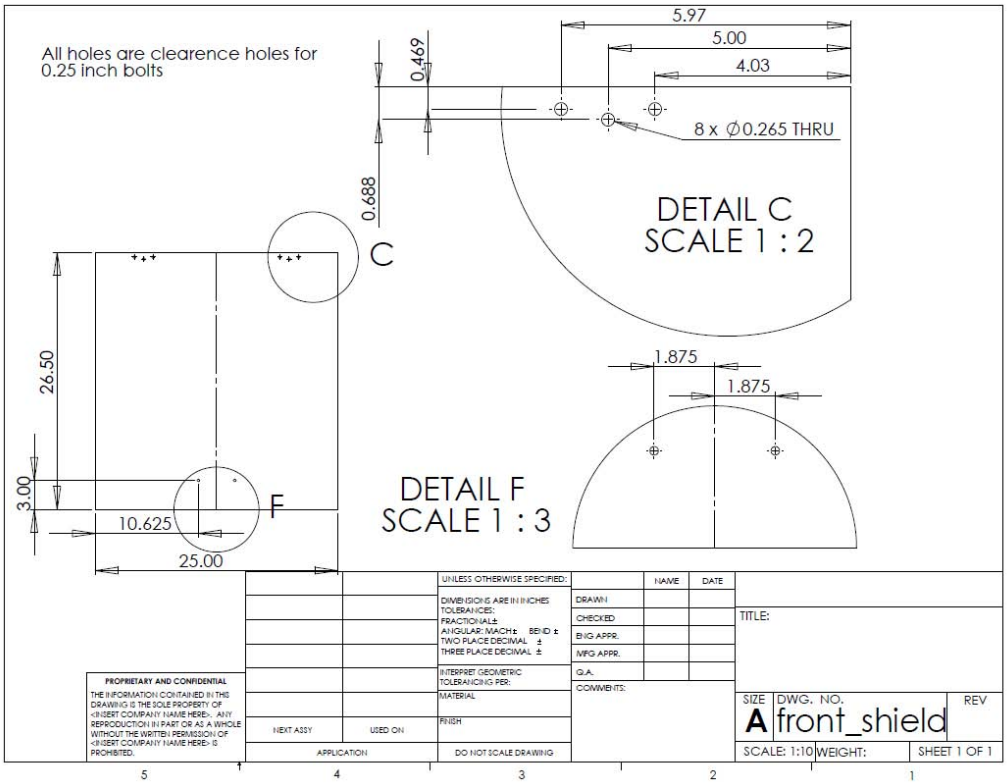

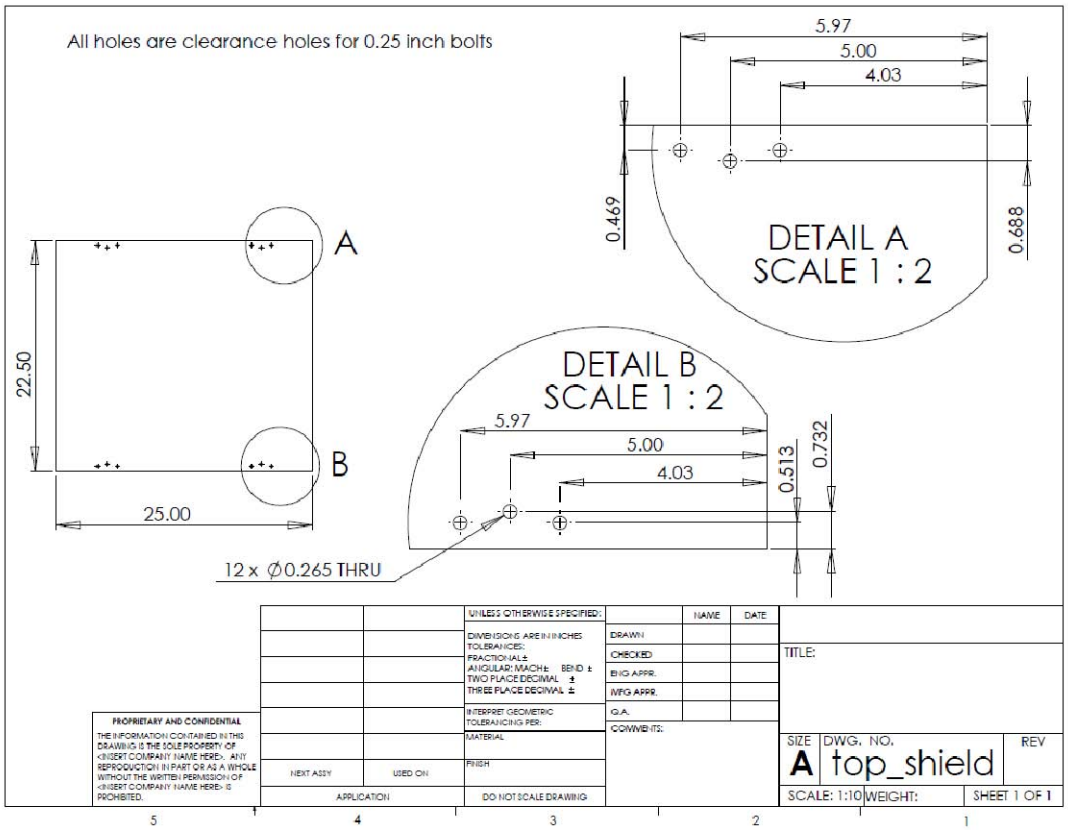

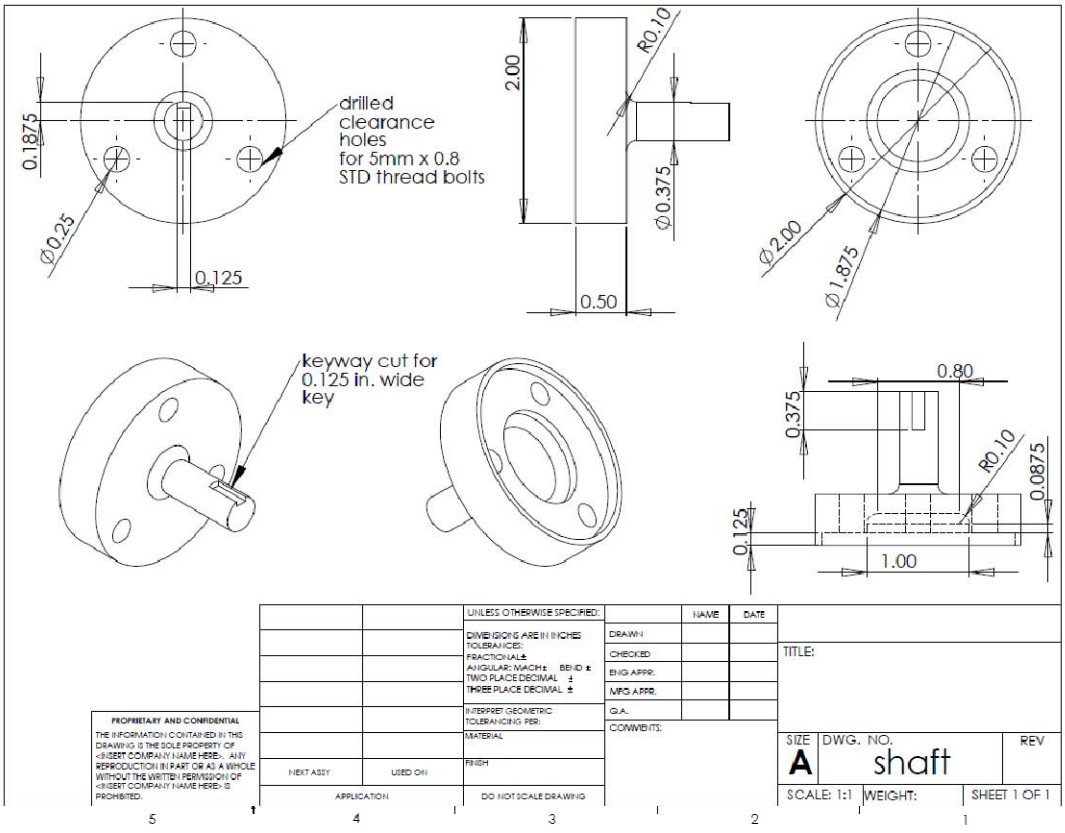

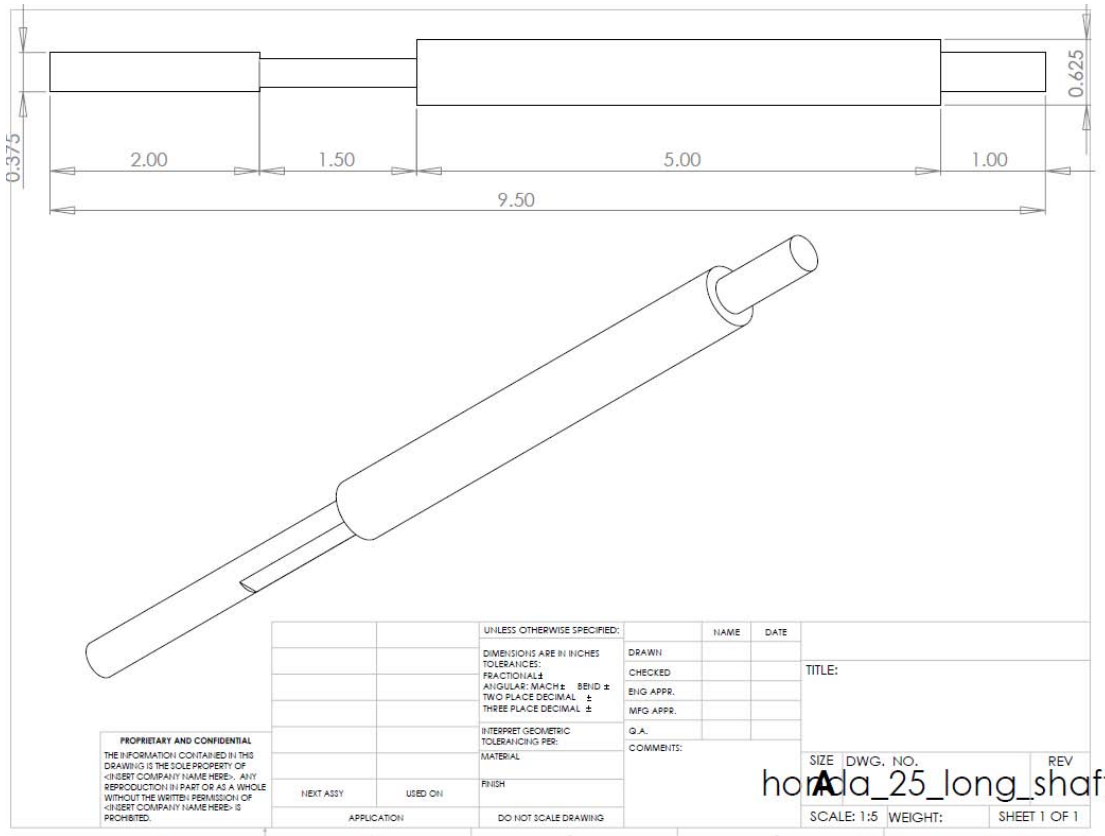

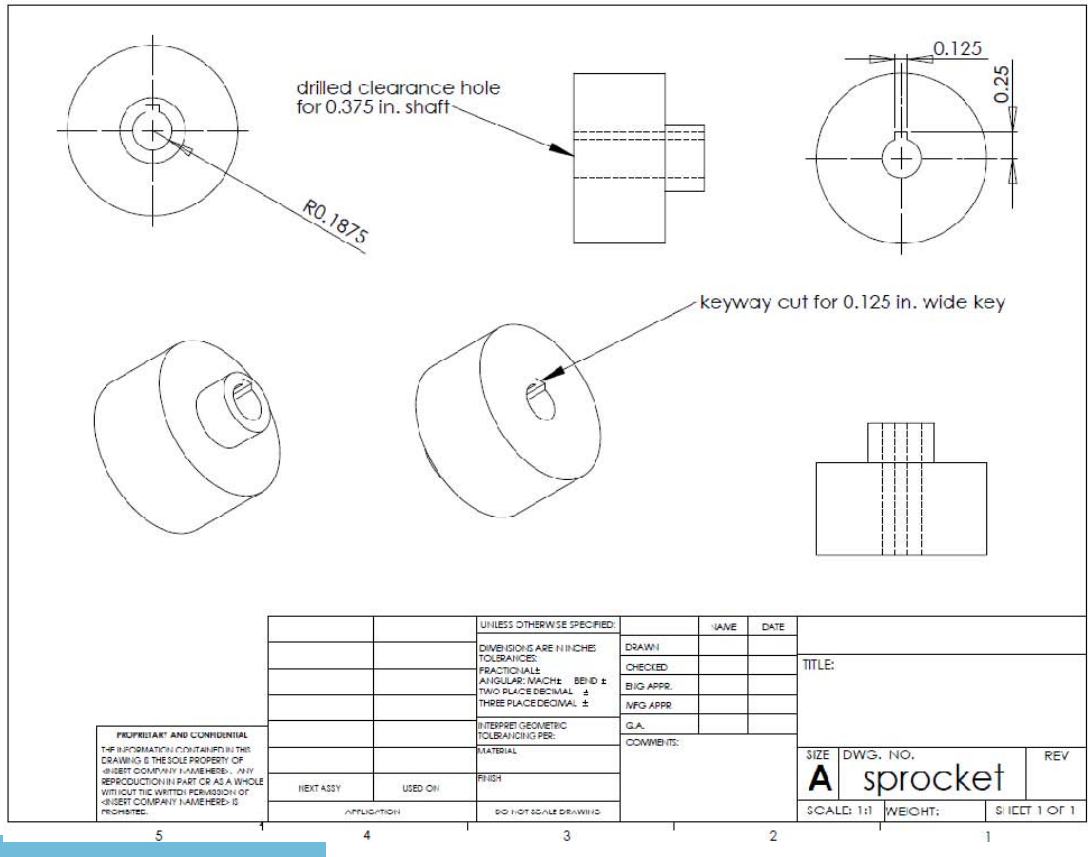

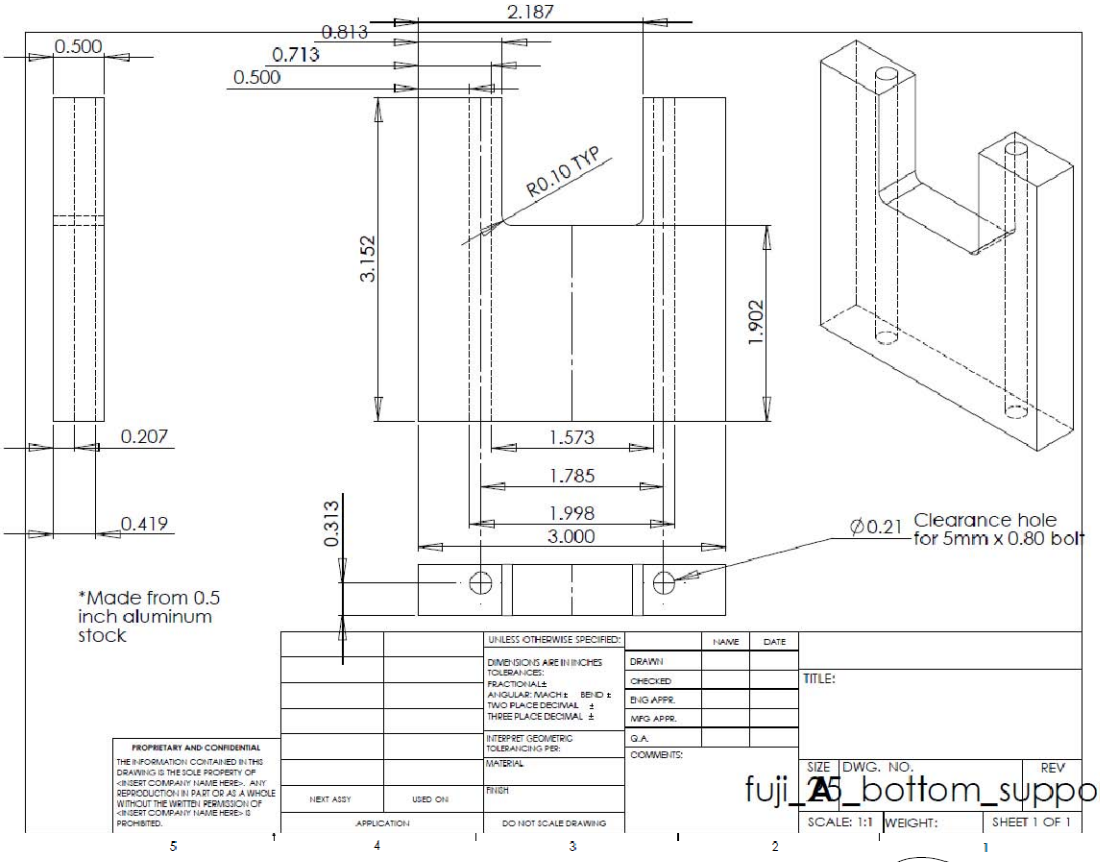

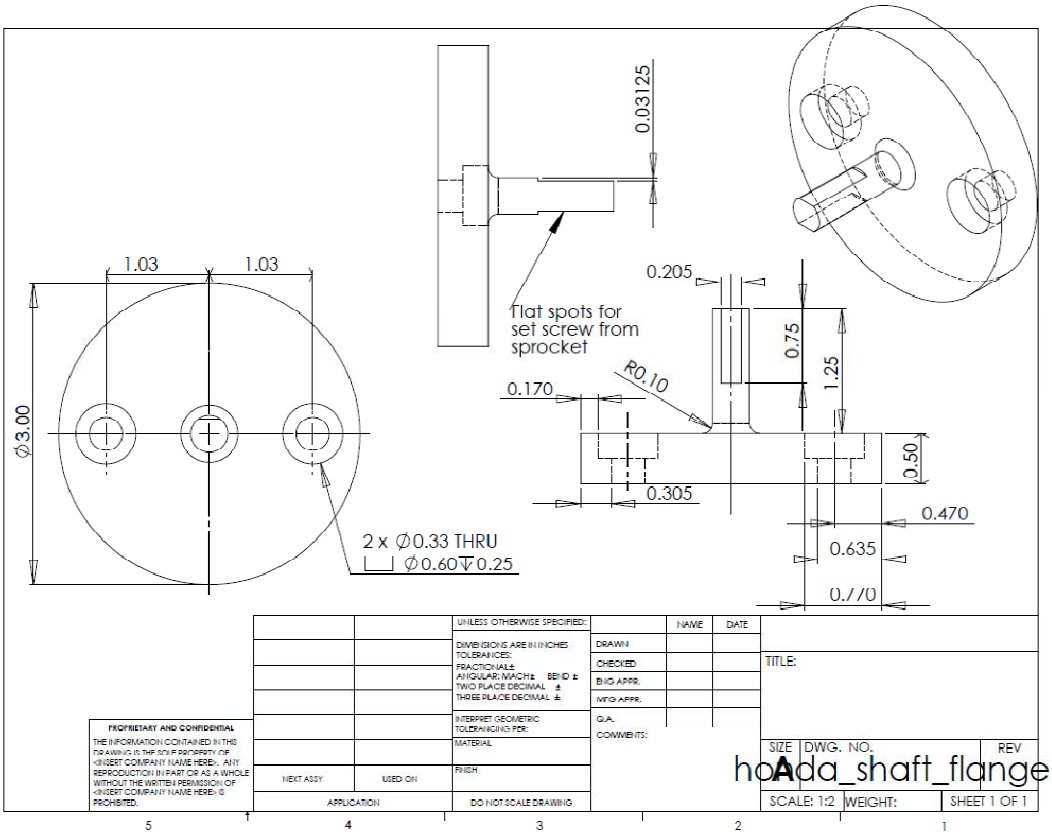

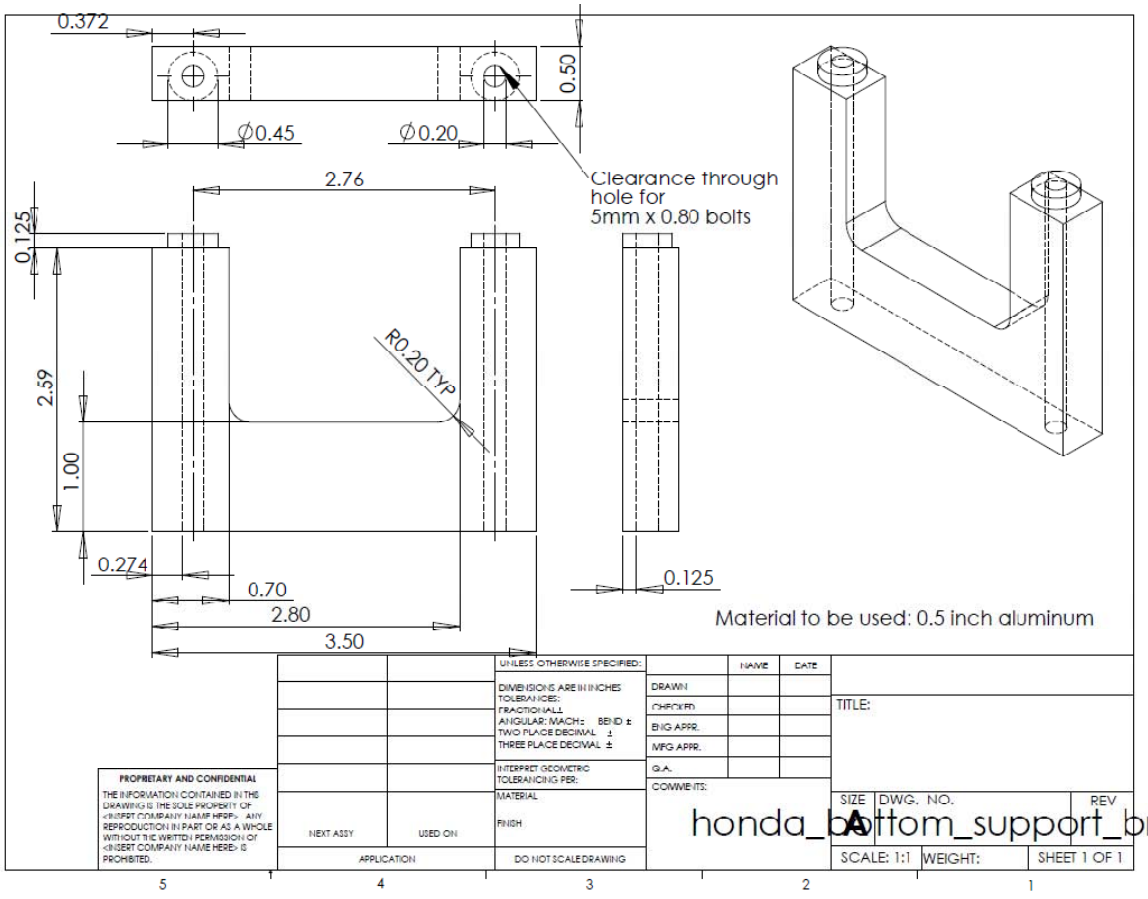

3. Appendix C: ENY Small Engine & Electric Motor Dynamometer Testing SOPs

DYNOmite Dynamometer Operation –

1. □ Ensure TrippLite surge protector/power-strip is plugged into 115V wall electrical outlet
2. □ Ensure TrippLite surge protector/power-strip "Protection" and "Line OK" status LEDs are green
3. □ Check and make sure data acquisition computer is on and not in sleep mode
4. □ Login to computer and open DYNO-MAX software program
5. □ Make sure eddy-current absorber and sprockets are free of debris and that no loose materials are close enough to become entangled during operation
6. □ Slowly rotate absorber (by hand) to guarantee it is completely free to revolve
7. □ Check data harness connections to data computer/controller and dynamometer sensors (Engine RPM sensor, Absorber/Load RPM sensor, fuel flow meter, etc.) are secure
8. □ Check that data computer/controller is powered (indicated by lit green LED on the side)
9. □ Check USB connections to data computer/controller and data acquisition computer are secure
10. □ Ensure eddy-current power supply control module is in OFF position and has its power cord plugged into 115V wall electrical outlet
11. □ Switch eddy-current power supply control module's load control switch to "Manual (Knob)" position
12. □ Ensure load knob is turned to "Zero" position
13. □ Connect 30 Amp "male" plug type power cord from dynamometer to 30 Amp "female" plug type power cord from eddy-current power supply control module
14. □ Turn eddy-current power supply control module ON when dynamometer is ready for operation
15. □ Operate dynamometer using DYNO-MAX software

Engine Operation –

1. □ Place new PIG® absorbent mats under the engine/dynamometer test stand
2. □ Ensure sprocket-engine flange is securely fastened to engine shaft
3. □ Check engine mounting hardware and fasteners are tight and secure
4. □ Check engine mounting plate is secured to dynamometer reaction cradle
5. □ Ensure Electric Ignition System (EIS) module is connected to a fully charged battery
6. □ Check EIS spark plug cover is secured over engine spark plug
7. □ Check EIS is securely connected to the engine's crankshaft position sensor
8. □ Ensure that EIS kill switch is wired between battery and EIS
9. □ Check oil level by examining oil pan dip stick to ensure sufficient oil is present in crankcase
10. □ Ensure exhaust and intake/throttle ports are clear of any obstructions
11. □ Check that throttle and choke valves are functioning and can be fully closed and opened via the servos
12. □ Ensure all fuel lines are unobstructed and connections (to fuel filters, carburetor, etc.) are tight
13. □ Make certain exhaust fan is connected to power supply and running by listening for sound of fan spinning
14. □ Fill fuel tank with fuel to be used (gasoline, JP-8, diesel)
15. □ Check that fuel tubing is secured away from cylinder head and other hot surfaces
16. □ Ensure all other fuel lines are unobstructed and connections (to fuel filters, carburetor, etc.) are tight
17. □ Place Lexan® shield/cover down over dynamometer test stand
18. □ Operate engine following engine starting procedure guideline
19. □ Run engine until fuel tank is completely empty and engine stops
20. □ Allow sufficient time for the engine to cool before further testing

VII. Bibliography

[1] Headquarters, United States Air Force, "United States Air Force Unmanned Aircraft Systems Flight Plan (2009-2047)," Washington DC, 18 May 2009.

[2] Department of the Air Force, "The U.S. Air Force Remotely Piloted Aircraft and Unmanned Aerial Vehicle Strategic Vision," Washington DC, 01 Jan 2005.

[3] Office of the Secretary of Defense, "Unmanned Aircraft Systems Roadmap (2005-2030)," Washington DC, 01 Jan 2005.

[4] Air Force Special Operations Command, Public Affairs Office. (2010, Jan) United States Air Force Factsheets. [Online]. http://www.af.mil/information/factsheets/factsheet.asp?id=10446

[5] Air Force Special Operations Command, Public Affairs Office. (2009, Nov) United States Air Force Factsheets. [Online]. http://www.af.mil/information/factsheets/factsheet.asp?id=10469

[6] Naval Research Laboratory. (14 Oct 2009) United States Naval Research Laboratory. [Online]. http://www.nrl.navy.mil/pao/pressRelease.php?Y=2009&R=99-09r

[7] Insitu, Inc. Insitu. [Online]. http://www.insitu.com/documents/Insitu%20Website/Marketing%20Collateral/ScanEagle%20Folder%20Insert.pdf

[8] Air Force Special Operations Command, Public Affairs Office. (2009, Nov) United States Air Force Factsheets. [Online]. http://www.af.mil/information/factsheets/factsheet.asp?fsID=10468

[9] Frederick G. Harmon, Andrew A. Frank, and Jean-Jacques Chattot, "Conceptual Design and Simulation of a Small Hybrid-Electric Unmanned Aerial Vehicle," *Journal of Aircraft*, vol. 43, no. 5, Sep 2006.

[10] Ryan M. Hiserote, "Analysis of Hybrid-Electric Propulsion System Designs for Small Unmanned Aircraft Systems," Air Force Institite of Technology, Mar 2010.

[11] Collin Greiser, "Implementation of a Rule-Based Open-Loop Control Strategy For a Hybrid-Electric Propulsion System on a Small RPA," Air Force Institute of Technology, Mar 2011.

[12] Todd A Rotramel, "Optimization of Hybrid-Electric Propulsion Systems for Small Remotely-Piloted Aircraft," Air Force Institute of Technology, Mar 2011.

[13] Paul Wolfowitz, "Department of Defense Directive: Number 4140.25," U.S. Department of Defense, Washington D.C., Apr 2004.

[14] M. John Miller, *Propulsion Systems for Hybrid Vehicles*. London: The Institution of Electrical Engineers, 2004.

[15] Philip G. Hill and Carl R. Peterson, *Mechanics and Thermodynamics of Propulsion*, 2nd ed. Reading, MA: Addison-Wesley Publishing Company, Inc., 1992.

[16] John B. Heywood, *Internal Combustion Engine Fundamentals*. New York: McGraw-Hill, 1988.

[17] Stephen R. Turns, *An Introduction to Combustion: Concepts and Application*, 2nd ed. Boston: McGraw-Hill, Inc., 2000.

[18] Encyclopedia Britannica, Inc. (2007) Encyclopedia Britannica. [Online]. http://www.britannica.com/bps/image/226592/89315/An-internal-combustion-engine-goes-through-four-strokes-intake-compression

[19] Colin R. Ferguson, *Internal Combsution Engines: Applied Thermosciences*. New York: John Wiley & Sons, Inc., 1986.

[20] Cary W. Wilson, "Performance of a Small Internal Combustion Engine Using n-heptane and iso-ocatane," Air Force Institute of Technology, Mar 2010.

[21] Stephen R. Turns, *An Introduction to Combustion: Concepts and Applications* , 2nd ed. Boston, United States of America: McGraw Hill, 2000.

[22] Mohmad Marouf Wani and M. Arif Wani, "Hybrid Neural Network Based Model for Predicting the Performance of a Two Stroke Spark Ignition Engine," in *Sixth International Conference on Machine Learning and Applications*, 2007, pp.

470-475.

[23] Shyam Menon and Christopher Cadou, "Experimental and computational investigations of small internal combustion engine performance," in *5th US Combustion Meeting: Organized by the Western States Section of the Combustion Institute*, Mar 2007.

[24] James G. Speight, *Fuel Science and Technology Handbook*. New York, United States of America: Marcel Dekker, Inc., 1990.

[25] E. M. Goodger, *Alternative Fuels: Chemical Energy Resources*. New York, United States of America: John Wiley & Sons, 1980.

[26] George E. Totten, *Fuels and Lubricants Handbook: Technology, Properties, Performance, and Testing*, Stephen R. Westbrook and Rajesh J. Shah, Eds. West Conshohocken, United States of America: ASTM International, 2003.

[27] John B. Heywood, *Internal Engine Combustion Fundamentals*. New York, United States of America: McGraw Hill, Inc., 1988.

[28] M. S. Shehata, "Cylinder pressure, performance parameters, heat release, specific heats ratio and duration of combustion for spark ignition engine," *Energy*, vol. 35, pp. 4710-4725, September 2010.

[29] American Honda Motor Co., Inc. (2011, February) Honda Engines - GX35 Mini 4-Stroke Engine. [Online]. http://engines.honda.com/models/model-detail/gx35

[30] Fuji-IMVAC. (2011) Fuji-IMVAC Engines 4-Stroke Engines: BF-25EI 25cc. [Online]. http://www.fuji-imvac.com/engines/fjig0225.html

[31] Fuji-IMVAC, Inc., "Operator's Manual for BF-25 and BF-34 EI 4-Stroke Engines," Hobbico, Inc., Champaign, IL,.

[32] SAE International. (2011, January) SAE International Standards. [Online]. http://standards.sae.org/wip/j1349/

[33] Grand Wing System U.S.A, Inc., "MT-1, the Multi-Tester Manual," City of Industry, CA,.

[34] Land and Sea, "DYNOmite Owner's Manual," 2006.

[35] Shyam Kumar Menon, "Performance measurement and scaling in small internal combustion engines," 2006.

[36] McMaster-Carr Supply Company. (2010) Aluminum Base-Mounted Stainless Steel Ball Bearing. [Online]. http://www.mcmaster.com/#8600n5/=ay7plg

[37] The Gates Rubber Company, "All You Ever Wanted to Know About Misalignment, But Were Afriaid to Ask: GatesFacts Technical Information Library," Denver, Colorado, 2008.

[38] The Gates Rubber Company, "Belt Drive Preventive Maintenance & Safety Manual," Denver, Colorado, 2008.

[39] American Honda Motor Co., Inc. (2011, February) Honda Engines - GX25 Mini 4-Stroke Engine. [Online]. http://engines.honda.com/models/model-detail/gx25

[40] Subaru Robin Industrial Engines. (2007) Subaru Robin - Features and Benefits - EH025. [Online]. http://209.62.29.198/pfeatures.aspx?pid=48

[41] Gates Corporation. (2006, October) Gates Corporatino Belt Drive Design Manuals. [Online]. http://www.gates.com/catalogs/file_display.cfm?file=PowerGrip_17195forweb.pdf&thisPath=gates\catalogs

[42] Max Macinery, Inc. (2010) Max Macinery, Inc. [Online]. http://www.maxmachinery.com/pdfs/213w.pdf

[43] TSI, Inc. (2010) Mass Flow-meters for Gases. [Online]. http://www.tsi.com/en-1033/products/2130/mass_flowmeters_for_laboratory_and_general_purpose_applications.aspx

[44] CTS Corporation. (2010) CTS Automotive Products. [Online]. http://www.ctscorp.com/automotive/datasheets/500-se.pdf

[45] Honda Motor Co., Ltd., "Honda Engines GX35 Owner's Manual,".

VIII. Vita

Captain Isseyas H. Mengistu graduated from Souderton Area High School in Souderton, PA in 2001. He completed his Bachelor of Science in Aerospace Engineering (B.S.E.) degree at Virginia Polytechnic Institute and State University, Blacksburg, VA, in 2005. He was commissioned as a second lieutenant in the United States Air Force on May 14, 2005 after completion of the Reserve Officer Training Corps program at Virginia Polytechnic Institute and State University.

His first assignment was with the Battlespace Environment Division of the Air Force Research Laboratory's Space Vehicles Directorate at Hanscom AFB, MA. There he served first as an Ionospheric Sensors Engineer and then as Chief of the Ionospheric Sensors Team in the Ionospheric Hazards and Specification group working to characterize, predict and mitigate the effects of the Ionosphere and space environment on defense systems such as GPS and SATCOM. In August 2009, he entered the Graduate School of Engineering and Management at the Air Force Institute of Technology in pursuit of a Master's degree in Aeronautical Engineering in March 2011. Following completion of the Master's he will move on to an assignment at the Global Positioning Systems Wing at the Air Force's Space and Missile Systems Center at Los Angeles AFB, CA.

REPORT DOCUMENTATION PAGE

Form Approved
OMB No. 074-0188

1. REPORT DATE *(DD-MM-YYYY)*	2. REPORT TYPE	3. DATES COVERED *(From – To)*
24-03-2011	Master's Thesis	Sept 2009 – Mar 2011

4. TITLE AND SUBTITLE
Small Internal Combustion Engine Testing for a Hybrid-Electric Remotely-Piloted Aircraft

5a. CONTRACT NUMBER

5b. GRANT NUMBER

5c. PROGRAM ELEMENT NUMBER

6. AUTHOR(S)
Mengistu, Isseyas H., Captain, USAF

5d. PROJECT NUMBER

5e. TASK NUMBER

5f. WORK UNIT NUMBER

7. PERFORMING ORGANIZATION NAMES(S) AND ADDRESS(S)
Air Force Institute of Technology
Graduate School of Engineering and Management (AFIT/ENY)
2950 Hobson Way, Building 640
WPAFB, OH 45433-8865

8. PERFORMING ORGANIZATION REPORT NUMBER
AFIT/GAE/ENY/11-M20

9. SPONSORING/MONITORING AGENCY NAME(S) AND ADDRESS(ES)
Dr. Fred Schauer (frederick.schauer@wpafb.af.mil)
Air Force Research Laboratory
1950 Fifth Street
WPAFB, OH 45433-7251

10. SPONSOR/MONITOR'S ACRONYM(S)
AFRL/RZTC

11. SPONSOR/MONITOR'S REPORT NUMBER(S)

12. DISTRIBUTION/AVAILABILITY STATEMENT
APPROVED FOR PUBLIC RELEASE; DISTRIBUTION UNLIMITED

13. SUPPLEMENTARY NOTES
This material is declared a work of the U.S. Government and is not subject to copyright protection in the United States.

14. ABSTRACT
Efficient operation of a hybrid-electric propulsion system (HEPS) powering a small remotely-piloted aircraft (RPA) requires that a controller have accurate and detailed engine and electric motor performance data. Many small internal combustion engines (ICEs) currently used on various small RPA were designed for use by the recreational hobbyist radio-control (R/C) aircraft market. Often, the manufacturers of these engines do not make accurate and reliable detailed engine performance data available for their engines. A dynamometer testing stand was assembled to test various small ICEs. These engines were tested with automotive unleaded gasoline (the manufacturer's recommended fuel) using the dynamometer setup. Torque, engine speed and fuel flow measurements were taken at varying load and throttle settings. Power and specific fuel consumption (SFC) data were calculated from these measurements. Engine performance maps were generated in which contours of SFC were mapped on a mean effective pressure (MEP) versus engine speed plot. These performance maps are to be utilized for performance testing of the controller and integrated HEPS in further research. Further follow-on research and development will be done to complete the goal of building a prototype hybrid-electric remotely piloted aircraft (HE-RPA) for flight testing. Minimum BSFC for the Honda GX35 engine was found to be 383.6 g/kW·hr (0.6307 lbm/hp·hr) at 4500 RPM and 60% throttle. The Honda GX35 was overall the better fit for incorporation into the HE-RPA.

15. SUBJECT TERMS
Internal combustion engine, Hybrid-electric, Propulsion, Unmanned, Performance maps

16. SECURITY CLASSIFICATION OF:			17. LIMITATION OF ABSTRACT	18. NUMBER OF PAGES	19a. NAME OF RESPONSIBLE PERSON
a. REPORT	b. ABSTRACT	c. THIS PAGE			Frederick G. Harmon, Lt Col, USAF
U	U	U	UU	124	19b. TELEPHONE NUMBER *(Include area code)* DSN 786-3636 x7478 (frederick.harmon@afit.edu)

Standard Form 298 (Rev. 8-98)
Prescribed by ANSI Std. Z39.18